Master's thesis

Nonlinear analysis of coupled dissipative systems with a conservation law

Submitted by

Tobias Frohoff-Hülsmann

September 29, 2017

First examiner
Prof. Dr. Uwe Thiele

Second examiner
Jun.-Prof. Dr. Raphael Wittkowski

Westfälische Wilhelms-Universität Münster
Fachbereich Physik
Institut für theoretische Physik

Contents

The Faraday instability [7] is a well-known fluid dynamics instability which describes the occurence of standing waves at fluid surfaces or in droplets. This instability is excited by vertical oscillations of the substrate underneath the liquid and is considered in various experimental and theoretical investigations [6, 15, 17]. Basically this instability is studied in two different geometrical situations: Either the instability grows in an infinite domain or it is confined to fixed boundaries. In the latter case it is observed that the geometry influences the unstable eigenmodes and thus the appearing spatial pattern as can be described via a Mathieu equation [2, 3].

Recently, experimental studies addressed an intermediate situation with flexible boundaries [20, 19]. Thereby, an experimental setup is studied where less viscous droplets floating on a viscous bath are excited by vertical oscillations. The main observation is an interplay of the drop shapes and the pattern within these droplets. One can find stationary states which are formed by a coevolution of the boundary and the wave pattern. One observes that various droplet shapes are related to different small-scaled structures. Besides stationary states non-stationary states are also observed. These dynamical structures basically consist of parallel standing waves and an increasing elongation of the droplet. The mechanism of this coupling between shape and wave field has been considered and explained from a hydrodynamical point of view [19].

In this work we pursue another approach to model a wide class of systems [11] where a large-scale structure (e.g. the floating drop) develops together with small-scale patterns (e.g. the Faraday waves) whose 'carrier' they form.

In particular, we consider a coupled system consisting of a conserved and a non-conserved quantity. In the framework of the presented experiment the conservation law applies to the liquid volume in the floating droplet and the other equation describes the evolution of the small-scale structures within the droplet.

For the conserved field we use the Cahn-Hilliard equation [9] and for the non-conserved one we choose the Swift-Hohenberg equation [10, 23]. The two well-known model equations are coupled by terms which represent the interaction between shape and small-scale structures.

Besides the motivation from an experimental point of view there is also a theoretical incentive. First, the Cahn-Hilliard and the Swift-Hohenberg equations differ from each other in their stability and their mass conservation behavior. Through their coupling we obtain an eighth order system in space which shows a great variety of possible instabilities in the interplay of a conserved and non-conserved quantity. Second, individually the two equations are variational, i.e. they form gradient dynamics on respective energy functionals, which limits the possible solutions to steady ones. However, with the freedom of choosing any coupling terms one can break this variational structure what allows us to study the transition from variational to nonvariational systems.

Note that the main purpose of this investigation is not to model a particular experimental system quantitatively, but to explore by theoretical analysis such promising coupled systems employing the simplest possible variational coupling terms.

Therefore, linear, weakly nonlinear as well as fully nonlinear considerations are employed and compared.
The bifurcation behavior is studied in connection to symmetry considerations.
At the end, an outlook is presented where the first analysis steps are done for a nonvariational coupling. For this kind of system one can find travelling wave instabilities which might lead to similar behavior as observed in the experiments.

1. Theoretical introduction

1.1. Weakly nonlinear analysis – Amplitude equations

Nonlinear partial differential equations (PDE) are in general not fully solvable, but there exist many methods how to find or approximate solutions. The weakly nonlinear analysis treats such a physical system near the onset of linear instability. This kind of analysis can be applied in many different models to obtain amplitude or phase equations, which can describe and explain qualitative as well as quantitative behavior of the fully nonlinear system (see [12, 13, 25, 8]). In this work this kind of analysis is employed to derive amplitude equations.
We start with a very general PDE in space and time of the form

$$\partial_t \vec{u} = \vec{M}[\vec{u}, \vec{p}]\,, \tag{1.1}$$

where $\vec{M}[\vec{u}, \vec{p}]$ is the nonlinear spatial differential operator applied on the vector field $\vec{u}(x,t)$ with the parameter set $\vec{p}$. Here, we only consider one space dimension, but it can be applied in more dimensions as well. If we find a steady state solution $\vec{u}(x,t) = \vec{u}_0(x)$ we introduce the deviation $\tilde{\vec{u}} = \vec{u} - \vec{u}_0$, insert this into (1.1) and drop the tilde:

$$\partial_t \vec{u} = \underline{\mathbf{J}}(\vec{p}) \cdot \vec{u} + \vec{N}[\vec{u}, \vec{p}]\,. \tag{1.2}$$

Thereby, we split the nonlinear problem into the linear part $\underline{\mathbf{J}} \cdot \vec{u}$ and the nonlinear one $\vec{N}[\vec{u}]$. To apply the weakly nonlinear analysis we assume that there exists a parameter set $\vec{p}_c$ at which the maximal eigenvalue of the linearized problem

$$\underline{\mathbf{J}}(\vec{p}) \cdot \vec{u} = \lambda \vec{u}\,, \tag{1.3}$$

has zero real part. That means, the system is adjusted to the onset of linear instability or equivalently the system passes through a bifurcation [1]. The amount of parameters of the parameter set which have to be adjusted exactly gives us the codimension of this bifurcation. Here, we assume that it is a codimension-1-bifurcation, but it can be easily expanded to the case of higher codimensions. So a parameter μ and a critical value $\mu = \mu_c$ exist at which $\mathrm{Re}(\lambda_{max}) = 0$. In general, the solution of the linearized problem is a Fourier integral

$$\vec{u}_{lin}(x,t) = \int_{-\infty}^{\infty} a(k)\vec{v}(k)e^{ikx+\lambda(k)t}dk\,, \tag{1.4}$$

with the eigenvalues $\lambda(k)$, the eigenvectors $\vec{v}(k)$ and the coefficients $a(k)$. However, at the onset of instability this integral can be reduced to a finite number of terms, since every contribution with $\mathrm{Re}(\lambda(k)) < 0$ is damped to zero. So only terms with the critical wavenumber(s) k_c at which $\mathrm{Re}(\lambda(k_c)) = \mathrm{Re}(\lambda_{max}) = 0$ have to be considered.
Then, the weakly nonlinear analysis can be used if the system is slightly removed from

[1] If the eigenvalue crosses the imaginary axis with non-zero velocity

the onset of instability. So one can introduce a smallness parameter ϵ and expand the control parameter in a series of ϵ:

$$\mu = \mu_c + \sum_i \epsilon^{p_i} \lambda_i \,. \tag{1.5}$$

Alternatively, $\mu - \mu_c$ defines a smallness parameter ϵ, e.g.

$$\epsilon^2 = \mu - \mu_c \,. \tag{1.6}$$

The idea of the weakly nonlinear analysis is that every term of equation (1.1) can be expanded in a series of ϵ such that one can solve it at each occuring order in ϵ. Slightly above the onset of linear instability the coefficient $a(k_c)$ becomes a space and time varying amplitude $A(X_1, X_2, ..., T_1, T_2, ...)$ of the critical mode $e^{ik_c x}$. It varies on slow time- and large spacescales. This dependencies reflect that for $\mu > \mu_c$ the fixpoint becomes unstable to further modes with wavenumbers around the critical one, too and moreover, $\mathrm{Re}(\lambda_{max}) > 0$. How the new time- and spacescales take these two changes into account is discussed in detail for explicit systems (e.g. in chapter 2.2). Often, only one slow time- and one large spacescale have to be introduced, which could be for example:

$$X = \epsilon x \quad T = \epsilon^2 t \,. \tag{1.7}$$

In general, there could be further scales which are proportional to other exponents in ϵ. The introduction of these new scales is also called multiscale method. With these multiscales the time and space derivatives have to be exchanged to

$$\partial_x \to \partial_x + \epsilon \partial_X \qquad \partial_t \to \partial_t + \epsilon^2 \partial_T \,. \tag{1.8}$$

Furthermore, the amplitude $A(X, T)$ of the critical mode is small at the onset of instability. Thus, nonlinearities lead to smaller expressions, i.e. the effect of nonlinearities are weak, but not neglectible (as in the linear regime). In order to solve (1.1) for different orders in ϵ one has to make an ansatz. This ansatz is quite problem-dependent. If we assume that there is no imaginary part of the eigenvalue at the onset of instability the ansatz could read:

$$\vec{u} = \epsilon^p \vec{A}_\epsilon(X, T) e^{ik_c x} + \epsilon^{2p} \left(\vec{C}_\epsilon(X, T) e^{2ik_c x} + \vec{B}_\epsilon(X, T) \right) + c.c. + h.h. \,. \tag{1.9}$$

Thereby *c.c.* and *h.h.* denote 'complex conjugate' and 'higher harmonics'. The subscript ϵ denotes that the amplitudes themselves have to be expanded in ϵ, i.e.

$$\vec{A}_\epsilon(X, T) = \sum_{m=0} \epsilon^{m/n} \vec{A}_m(X, T) \qquad . \tag{1.10}$$

Often the most challenging thing is to choose the proper multiscales X_i and T_i as well as to expand the physical field (see (1.9)) in such an appropriate ansatz that the final system of algebraic, ordinary differential and amplitude equations is self-contained.

1.1.1. Fredholm alternative

The Fredholm alternative is a theorem of the linear algebra which is often employed in the following calculations. Here, we formulate the theorem, but we do not give the proof. Furthermore we do not go into details of the mathematical requirements because in the cases presented in this work they are always fulfilled. If interested in the proof and mathematical details see [1].
Given a linear (differential) operator $\underline{\mathbf{J}}$ the Fredholm alternative says that **either**

$$\underline{\mathbf{J}} \cdot \vec{x} = \vec{q} \tag{1.11}$$

has unique solution $\vec{x}$ **or** the adjoint homogeneous problem

$$\underline{\mathbf{J}}^\dagger \cdot \vec{y} = \vec{0} \tag{1.12}$$

has a solution $\vec{y}$ with $< \vec{y}|\vec{q} > \neq 0$. Thereby, $\underline{\mathbf{J}}^\dagger$ denotes the adjoint (transposed and complex conjugated) operator of $\underline{\mathbf{J}}$ and $< \cdot|\cdot >$ is the scalar product of the underlying vector space. Another formulation of the Fredholm alternative is that the existence of an unique solution of the inhomogeneous problem (1.11) requires that $\vec{q} \notin ker\underline{\mathbf{J}}^\dagger$. This yields the so-called solvability condition:

$$< \vec{y}|\vec{q} >= 0 \quad \forall \vec{y} \in ker\underline{\mathbf{J}}^\dagger \,. \tag{1.13}$$

Often the physical field ansatz has the form (1.9). Then the solution $\vec{y}$ is given by

$$\vec{y} = \vec{v}e^{ik_c x} \,, \tag{1.14}$$

i.e. it is one critical fourier mode with eigenvector $\vec{v}$. Then the solvability condition (1.13) yields

$$< \vec{y}|\vec{q} >= \int_0^{2\pi} \vec{v}^* e^{-ik_c x} \cdot \vec{q} = 0 \,. \tag{1.15}$$

Due to the integration the solvability condition only affects the mode $\sim e^{ik_c x}$ of $\vec{q}$ since any other mode vanishes in (1.15) automatically.

1.2. Cahn-Hilliard equation – A long-scale instability

The Cahn-Hilliard equation is:

$$\partial_t \phi = \partial_x M \partial_x \left(-\kappa^2 \partial_{xx}\phi + a\phi + \phi^3 \right) \,, \tag{1.16}$$

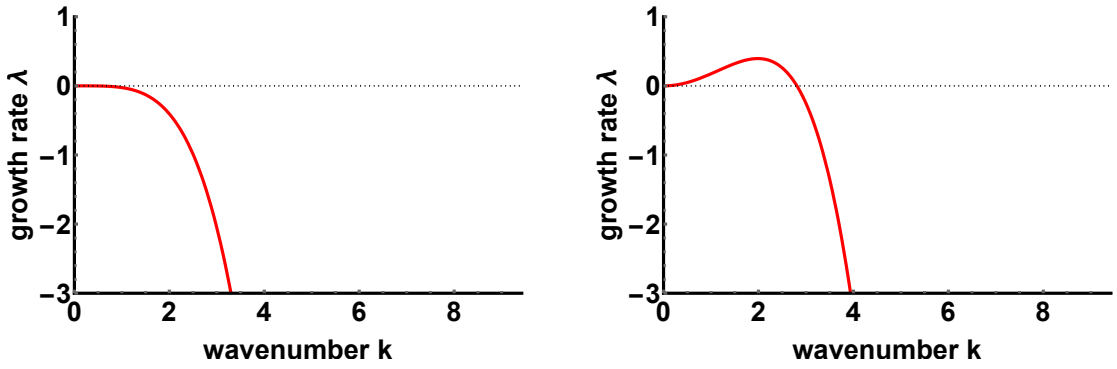

Figure 1.1: Dispersion relations of the Cahn-Hilliard equation (1.25) with respect to the trivial fixpoint $\phi_0 = 0$ at the onset of instability (a), $a = a_c = 0$) and slightly above the instability (b), $a = -0.2 < a_c$). The fixed parameters are $\kappa = 1$ and $L = 2\pi$.

with the mobility M, the tension κ and the parameter a?
It is common to nondimensionalize the Cahn-Hilliard equation via

$$x = L\tilde{x}, \quad t = \tau\tilde{t}\,, \tag{1.17}$$

where the tilde indicates nondimensionalized quantities. Furthermore, we set

$$\tau = \frac{1}{ML^2}. \tag{1.18}$$

We drop the tildes, thus the nondimensionalised Cahn-Hilliard equation is given by

$$\partial_t \phi = \partial_{xx}\left(-\frac{\kappa^2}{L^2}\partial_{xx}\phi + a\phi + \phi^3\right), \tag{1.19}$$

which can be written as gradient dynamics

$$\partial_t \phi = \partial_{xx}\frac{\delta \mathcal{F}_{CH}}{\delta \phi} \tag{1.20}$$

with the Cahn-Hilliard free energy

$$\mathcal{F}_{CH} = \int \left(\frac{\kappa^2}{L^2}\left(\partial_x \phi\right)^2 + \frac{a}{2}\phi^2 + \frac{1}{4}\phi^4\right) dx\,. \tag{1.21}$$

(1.19) can also be written as a conservation law

$$\partial_t \phi = \partial_x j\,, \tag{1.22}$$

and its symmetries are field inversion as well as spatial reflection (parity) and translation, i.e.

$$\phi \to -\phi \qquad x \to -x \qquad x \to x + \Theta\,. \tag{1.23}$$

The trivial fixpoint is

$$\phi(x,t) = \phi_0 = const\,, \tag{1.24}$$

which becomes unstable at $a = a_c = -3\phi_0^2$ due to a long-scale instability, also called a type-III instability. The corresponding dispersion relation

$$\lambda(k) = -k^2(\frac{\kappa^2}{L^2}k^2 + a + 3\phi_0^2) \tag{1.25}$$

is obtained via linear stability analysis and is depicted in figure 1.1 for the case $\phi_0 = 0$. The left panel shows that for $a = a_c$ the dispersion relation has a saddle-node at $k = k_c = 0$. Then in the right panel for $a > a_c$ the fixpoint becomes unstable, whereby the eigenvalue at $k = 0$ stays zero and the most critical wavenumber is greater than zero. For $a \to a_c$ the critical wavelength $\lambda_c = \frac{2\pi}{k_c}$ tends to infinity. Therefore, it is called a long-scale instability.

1.2.1. Weakly nonlinear analysis of the Cahn-Hilliard equation

The common ansatz for a weakly nonlinear analysis for a type-III instability [4] is

$$u(x,t) = u_0(x + \Theta(X,T)) + \epsilon^s u_1(x,X,T) + O(\epsilon^{s+1})\,, \tag{1.26}$$

where $u_0(x)$ is the fixpoint solution, $\Theta(X,T)$ is a phase that may vary on a large timescale $T = \epsilon^r t$ and a largespatial scale $X = \epsilon^p x$ and u_1 is the first small amplitude correction to u_0. Applying a weakly nonlinear analysis one obtains a phase equation for $\Theta(X,T)$ and an amplitude equation for u_1.
Here, the fixpoint solution is the homogeneous solution, i.e. $\phi_0(x + \Theta(X,T)) = \phi_0$. Therefore, we do not obtain a phase equation and our ansatz reduces to

$$\phi(x,t) = \phi_0 + \epsilon^s A_0(X,T) + \epsilon^{s+1} A_1(X,T) + O(\epsilon^{s+2})\,, \tag{1.27}$$

where A_i are real 'amplitudes'. Due to the dispersion relation (1.25) we choose the scalings

$$a = -3\phi_0^2 + \tilde{a}\epsilon^2 \qquad X = \epsilon x \qquad T = \epsilon^4 t \tag{1.28}$$

in order to keep every term in (1.25) at the same magnitude [2]. Next, we consider the possible nonlinearity which satisfies the symmetries (1.23).
In the special case of $\phi_0 = 0$, the first possible nonlinearity is $\partial_{XX} A_0(X,T)^3$. With the

[2] In (1.25) the wavenumber k is scaled as X and the growth rate λ is scaled as T. More explanation on the connection between the dispersion relation and the introduced multiscales will follow in chapter 2.2

ansatz

$$\phi(x,t) = \phi_0 + \epsilon A_0(X,T) + O(\epsilon^2)\,, \tag{1.29}$$

we ensure that this nonlinearity contributes at the same order in ϵ as the linear terms. Therefore, we obtain the amplitude equation for $A_0(X,T)$ at fifth order in ϵ:

$$\partial_T A_0 = \partial_{XX}\left(-\frac{\kappa^2}{L^2}\partial_{XX}A_0 + \tilde{a}A_0 + A_0^3\right)\,. \tag{1.30}$$

This is again the Cahn-Hilliard equation.
In the case of arbitrary ϕ_0, as long as it is of order 1, there is the quadratic nonlinearity in the small amplitude namely $\phi_0\partial_{XX}A_0(X,T)^2$ which could occur and which satisfies the symmetries. If we choose now

$$\phi(x,t) = \phi_0 + \epsilon^2 A_0(X,T) + O(\epsilon^3)\,, \tag{1.31}$$

then the quadratic nonlinearity contributes at the same order as the linear terms thus the amplitude equation (found at order ϵ^6) reads:

$$\partial_T A_0 = \partial_{XX}\left(-\frac{\kappa^2}{L^2}\partial_{XX}A_0 + \tilde{a}A_0 + 6\phi_0 A_0^2\right)\,. \tag{1.32}$$

This is known as the Sivashinsky equation [22]. It conserves the $\phi \to -\phi$ symmetry since that means $\phi_0 \to -\phi_0$ and $A_0 \to -A_0$, but in contrast to the Cahn-Hilliard equation for the amplitude (1.30) it breaks the up-down symmetry in A_0.
The Sivashinsky equation in the form of (1.32) exhibits a finite time blow up and is therefore not physically meaningful. In order to prevent this behavior one has to incorporate higher orders in (1.32) which stabilized the solutions of (1.32) to finite amplitudes.
A third case can be considered where $\phi_0 \sim \epsilon$. Then higher order nonlinearities become important in (1.32). To balance linear and nonlinear terms we choose again ansatz (1.29) and obtain the following evolution equation for $A_0(X,T)$:

$$\partial_T A_0 = \partial_{XX}\left(-\frac{\kappa^2}{L^2}\partial_{XX}A_0 + \tilde{a}A_0 + 6\phi_0 A_0^2 + A_0^3\right)\,. \tag{1.33}$$

1.3. Swift-Hohenberg equation – A short-scale instability

The Swift-Hohenberg equation is given by:

$$\partial_t\psi = r\psi - \left(q_c^2 + \partial_{xx}\right)^2\psi + \delta\psi^2 - \psi^3\,. \tag{1.34}$$

It is common to nondimensionalise (1.39) via

$$x = \frac{1}{q_c}\tilde{x}, \quad t = \tau\tilde{t}, \quad \psi = \psi_0\tilde{\psi}\,. \tag{1.35}$$

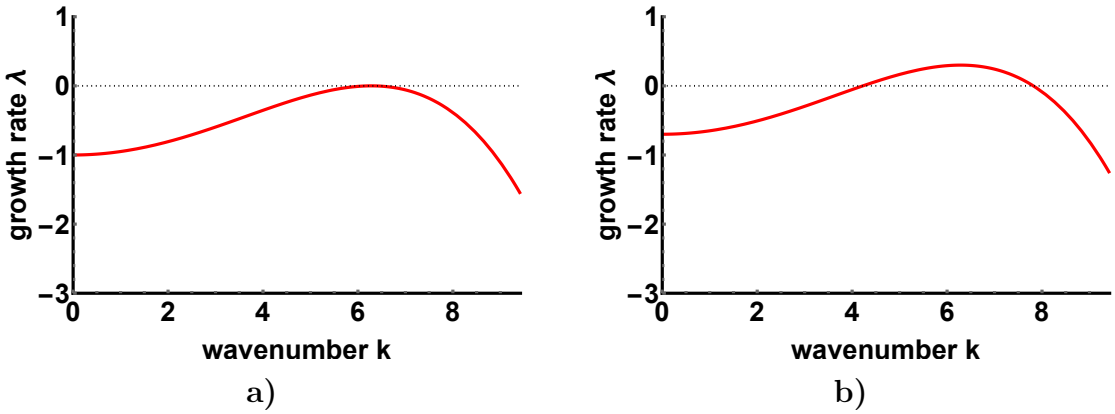

Figure 1.2: Dispersion relations of the Cahn-Hilliard equation (1.43) at the onset of instability (a), $r = r_c = 0$) and slightly above the instability (b), $r = 0.3 > r_c$). The fixed parameters are $\kappa = 1$ and $L = 2\pi$.

Then (1.34) becomes

$$\partial_{\tilde{t}}\tilde{\psi} = \tau r\tilde{\psi} - \tau q_c^2 \left(1 + \partial_{\tilde{x}\tilde{x}}\right)^2 \tilde{\psi} + \tau\delta\psi_0\tilde{\psi}^2 - \tau\psi_0^2\tilde{\psi}^3 \,. \tag{1.36}$$

We set

$$\tau = \frac{1}{q_c^2}, \quad \psi_0 = \frac{1}{\sqrt{\tau}}, \quad \tilde{r} = \tau r, \quad \tilde{\delta} = \tau\delta\psi_0, \tag{1.37}$$

and use a second spatial scaling

$$\tilde{x} = L\hat{x} \,. \tag{1.38}$$

Leaving tildes and hats yields the nondimensionalised and rescaled Swift-Hohenberg equation

$$\partial_t\psi = r\psi - \left(1 + \frac{1}{L^2}\partial_{xx}\right)^2 \psi + \delta\psi^2 - \psi^3 \,. \tag{1.39}$$

Similarly to the Cahn-Hilliard equation we can write (1.39) as a gradient dynamics on a free energy

$$\partial_t\psi = -\frac{\delta\mathcal{F}_{\mathcal{SH}}}{\delta\psi} \tag{1.40}$$

with the Swift-Hohenberg free energy

$$\mathcal{F}_{SH} = \int \left(\frac{1}{L^4}\left(\partial_{xx}\psi\right)^2 - \frac{1}{L^2}\left(\partial_x\psi\right)^2 + \frac{1-r}{2}\psi^2 - \frac{\delta}{3}\psi^3 + \frac{1}{4}\psi^4\right) dx \,. \tag{1.41}$$

The trivial fixpoint of (1.39) is

$$\psi(x,t) = 0 \,. \tag{1.42}$$

In figure 1.2 the dispersion relation

$$\lambda(k) = r - \left(1 - \frac{k^2}{L^2}\right)^2 \tag{1.43}$$

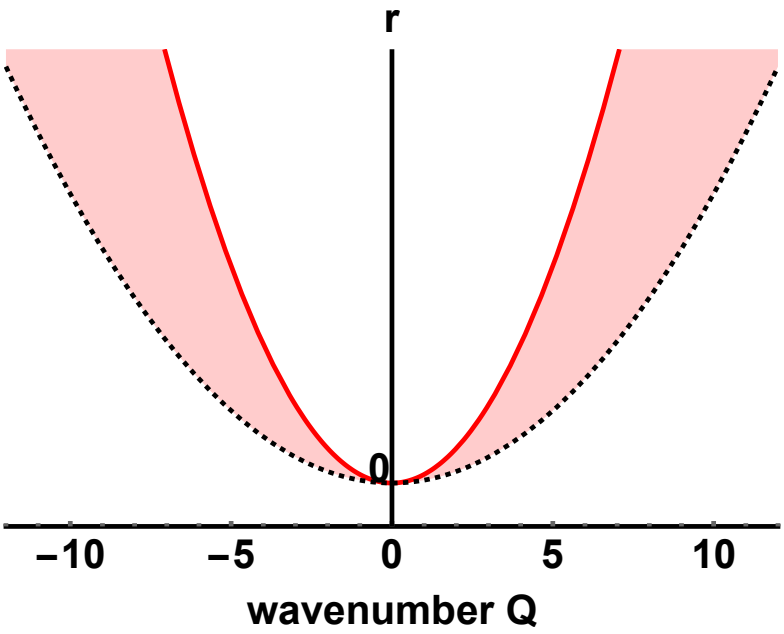

Figure 1.3: Illustration of the Eckhaus instability. The existence condition (1.48) is depicted by the black dashed curve and the stability condition by the red solid one. The red shaded area in between these curves is the Eckhaus band. There, the corresponding solutions are unstable.

obtained from the linear stability analysis around the trivial fixpoint is illustrated. We see that the trivial fixpoint becomes unstable in a short-scale instability for $r \geq 0$ at $k = k_c = L$. That means, that the system has a most critical wavelength

$$\lambda_c = \frac{2\pi}{L} < \infty \,. \tag{1.44}$$

Therefore, it is called a short-scale or a type-I instability.

1.3.1. Weakly nonlinear analysis of the Swift-Hohenberg equation

The weakly nonlinear analysis can be applied for $r = \epsilon^2 << 1$ with the proper ansatz

$$\begin{aligned}\psi(x,t) =& \epsilon \left(A_0(X,T) e^{ik_c x} + c.c. \right) \\ &+ \epsilon^2 \left(A_1(X,T) e^{ik_c x} + C_0(X,T) e^{2ik_c x} + c.c. + B_0(X,T) \right) + O(\epsilon^3) \,,\end{aligned} \tag{1.45}$$

where the slow time scale $T = \epsilon^2 t$ and long space scale $X = \epsilon x$ are introduced. At order ϵ^3 one obtains the real Ginzburg-Landau equation as amplitude equation for A_0:

$$\partial_T A_0 = r A_0 - (1 - \frac{\delta^2}{9}) |A_0|^2 A_0 + \frac{4}{L^2} \partial_{XX} A_0 \tag{1.46}$$

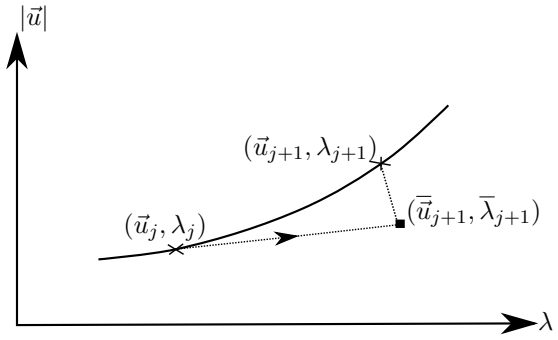

Figure 1.4: Illustration of the Predictor-Corrector method

Amplitude equations such as (1.46) are useful to describe solution behavior like secondary bifurcations [3]. Steady solutions of equation (1.46) are

$$A_0(x) = a_0 e^{iQx} \text{ with } a_0 = \sqrt{\frac{r - \left(\frac{2Q}{L}\right)^2}{1 - \frac{\delta^2}{9}}}\,. \tag{1.47}$$

These so-called phase winding solutions only exist if

$$r > \left(\frac{2Q}{L}\right)^2 \tag{1.48}$$

and a linear stability analysis yields that only the primary solution with $Q = 0$ is always stable. Additional to the existence condition (1.48) there is a stability condition for any other solution with $Q \neq 0$. This second condition has to be fulfilled, otherwise the solution is unstable. That is for any $r > 0$ there exists a band of phase winding solution in the (Q, r)-plane which are unstable. This unstable band is depicted as red shaded region in figure 1.3 and is called Eckhaus band. The corresponding instability is the Eckhaus instability [14].

1.4. Continuation – basic principles

Throughout this work fully nonlinear examinations are computed by a numerical continuation program *pde2path*. Therefore, the basic principles of continuation are explained in this chapter. For further information of this subject see [24, 21].
The main task of continuation is to trace a branch of solutions which are described by a system of nonlinear algebraic equations

$$\vec{G}(\vec{u}, \lambda) = 0\,, \tag{1.49}$$

[3] We assume that $1 - \frac{\delta^2}{9} > 0$, i.e. the amplitude solutions of (1.46) are saturated by the negative sign of the cubic nonlinearity

where $\vec{u}$ is the n-dimensional vector, λ is the control parameter and $\vec{G}$ is a nonlinear differential operator. Tracing a branch of solutions means that for a given first solution $(\vec{u}_0, \lambda_0)$ further solutions $(\vec{u}_1, \lambda_1), (\vec{u}_2, \lambda_2), ...$ are calculated to complete the branch. The continuation method is combined with devices to detect special points such as bifurcation and fold points. The linear stability of the current solution is also analyzed and branch switching at bifurcation points is also possible. One uses these numerical methods to obtain a bifurcation diagram of system (1.49). Here, we just consider the simple branch tracing method which consists of two parts. As depicted in figure 1.4 we start from the given solution point $(\vec{u}_j, \lambda_j)$, make a prediction $(\overline{\vec{u}}_{j+1}, \overline{\lambda}_{j+1})$ and correct this predictor to the next solution $(\vec{u}_{j+1}, \lambda_{j+1})$. In this so-called predictor-corrector method the solution is often parameterized by the arclength s of the branch, i.e. $(\vec{u}_j, \lambda_j) = (\vec{u}(s_j), \lambda(s_j))$. Then the step-length is defined by $\Delta s = s_{j+1} - s_j$. So the main ingredients of branch tracing are

- parametrization
- predictor
- corrector
- step-length control .

Besides the arclength parametrization the natural parametrization $(\vec{u}_j, \lambda_j) = (\vec{u}(\lambda_j), \lambda_j)$ is common. However, this parametrization can not be used in general, since the continuation with this parametrization at fold points where $\partial_s \lambda$ changes its sign breaks down. This is not the case for arclength parametrization. The continuation program is able to switch between these two parametrizations.
Within this program the tangent predictor is used in the framework of arclength parametrization. We differentiate (1.49) with respect to the arclength s and obtain

$$0 = \vec{G}_{\vec{u}} \cdot \frac{d\vec{u}}{ds} + \vec{G}_{\lambda} \frac{d\lambda}{ds} = \left(\vec{G}_{\vec{u}} | \vec{G}_{\lambda} \right) \cdot \begin{pmatrix} \frac{d\vec{u}}{ds} \\ \frac{d\lambda}{ds} \end{pmatrix} . \tag{1.50}$$

Equation (1.50) is solved at the given solution $(\vec{u}(s_j), \lambda(s_j))$ to obtain the tangent vector after proper normalization and orientation as

$$\vec{\tau}(s_j) = (\dot{\vec{u}}(s_j), \dot{\lambda}(s_j) = \frac{d}{ds} \left(\vec{u}(s), \lambda(s) \right) |_{s=s_j} . \tag{1.51}$$

Then one calculates the predictor by a step of the Euler method with the stepsize Δs:

$$(\overline{\vec{u}}(s_{j+1}), \overline{\lambda}(s_{j+1}) = (\vec{u}(s_j), \lambda(s_j) + \Delta s \vec{\tau} . \tag{1.52}$$

Afterwards this predictor has to be corrected. The Newton method is mostly used for it. Here, the main aspects of branch tracing have been discussed but practical details such as pseudo arclength parametrization and step-length control methods have been neglected.

2. Fully and weakly nonlinear analysis of coupled system with variational structure

Now, we start the analysis of a two-field system consisting of a Cahn-Hilliard part ϕ (1.19) and a Swift-Hohenberg part ψ (1.39) which are coupled by the mathematically simplest term that preserves the variational structure. We can write this term as coupling energy $\mathcal{F}_{Coupling}$ with coupling strength γ of the form

$$\mathcal{F}_{Coupling} = \gamma \int \phi\psi dx \,. \tag{2.1}$$

The resulting total free energy is

$$\mathcal{F} = \mathcal{F}_{CH} + \mathcal{F}_{SH} + \mathcal{F}_{Coupling} \,, \tag{2.2}$$

with $\mathcal{F}_{CH}$ and $\mathcal{F}_{SH}$ defined in (1.21) and (1.41), respectively. Then the two-field system, called $\vec{u}$ from now on, in one spatial dimension reads

$$\partial_t \vec{u} = \partial_t \begin{pmatrix} \phi \\ \psi \end{pmatrix} = \begin{pmatrix} \partial_{xx} \frac{\delta \mathcal{F}}{\delta \phi} \\ -\frac{\delta \mathcal{F}}{\delta \psi} \end{pmatrix} \tag{2.3}$$

$$= \begin{pmatrix} \partial_{xx} \left(-\frac{\kappa^2}{L^2} \partial_{xx} \phi + a\phi + \phi^3 + \gamma\psi \right) \\ r\psi - (\frac{1}{L^2}\partial_{xx} + 1)^2 \psi + \delta\psi^2 - \psi^3 - \gamma\phi \end{pmatrix} , \tag{2.4}$$

where κ, L, a, r, δ and γ are system parameters.
The differential equation system (2.4) is invariant under spatial translation ($x \to x + x_0$) and spatial reflection ($x \to -x$) as well as under $(\gamma, \phi, \psi) \to (-\gamma, -\phi, \psi)$ transformation. If the quadratic nonlinearity is turned off, i.e. if $\delta = 0$, it also has an inversion symmetry ($(x, \phi, \psi) \to (-x, -\phi, -\psi)$).

2.1. Linearized problem

We begin analysing system (2.4) by linearizing it around the trivial fixpoint

$$\begin{pmatrix} \phi_0 \\ \psi_0 \end{pmatrix} = \begin{pmatrix} 0 \\ 0 \end{pmatrix} \tag{2.5}$$

As mentioned in the introduction we expect qualitative different instabilities in the linearized regime. Therefore, we apply the linear stability analysis. We consider a small perturbation, build a Fourier decomposition, i.e. we examine decoupled harmonic perturbation modes

$$\begin{pmatrix} \phi_1 \\ \psi_1 \end{pmatrix} = \epsilon \vec{v}(k) e^{\lambda t + ikx} + O(\epsilon^2) \,, \tag{2.6}$$

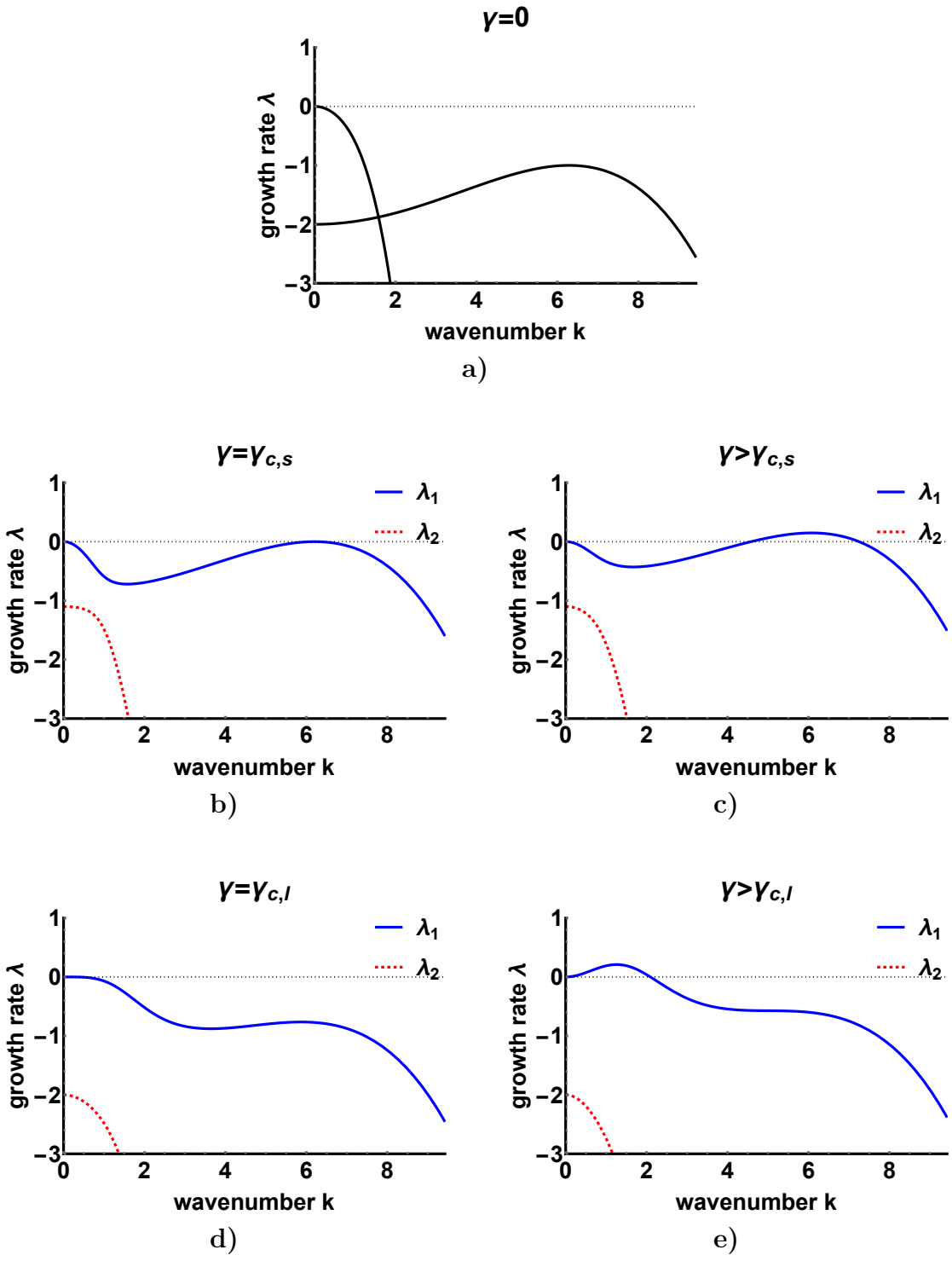

Figure 2.1: Dispersion relations of (2.8) for different cases. The uncoupled case a) ($\gamma = 0$) shows the unchanged dispersion relations of the Cahn-Hilliard and the Swift-Hohenberg part together. Panels b) and c) depict the long-scale instability at onset (b), $\gamma = \gamma_{c,l}$) and slightly above the onset (c), $\gamma > \gamma_{c,l}$), respectively, with $\gamma_{c,l}$ from (2.17). The fixed parameters for panels a), b) and c) are $a = 0.5$, $r = -1$, $\kappa = 2$ and $L = 2\pi$. Panels d) and e) depict the short-scale instability at onset (d), $\gamma = \gamma_{c,s}$) and slightly above the onset (e), $\gamma > \gamma_{c,s}$), respectively, with $\gamma_{c,s}$ from (2.11).

and linearize in ϵ around the trivial fixpoint. We obtain the eigenvalue problem

$$\underbrace{\begin{pmatrix} -k^2\left(\frac{\kappa^2}{L^2}k^2+a\right) & -\gamma k^2 \\ -\gamma & r-\left(-\frac{1}{L^2}k^2+1\right)^2 \end{pmatrix}}_{:=\underline{\mathbf{J}}}\vec{v}=\lambda\vec{v}\,, \tag{2.7}$$

where $\underline{\mathbf{J}}$ is the Jacobian and $\vec{v}$ is the eigenvector to the particular eigenvalue λ. The eigenvalue λ is automatically the growth rate given that for a gradient dynamics all eigenvalues are real. Both, eigenvector and eigenvalue, are functions of the wavenumber k. Explicitly the eigenvalues are

$$\begin{aligned}\lambda_{1,2}(k) =& \frac{1}{2}\Bigg[-k^2\left(\frac{\kappa^2}{L^2}k^2+a\right)+r-\left(-\frac{1}{L^2}k^2+1\right)^2 \\ &\pm\sqrt{\left[k^2\left(\frac{\kappa^2}{L^2}k^2+a\right)+r-\left(-\frac{1}{L^2}k^2+1\right)^2\right]^2+4k^2\gamma^2}\Bigg]\,.\end{aligned} \tag{2.8}$$

Since the coupling energy (2.1) influences ϕ as well as ψ directly, we choose the coupling strength γ as our main control parameter. This means that we use the coupling strength as critical parameter which controls the occurance of instability. For $\gamma \neq 0$ the eigenvalue with positive sign increases. Thus, every $\gamma \neq 0$ destabilizes the system. Therefore, we obtain some finite parameter intervalls in which the coupling strength can initiate an instability. For example the Cahn-Hilliard part as well as the Swift-Hohenberg part must not be unstable without any coupling, i.e.

$$a > 0 \qquad r < 0\,, \tag{2.9}$$

otherwise the instability is already initiated without any coupling and the coupling strength can only enhance this instability.
In the framework of these restrictions we find two different linear instabilities for some particular parameter intervall [4]. We can have a long-scale (type III-) instability due to the Cahn-Hilliard equation as well as a short-scale (type I-) instability resulting from the Swift-Hohenberg equation.
At first we examine the short-scale instability.

Short-scale instability

The onset of a type I-instability occurs at a critical coupling strength $\gamma_{c,s}$, as shown in figure 2.1. Here the subscripts c and s stand for 'critical' and 'short', respectively. Solving the eigenvalue problem (2.7) with eigenvalue $\lambda(k_c) = 0$ and critical wavenumber

[4] Here we only mean codimension-1 instabilities. The occurence of a codimension-2 instability is explained in chapter 2.6

$k_c \neq 0$ yields (from 2nd equation of (2.7))

$$\vec{v} = \left(\frac{r - \left(-\frac{1}{L^2}k_c^2 + 1\right)^2}{\gamma_{c,s}}, 1 \right) . \tag{2.10}$$

Inserting (2.10) into the first equation of (2.7) one obtains for the critical coupling strength:

$$\gamma_{c,s} = \pm \sqrt{\left(\frac{\kappa^2}{L^2}k_c^2 + a\right)\left[\left(1 - \frac{1}{L^2}k_c^2\right)^2 - r\right]} . \tag{2.11}$$

Furthermore, one obtains the critical wavenumber k_c by the condition

$$\partial_k \lambda_1(k)\Big|_{k=k_c} \stackrel{!}{=} 0 , \tag{2.12}$$

or, equivalent, in the second order of the multiscale analysis which will follow below. The conserved character of the Cahn-Hilliard field ϕ always results in a zero growth rate at $k = 0$ with eigenvector

$$\vec{w} = \begin{pmatrix} 1 \\ \frac{\gamma}{r-1} \end{pmatrix} . \tag{2.13}$$

Hence, the solution of (2.7) at the onset of the short-scale instability with $\lambda = 0$ is composed of two parts:

$$\vec{u} = \begin{pmatrix} \phi \\ \psi \end{pmatrix} = c_0 \vec{w} + \vec{v}\left(c_1 e^{ik_c x} + c_1^* e^{-ik_c x}\right) . \tag{2.14}$$

Next, we turn to the long-scale instability.

Long-scale instability

As mentioned above, the system always has a zero growth rate $\lambda_1 = 0$ at $k = 0$. For a long-scale instability, λ_1 must have a minimum at $k = 0$, i.e

$$\partial_{kk} \lambda_1(k)\Big|_{k=0} \stackrel{!}{>} 0 , \tag{2.15}$$

which gives a condition for the coupling strength

$$\gamma^2 > (1 - r)a . \tag{2.16}$$

So the onset of the long-scale instability occurs at a critical value $\gamma_{c,l}$:

$$\gamma_{c,l} = \pm\sqrt{(1 - r)a} . \tag{2.17}$$

Here the subscripts c and l stand for 'critical' and 'long', respectively.
The solution of (2.7) at the onset of the long-scale instability with $\lambda = 0$ is given by

$$\vec{u} = \begin{pmatrix} \phi \\ \psi \end{pmatrix} = c_0 \vec{w} \,. \tag{2.18}$$

In the following, we examine (2.3) in the framework of multiscale analysis in different instability cases and compare steady state solutions of the obtained amplitude equations with results of a fully nonlinear analysis determined by continuation in pde2path.
Thereby, we use periodic boundary conditions.

2.2. Weakly nonlinear analysis – Short-scale instability

2.2.1. Derivation of amplitude equations

We start with the general solution of the linearized problem with zero eigenvalue for $\gamma = \gamma_{c,s}$:

$$\begin{pmatrix} \phi \\ \psi \end{pmatrix} = c_0 \vec{w} + \vec{v} \left(c_1 e^{ik_c x} + c_1^* e^{-ik_c x} \right) . \tag{2.19}$$

The idea of the following multiscale analysis in the weakly nonlinear regime is that the control parameter γ is slightly above the critical coupling strength $\gamma_{c,s}$, i.e $\gamma - \gamma_{c,s} \sim \epsilon^2$ with the smallness parameter $0 < \epsilon \ll 1$. Therefore the critical mode $\vec{v}$ gets linearly unstable, i.e. the constant c_1 has to be replaced by an amplitude $A^0(X,T)$ which will linearly grow proportional to $e^{\lambda(k_c)t}$. By considering the growth rate as a function of the smallness parameter one obtains via a Taylor expansion that $\lambda(k_c) \sim \epsilon^2$. So the mode is linearly unstable, but very weak, precisely, it grows on the slow timescale $T = \epsilon^2 t$. Furthermore, while the eigenvalue at $k = k_c$ crosses zero, further wavenumbers in a small band of width Δk around $k = k_c$ become unstable as well. Instead of introducing all these additional modes with their own amplitudes, one incorporates this effect by a spatial dependence of the amplitude $A^0(X,T)$. Since $\Delta k \ll k_c$ one also seperates these two spatial scales by $X = \epsilon x$. This explicit relation can be obtained by calculating the roots $k_0 \neq 0$ of the eigenvalue λ_1 as functions of ϵ and finally expand the relations about $\epsilon = 0$. To zeroth order one otains $k_0 = k_c$ and the first order term is not zero so to linear order the width of the band of unstable wavenumbers is of order ϵ. This means that the physical field can have a wavenumber q with $q - k_c \sim \epsilon$, i.e. it can vary from the maximally unstable mode on a spatial scale $X = \epsilon x$, because

$$e^{iqx} = e^{ik_c x} \underbrace{e^{i(q-k_c)x}}_{\sim e^{i\epsilon x} = e^{iX}} \tag{2.20}$$

With the introduced time and spatial scales T and X the spatial and temporal derivatives change in the multiscale analysis to

$$\frac{\partial}{\partial x} \to \frac{\partial}{\partial x} + \epsilon \frac{\partial}{\partial X} \qquad \frac{\partial}{\partial t} \to \frac{\partial}{\partial t} + \epsilon^2 \frac{\partial}{\partial T}\,. \tag{2.21}$$

Being close to the onset of instability we get an interaction between linear and nonlinear behavior and can finally obtain an amplitude equation. For that we use the following ansatz:

$$\begin{aligned}
\vec{u} = \begin{pmatrix} \phi_1 \\ \psi_1 \end{pmatrix} =& \epsilon \vec{v} \left(A^0(X,T) e^{ik_c x} + c.c \right) \\
&+ \epsilon^2 \left[\begin{pmatrix} A^1_\phi(X,T) \\ A^1_\psi(X,T) \end{pmatrix} e^{ik_c x} + \begin{pmatrix} C^0_\phi(X,T) \\ C^0_\psi(X,T) \end{pmatrix} e^{2ik_c x} + c.c. \right. \\
&\quad \left. + \begin{pmatrix} B^0_\phi(X,T) \\ B^0_\psi(X,T) \end{pmatrix} \right] \\
&+ \epsilon^3 \left[\begin{pmatrix} A^2_\phi(X,T) \\ A^2_\psi(X,T) \end{pmatrix} e^{ik_c x} + \begin{pmatrix} C^1_\phi(X,T) \\ C^1_\psi(X,T) \end{pmatrix} e^{2ik_c x} + \begin{pmatrix} D^0_\phi(X,T) \\ D^0_\psi(X,T) \end{pmatrix} e^{3ik_c x} + c.c. \right. \\
&\quad \left. + \begin{pmatrix} B^1_\phi(X,T) \\ B^1_\psi(X,T) \end{pmatrix} \right] + O(\epsilon^4)
\end{aligned} \tag{2.22}$$

We see that in this case the bifurcation from the trivial state is pitchfork like, i.e $\left| \begin{pmatrix} \phi_1 \\ \psi_1 \end{pmatrix} \right| \sim \sqrt{\gamma - \gamma_{c,s}} = \epsilon$, so that we can start with the solution at linear order in ϵ. One could wonder why the neutral mode (wavenumber $k = 0$) does not occur to linear order although it is one part of the linear solution with zero eigenvalue. The reason is that due to the conservation behavior of the Cahn-Hilliard equation this eigenvalue does not cross the imaginary axis but always remains on it while the control parameter is varied above the critical value.

To quadratic order new modes and amplitudes occur. The first term also oscillates with the critical wavenumber k_c, but the second one with the first higher harmonic $2k_c$ and the third one is the neutral mode.

Without calculating it explicitly one can already see why and how these terms arise to second order. All three are connected directly with the linearly unstable pattern mode ($k = k_c$) and its amplitude $A^0(X,T)$. The higher harmonic amplitudes $C^0_\phi(X,T)$ and $C^0_\psi(X,T)$ are induced by the quadratic nonlinearity of the linear mode with k_c with the simple reason that $\left(e^{ik_c x}\right)^2 = e^{2ik_c x}$. The same holds for the neutral mode where the linear unstable pattern mode is not multiplied with itself but with its complex conjugated part, i.e. $e^{ik_c x} e^{-ik_c x} = 1$. The new amplitudes of the critical wavenumber which appear to second order are related to the first spatial X-derivative of $A^0(X,T)$ as it is of order ϵ^2 due to $X = \epsilon x$. Analogously one can construct the third order.

By comparing the symmetries of the original equation system (2.3) (translation and re-

flection symmetry) with the choosen ansatz (2.22) we can already see which symmetries all equations which we will obtain through the weakly nonlinear analysis have to fulfill. Ansatz (2.22) is invariant under translation symmetry $x \to x + x_0$ if

$$A \to Ae^{i\varphi} \quad B \to B \quad C \to Ce^{2i\varphi} \quad D \to De^{3i\varphi}\,, \tag{2.23}$$

with

$$\varphi = k_c x_0\,. \tag{2.24}$$

As explicit x-dependencies appear only as spatial derivatives in (2.3) it will be the same for any equation in the following analysis. Due to the invariance of any derivative to translation, i.e

$$\partial_{x+x_0} = \partial_x\,, \tag{2.25}$$

we can conclude that we can always add an arbitrary phase to any solution of the amplitudes according to (2.23).
For reflection symmetry ansatz (2.3) is invariant under

$$x \to -x \quad (A, C, D) \to (A^*, C^*, D^*) \quad B \to B\,. \tag{2.26}$$

This yields further restriction on the amplitude equations. We see that for example odd x-derivatives can not occur in the amplitude equation for B and have to go with a pure complex prefactor for the other amplitude equations we will obtain through the weakly nonlinear analysis.
These symmetry arguments can help to construct amplitude equations qualitativly, but now we want to do it step by step in the framework of the weakly nonlinear analysis. By inserting the ansatz (2.22) into (2.3) as well as replacing the derivatives with (2.21), expanding all polynomials and sorting in orders of ϵ and projecting onto every occuring wavenumber, we get relations between the amplitudes. To derive the amplitude equations we apply the Fredholm alternative, i.e. we need the adjoint eigenvector.
One finds the adjoint eigenvector [5] to be

$$\vec{v}^\dagger = \frac{1}{N}\left(\frac{r - \left(-\frac{1}{L^2}k_c^2 + 1\right)^2}{k_c^2\gamma_{c,s}}, 1\right) \tag{2.28}$$

with

$$N = 1 + \left(\frac{r - \left(-\frac{1}{L^2}k_c^2 + 1\right)^2}{k_c\gamma_{c,s}}\right)^2\,. \tag{2.29}$$

[5] In this case the adjoint Jacobian is

$$\underline{\mathbf{J}}^\dagger = \underline{\mathbf{J}}^\intercal = \begin{pmatrix} -k^2\left(\frac{\kappa^2}{L^2}k^2 + a\right) & -\gamma \\ -\gamma k^2 & r - \left(-\frac{1}{L^2}k^2 + 1\right)^2 \end{pmatrix} \tag{2.27}$$

Now we go successively through the different orders in ϵ.

$$O(\epsilon): \qquad 0 = 0$$

The linear order is automatically fulfilled because we have already incorporated the solution of the linear problem obtained in the previous chapter into our ansatz. Otherwise one would have found the eigenvector $\vec{v}$ and the critical coupling strength $\gamma_{c,s}$ to this order.
In second order we project onto the appearing wavenumbers:

$$\begin{aligned}
O(\epsilon^2): & \\
\sim 1: \qquad & 0 = 0 && (2.30)\\
& B^0_\psi = -\frac{\gamma_{c,s}}{1-r} B^0_\phi + \frac{2\delta}{1-r}|A^0|^2 && (2.31)
\end{aligned}$$

$$\begin{aligned}
\sim e^{ik_c x}: \qquad & -k_c^2\left(\frac{\kappa^2}{L^2}k_c^2 + a\right) A^1_\phi - \gamma_{c,s} k_c^2 A^1_\psi \\
& = \frac{2i}{\gamma_{c,s}}\left(\frac{\kappa}{L}\right)^2 k_c^3 \left[\left(1-\frac{k_c^2}{L^2}\right)^2 - r\right]\partial_X A^0 && (2.32)\\
& -\gamma_{c,s} A^1_\phi + \left[r - \left(1-\frac{k_c^2}{L^2}\right)^2\right] A^1_\psi \\
& = 4i\frac{k_c}{L^2}\left(1-\frac{k_c^2}{L^2}\right)\partial_X A^0 && (2.33)
\end{aligned}$$

$$\begin{aligned}
\sim e^{2ik_c x}: \qquad & C^0_\phi = -\frac{\gamma_{c,s}}{4\frac{\kappa^2}{L^2}k_c^2 + a} C^0_\psi && (2.34)\\
& C^0_\phi = \frac{1}{\gamma_{c,s}} r - \left(1 - 4\frac{k_c^2}{L^2}\right)^2 C^0_\psi + \frac{\delta}{\gamma_{c,s}}\left(A^0\right)^2 && (2.35)
\end{aligned}$$

These six equations and their complex conjugated ones (not shown here) form the algebraic/ode system at order ϵ^2. Each pair of equations shows different behavior, that we want to discuss briefly. First, equations (2.34) and (2.35) determine the amplitudes of the wavenumber $2k_c$ and one sees that $C^0_\phi(X,T) \sim C^0_\psi(X,T) \sim \left(A^0(X,T)\right)^2$.
Whereas the C^0's are completely determined by these two equations, this is not the case for the neutral modes $B^0_\phi(X,T)$ and $B^0_\psi(X,T)$ as only one relation between them can be reveived from (2.30) and (2.31). The reason is again the conserved dynamics of the Cahn-Hilliard equation which leads to the double x derivative in front of the whole term. For the projection onto wavenumber zero there is no small/original space scale present and this double spatial derivative always leads to an ϵ^2 so that there are not any amplitudes or combinations of them which contribute in the Cahn-Hilliard part (2.30) on order ϵ^2.

Equations (2.32) and (2.33) can be written as inhomogeneous linear equations for $\left(A^1_\phi(X,T), A^1_\psi(X,T)\right)$:

$$\underline{\mathbf{J}}\Big|_{k=k_c} \begin{pmatrix} A^1_\phi \\ A^1_\psi \end{pmatrix} = \begin{pmatrix} \frac{\kappa^2 k_c^2}{\gamma_{c,s}} \left[\left(1-\frac{k_c^2}{L^2}\right)^2 - r\right] \\ 2\left(1-\frac{k_c^2}{L^2}\right) \end{pmatrix} 2i\frac{k_c}{L^2}\partial_X A^0 \tag{2.36}$$

As explained in chapter 1.1.1 one can apply the Fredholm alternative, i.e.

$$\vec{v}^\dagger \cdot \begin{pmatrix} \frac{\kappa^2 k_c^2}{\gamma_{c,s}} \left[\left(1-\frac{k_c^2}{L^2}\right)^2 - r\right] \\ 2\left(1-\frac{k_c^2}{L^2}\right) \end{pmatrix} 2i\frac{k_c}{L^2}\partial_X A^0 \stackrel{!}{=} 0 \tag{2.37}$$

$$\Leftrightarrow \left[L^4(2a+(-1+r)\kappa^2) - 2L^2(a-2\kappa^2)k_c^2 - 3\kappa^2 k_c^4\right]\partial_X A^0 = 0 \tag{2.38}$$

As explained above, the amplitude $A^0(X,T)$ should be a function of X, so the bracket in (2.38) should be zero. This recovers condition (2.12), i.e. the expression for the critical wavenumber k_c at onset:

$$k_c^2 = \frac{L^2}{3}\left[2 - \frac{a}{\kappa^2} + \frac{\sqrt{(a+\kappa^2)^2 + 3r\kappa^4}}{\kappa^2}\right]. \tag{2.39}$$

Second, (2.36) provides

$$A^1_\phi = \frac{1}{\gamma_{c,s}}\left[r - \left(1-\frac{k_c^2}{L^2}\right)^2\right] A^1_\psi - \frac{4}{\gamma_{c,s}} i\frac{k_c}{L^2}\left(1-\frac{k_c^2}{L^2}\right)\partial_X A^0 \tag{2.40}$$

To obtain the amplitude equation the third order in ϵ is required. Projecting onto wavenumber $e^{ik_c x}$ yields

$$\underline{\mathbf{J}}\Big|_{k=k_c} \begin{pmatrix} A^2_\phi \\ A^2_\psi \end{pmatrix} = \vec{b}\,, \tag{2.41}$$

where the inhomogenity $\vec{b}$ contains $\partial_T A^0(X,T)$. Applying the Fredholm alternative leads to the amplitude equation for the pattern mode,

$$\partial_T A^0 = \alpha_1 A^0 + \alpha_2 A^0 B^0_\phi + \alpha_3 |A^0|^2 A^0 + \alpha_4 \partial_{XX} A^0\,, \tag{2.42}$$

where all known relations have already been incorporated and where the α_i with $i = \{1,2,3,4\}$ are parameters which are listed in table B.1. The weak linear instability discussed above arises here in form of the parameter $\alpha_1 \sim (\gamma - \gamma_{c,s})$. If the bifurcation is supercritical then $\alpha_3 < 0$.

To obtain a self-contained system one also needs an amplitude equation for B^0_ϕ because a determination of this neutral mode has not been possible due to equation (2.30), i.e. due to the conservation law.

This second amplitude equation is found to fourth order of ϵ and reads

$$\partial_T B^0_\phi = \partial_{XX}\left[\beta_1 B^0_\phi + \beta_2 |A^0|^2\right]. \tag{2.43}$$

So we have a coupled system of two amplitude equations, which can be written in variational form

$$\partial_T A^0 = -\frac{\delta F}{\delta \left(A^0\right)^*} \tag{2.44}$$

$$\partial_T B^0_\phi = \partial_X \left(M \partial_X \frac{\delta F}{\delta B^0_\phi} \right) \tag{2.45}$$

$$\text{with } F = \int \left[-|A^0|^2 \left(\alpha_1 + \alpha_2 B^0_\phi\right) - \frac{\alpha_3}{2}|A^0|^4 + \alpha_4 |\partial_X A^0|^2 - \frac{\beta_1 \alpha_2}{2\beta_2}\left(B^0_\phi\right)^2 \right] dx \tag{2.46}$$

$$\text{and } M = -\frac{\beta_2}{\alpha_2} \tag{2.47}$$

If we want to include higher order terms in ϵ, especially important if the coefficient $\alpha_3 \approx 0$ in (2.42) we have to derive further amplitude equations which contain more terms that fulfill the symmetry

$$X \to -X \qquad A \to A^* \qquad B \to B\,, \tag{2.48}$$

but one can not solve each order successively. Instead one has to incorporate all amplitude equation into one. We will do this by considering here the next order in our weak nonlinear expansion.
At next order we find [6]:

$$\begin{aligned}\partial_T A^1_\psi =& \alpha_1 A^1_\psi + \alpha_2 \left(A^0 B^1_\phi + A^1_\psi B^0_\phi\right) \\ &+ \alpha_3 \left(2A^1_\psi |A^0|^2 + \left(A^1\right)^*_\psi \left(A^0\right)^2\right) + \alpha_4 \partial_{XX} A^1_\psi \\ &+ i\left[\alpha_5 \partial_{XT} A^0 + \alpha_6 \partial_X A^0 + \alpha_7 \partial_X \left(A^0 B^0_\phi\right) + \alpha_8 \partial_X \left(A^0 |A^0|^2\right) + \alpha_9 \partial_{XXX} A^0\right]\end{aligned} \tag{2.49}$$

$$\partial_T B^1_\phi = \partial_{XX}\left[\beta_1 B^1_\phi + \beta_2 \left(\left(A^1_\psi\right)^* A^0 + \left(A^0\right)^* A^1_\psi \right)\right] \tag{2.50}$$

These two amplitude equations have to be combined with the algebraic equations (2.34), (2.35) and (2.40) in order to have a self-contained system of the physical field with

[6] The occuring prefactors α_i, β_i and γ_i are listed in table B.1

amplitudes up to order ϵ^2:

$$A^1_\phi = v_1 A^1_\psi + i\alpha_{10}\partial_X A^0 \tag{2.51}$$
$$B^0_\psi = \beta_3 B^0_\phi + \beta_4 |A^0|^2 \tag{2.52}$$
$$C^0_\phi = \gamma_1 \left(A^0\right)^2 \tag{2.53}$$
$$C^0_\psi = \gamma_2 \left(A^0\right)^2 \tag{2.54}$$

In (2.51) we have identified the prefactor of A^1_ψ as the first component of the eigenvector $\vec{v}$, named v_1, and have defined the other prefactor as α_{10}. In (2.53) and (2.54) the occuring prefactors are defined as γ_1 and γ_2 and can be calculated easily from (2.34) and (2.35).
Now, to get the amplitude equations in higher order one has to look at the general ansatz (1.9) where we have one amplitude for each mode. The amplitudes itself are expansions of the order parameter ϵ (see (1.10)).
The order of the amplitude equations depends on the truncation we use in these expansions. Therefore we define $\vec{A}(X,T)$, $\vec{B}(X,T)$, $\vec{C}(X,T)$ by

$$\vec{A} \equiv \begin{pmatrix} A_\phi \\ A_\psi \end{pmatrix} \equiv \vec{v}A^0 + \epsilon \begin{pmatrix} A^1_\phi \\ A^1_\psi \end{pmatrix} \tag{2.55}$$
$$\vec{B} \equiv \begin{pmatrix} B_\phi \\ B_\psi \end{pmatrix} \equiv \begin{pmatrix} B^0_\phi \\ B^0_\psi \end{pmatrix} + \epsilon \begin{pmatrix} B^1_\phi \\ B^1_\psi \end{pmatrix} \tag{2.56}$$
$$\vec{C} \equiv \begin{pmatrix} C_\phi \\ C_\psi \end{pmatrix} \equiv \begin{pmatrix} C^0_\phi \\ C^0_\psi \end{pmatrix} \tag{2.57}$$

as the amplitudes in first order.
The corresponding system of algebraic and amplitude equations is given by

$$\begin{aligned}
\partial_T A_\psi =& \partial_T A^0 + \epsilon \partial_T A^1_\psi \\
=& \alpha_1 \left(A^0 + \epsilon A^1_\psi\right) + \alpha_2 \Big(A^0 B^0_\phi + \epsilon \left(A^0 B^1_\phi + A^1_\psi B^0_\phi\right) \Big) \\
&+ \alpha_3 \Big(|A^0|^2 A^0 + \epsilon \left(2A^1_\psi |A^0|^2 + \left(A^1\right)^*_\psi \left(A^0\right)^2 \right) \Big) + \alpha_4 \partial_{XX} \left(A^0 + \epsilon A^1_\psi\right) \\
&+ i\epsilon \Big[\alpha_5 \left(\alpha_1 \partial_X A^0 + \alpha_2 \partial_X \left(A^0 B^0_\phi\right) + \alpha_3 \partial_X \left(|A^0|^2 A^0\right) + \alpha_4 \partial_{XXX} A^0 \right) \\
&+ \alpha_6 \partial_X A^0 + \alpha_7 \partial_X \left(A^0 B^0_\phi\right) + \alpha_8 \partial_X \left(A^0 |A^0|^2\right) + \alpha_9 \partial_{XXX} A^0 \Big]
\end{aligned} \tag{2.58}$$
$$A_\phi = v_1 \left(A^0 + \epsilon A^1_\psi\right) + i\epsilon\alpha_{10}\partial_X A^0 \tag{2.59}$$
$$\begin{aligned}
\partial_T B_\phi =& \partial_T B^0_\phi + \epsilon \partial_T B^1_\psi \\
=& \partial_{XX} \Big[\beta_1 \left(B^0_\phi + \epsilon B^1_\phi\right) + \beta_2 \Big(|A^0|^2 + \epsilon \left(\left(A^1_\psi\right)^* A^0 + \left(A^0\right)^* A^1_\psi \right) \Big) \Big]
\end{aligned} \tag{2.60}$$

The last step is to replace all occuring terms by the new amplitudes. In doing so we make mistakes, but they are all at order ϵ^2 and can be neglected as we have expanded the new amplitudes up to ϵ. So for example we rewrite the cubic term in (2.58) into

$$|A^0|^2A^0 + \epsilon\left(2A^1_\psi|A^0|^2 + \left(A^1_\psi\right)^*\left(A^0\right)^2\right) \tag{2.61}$$

$$=|A_\psi|^2A_\psi - \epsilon^2\left(2A^0|A^1_\psi|^2 + \left(A^0\right)^*\left(A^1_\psi\right)^2\right) - \epsilon^3A^1_\psi|A^1_\psi|^2 \tag{2.62}$$

$$=|A_\psi|^2A_\psi + O(\epsilon^2)\,. \tag{2.63}$$

All in all this leads to

$$\begin{aligned}\partial_T A_\psi \;=&\alpha_1 A_\psi + \alpha_2 A_\psi B_\phi + \alpha_3|A_\psi|^2A_\psi + \alpha_4\partial_{XX}A_\psi\\ &+ i\epsilon\left[\tilde\alpha_1\partial_X A_\psi + \tilde\alpha_2\partial_X\left(A_\psi B_\phi\right) + \tilde\alpha_3\partial_X\left(|A_\psi|^2A_\psi\right) + \tilde\alpha_4\partial_{XXX}A_\psi\right]\\ &+ O(\epsilon^2)^7 \end{aligned}\tag{2.64}$$

$$\partial_T B_\phi = \partial_{XX}\left[\beta_1 B_\phi + \beta_2|A_\psi|^2\right] + O(\epsilon^2) \tag{2.65}$$

$$A_\phi = v_1 A_\psi + i\epsilon\alpha_{10}\partial_X A_\psi + O(\epsilon^2) \tag{2.66}$$

$$B_\psi = \beta_3 B_\phi + \beta_4|A_\psi|^2 + O(\epsilon^2) \tag{2.67}$$

$$C_\phi = \gamma_1\left(A_\psi\right)^2 + O(\epsilon) \tag{2.68}$$

$$C_\psi = \gamma_2\left(A_\psi\right)^2 + O(\epsilon) \tag{2.69}$$

We can check if system (2.64) - (2.69) still fulfills the required symmetries. Translation symmetry is obviously fulfilled. For reflection symmetry these equations have to fulfill symmetry (2.26). To check this invariance we take the complex conjugate of system (2.64) - (2.69). Then (2.64) and (2.66) become (here with truncation of terms in $O(\epsilon^2)$)

$$\begin{aligned}\partial_T A^*_\psi \;=&\alpha_1 A^*_\psi + \alpha_2 A^*_\psi B_\phi + \alpha_3|A_\psi|^2A^*_\psi + \alpha_4\partial_{XX}A^*_\psi\\ &- i\epsilon\left[\tilde\alpha_1\partial_X A^*_\psi + \tilde\alpha_2\partial_X\left(A^*_\psi B_\phi\right) + \tilde\alpha_3\partial_X\left(|A_\psi|^2A^*_\psi\right) + \tilde\alpha_4\partial_{XXX}A^*_\psi\right]\end{aligned}\tag{2.70}$$

$$A^*_\phi = v_1 A^*_\psi + i\epsilon\alpha_{10}\partial_X A^*_\psi\,. \tag{2.71}$$

which are the amplitude equations for the complex conjugates amplitudes A^*_ψ and A^*_ϕ. We see that equations (2.64) and (2.66) are related to equations (2.70) and (2.71) by the symmetry (2.26). As requested, this symmetry is still present in all of the equations (2.64) - (2.69) [8] due to the reflection symmetry of the original system (2.3).
In this representation ϵ indicates as prefactor the additional terms, i.e. the qualitative change in the amplitude equation (2.66) due to the investigation of the next order. In contrast to the amplitude equation in first order we do not find a free energy functional

[7] We have defined $\tilde\alpha_1 \equiv \alpha_5\alpha_1 + \alpha_6$, $\tilde\alpha_2 \equiv \alpha_5\alpha_2 + \alpha_7$, $\tilde\alpha_3 \equiv \alpha_5\alpha_3 + \alpha_8$ and $\tilde\alpha_4 \equiv \alpha_5\alpha_4 + \alpha_9$

[8] This symmetry is trivially fulfilled for the remaining equations (2.65),(2.67),(2.68) and (2.69)

such that we could write the amplitude equations (2.64) and (2.65) as gradient dynamics. The next order terms inhibit this property. Although the full system is always described by gradient dynamics, we do not see this property at this order of approximation anymore. There are two things which could cause that loss. One thing is that there might be higher order terms which do not show up in (2.64) and (2.65) but which have to be incorporated to form gradient dynamics. The other thing might be that the algebraic equations (2.64) - (2.69) also carry information about the system. These equations are solution of completed time evolutions on faster timescales that T_2. Since, we do not consider their time evolution we might loose the obvious gradient dynamics in the amplitude equations. A task of further studies could be to verifiy or refute these assumptions.

Before we go on and solve system (2.58) - (2.69) there are two notes to mention.

First, in (2.68) and in (2.69) terms of order ϵ have been neglected, but this is allowed. The crucial difference between amplitudes of the most critical mode ($\sim k_c x$) and ones of the neutral or higher harmonic mode is the lowest order in which they appear. The first ones come with ϵ and the other ones come with ϵ^2. Constructing the physical field up to order ϵ^2 is equivalent to consider amplitude equation for A at order ϵ and solve the equations for B and C to zeroth order. Though (2.65) has also to be at order ϵ, due to the coupling between the amplitude equations (2.64) and (2.65). Only by considering both coupled equations at the same order we can say that we solve the system for amplitude A at this order. Therefore we have to request Equation (2.65) in order ϵ. In contrast, the first order is not required in the algebraic equation (2.67), however automatically fulfilled in this case.

Second, we have to discuss how to deal with the smallness parameter ϵ appearing both in the ansatz (2.22) and in the amplitude equation system (see (2.64) and (2.66)). In the beginning of the analysis we have set

$$\epsilon^2 = \gamma - \gamma_{c,s} \tag{2.72}$$

and one could conceive of resubstituting (2.72) into amplitude equations and into the ansatz, but that would be wrong.

The crucial difference between the term $\gamma - \gamma_{c,s}$ which can be found in some parameters of system (2.64) - (2.69) and ϵ is that this term stand for the real (experimental) difference between actual and critical coupling strength whereas ϵ just indicates as prefactor the size scale of the associated term.

For the same reason the ansatz (2.22) must not be seen as a taylor expansion in $\gamma - \gamma_{c,s}$ (if so then the amplitudes should be independent of this term) but as an expansion in size scale, i.e. an expansion in relevance if ϵ is small enough.

As the name implies the smallness parameter ϵ just helps to order the different contribution to the physical field, but have no further physical meaning. Therefore we have to drop ϵ from now on or in other words we give the associated terms their size scale back

by reincorporating ϵ into them. This is done for the amplitude terms as well as for the derivatives with respect to T or X.
With that discussion we know how to deal with the system (2.64) - (2.69) and how to construct the physical solution.

2.2.2. Solutions of the amplitude equations

Steady state solutions are presented here for the amplitude equations in first and second order. Furthermore, we distinguish two different cases in δ, the coefficient of the quadratic nonlinearity. This prefactor plays an essential role as it enables the pattern mode A to couple with the neutral mode B. We start with the general case.

General Case: $\delta \neq 0$

To solve system (2.64) - (2.69) for steady states we make the ansatz [9]

$$A_\psi(x) = a_\psi e^{iQx}\,, \quad A_\phi(x) = a_\phi e^{iQx}\,, \tag{2.73}$$

$$B_\psi(x) = b_\psi\,, \qquad B_\phi(x) = 0\,, \tag{2.74}$$

$$C_\psi(x) = c_\psi e^{2iQx}\,, \quad C_\phi(x) = c_\phi e^{2iQx}\,, \tag{2.75}$$

and insert it into (2.64) - (2.69):

$$(2.64) \Rightarrow \quad a_\psi = \sqrt{\frac{\alpha_1 - \alpha_4 Q^2 - Q\left(\tilde{\alpha}_1 - \tilde{\alpha}_4 Q^2\right)}{-\alpha_3 + \tilde{\alpha}_3 Q}} \tag{2.76}$$

$$(2.65) \Rightarrow \quad 0 = 0 \tag{2.77}$$

$$(2.66) \Rightarrow \quad a_\phi = \left(v_1 - \alpha_{10} Q\right) a_\psi \tag{2.78}$$

$$(2.67) \Rightarrow \quad b_\psi = \beta_4 a_\psi^2 \tag{2.79}$$

$$(2.68) \Rightarrow \quad c_\phi = \gamma_1 a_\psi^2 \tag{2.80}$$

$$(2.69) \Rightarrow \quad c_\psi = \gamma_2 a_\psi^2 \tag{2.81}$$

Finally we insert (2.76) - (2.81) into the physical field ansatz (2.22) and obtain

$$\vec{u} = \begin{pmatrix} \phi_1 \\ \psi_1 \end{pmatrix} = 2 \begin{pmatrix} a_\phi \\ a_\psi \end{pmatrix} \cos((Q+k_c)x) + \begin{pmatrix} 0 \\ b_\psi \end{pmatrix} + 2 \begin{pmatrix} c_\phi \\ c_\psi \end{pmatrix} \cos\left(2(Q+k_c)x\right)\,. \tag{2.82}$$

This is the steady state solution of the physical field up to order ϵ^2 in the framework of the weakly nonlinear analysis.
In the simpler case of solving system (2.64) - (2.69) in first order, we can drop equations

[9] We could add an additional phase φ in the exponential terms of (2.73) - (2.75), but here we consider periodic boundary conditions. Therefore we have translational symmetry of all solutions, i.e. the free choice of the phase φ. We simply choose $\varphi = 0$.

(2.67) - (2.69) as well as terms in (2.64) and (2.66) which go with ϵ and obtain:

$$\partial_T A_\psi = \alpha_1 A_\psi + \alpha_2 A_\psi B_\phi + \alpha_3 |A_\psi|^2 A_\psi + \alpha_4 \partial_{XX} A_\psi \tag{2.83}$$

$$\partial_T B_\phi = \beta_1 (B_\phi)_{XX} + \beta_2 \left(|A_\psi|^2\right)_{XX} \tag{2.84}$$

$$A_\phi = v_1 A_\psi \tag{2.85}$$

With the same ansatz for A_ψ, A_ϕ and B_ϕ as above (Equations (2.73) - (2.75)) we obtain by inserting in system (2.83) - (2.85):

$$(2.83) \Rightarrow \quad a_\psi = \sqrt{\frac{\alpha_1 - \alpha_4 Q^2}{-\alpha_3}} \tag{2.86}$$

$$(2.84) \Rightarrow \quad 0 = 0 \tag{2.87}$$

$$(2.85) \Rightarrow \quad a_\phi = v_1 a_\psi \tag{2.88}$$

Then the physical field solution in first order is

$$\vec{u} = \begin{pmatrix} \phi_1 \\ \psi_1 \end{pmatrix} = 2 \begin{pmatrix} a_\phi \\ a_\psi \end{pmatrix} \cos((Q + k_c)x) \,. \tag{2.89}$$

Note, that the amplitudes a_ϕ and a_ψ in equations (2.82) and (2.89) are different.

Special case: $\delta = 0$

Without quadratic nonlinearity the pattern mode A does not couple with the neutral mode B or the first harmonic mode C. This is reflected in the coefficients of the amplitude equations (2.64) - (2.69) which become zero in this case:

$$\alpha_2 = \tilde{\alpha}_2 = \beta_2 = \beta_4 = \gamma_1 = \gamma_2 = 0 \tag{2.90}$$

We also notice that other parameters (such as α_3) also depend on δ (for α_3 it is the recoupling between A and C which has a contribution of $|A|^2 A$ in (2.64)), but they do not vanish for $\delta = 0$.

Due to the absence of coupling of neutral as well as first harmonic mode with the pattern mode, we just have to consider (2.64) and (2.66) to construct the weakly nonlinear solution (2.22) to first and second order in ϵ. The amplitudes are

$$\vec{A} = \begin{pmatrix} a_\phi \\ a_\psi \end{pmatrix} = \begin{pmatrix} v_1 \\ 1 \end{pmatrix} \sqrt{\frac{\alpha_1 - \alpha_4 Q^2}{-\alpha_3}} e^{iQx} \tag{2.91}$$

to $O(\epsilon)$ and

$$\vec{A} = \begin{pmatrix} a_\phi \\ a_\psi \end{pmatrix} = \begin{pmatrix} v_1 - \alpha_{10} Q \\ 1 \end{pmatrix} \sqrt{\frac{\alpha_1 - \alpha_4 Q^2 - Q\left(\tilde{\alpha}_1 - \tilde{\alpha}_4 Q^2\right)}{-\alpha_3 + \tilde{\alpha}_3 Q}} e^{iQx} \tag{2.92}$$

to $O(\epsilon^2)$. Then the physical field $\vec{u}$ becomes

$$\vec{u} = 2 \begin{pmatrix} v_1 \\ 1 \end{pmatrix} \sqrt{\frac{\alpha_1 - \alpha_4 Q^2}{-\alpha_3}} \cos((Q + k_c)x) \tag{2.93}$$

to $O(\epsilon)$ and

$$\vec{u} = 2 \begin{pmatrix} v_1 - \alpha_{10} Q \\ 1 \end{pmatrix} \sqrt{\frac{\alpha_1 - \alpha_4 Q^2 - Q\left(\tilde{\alpha}_1 - \tilde{\alpha}_4 Q^2\right)}{-\alpha_3 + \tilde{\alpha}_3 Q}} \cos((Q + k_c)x) \tag{2.94}$$

to $O(\epsilon^2)$, respectively.

Finally, we have to include the boundary condition which constrains the possible wavenumbers. In our case we use periodic boundary conditions with domain size l_x, i.e. the suitable wavenumbers are

$$k_n = \frac{2n\pi}{l_x} \quad n \in N\,. \tag{2.95}$$

Inserting the amplitudes of (2.73) - (2.75) into the ansatz (2.22) for the physical field yields terms proportional to

$$e^{\pm im(k_c+Q)x} \quad \text{with } m \in [0, 1, 2]\,, \tag{2.96}$$

i.e. wavenumber Q has to fulfill

$$Q = \frac{2n\pi}{l_x} - k_c \quad n \in \mathbb{N}\,. \tag{2.97}$$

In the following we will examine different solution behaviors with or without the quadratic nonlinearity ($\delta \neq 0$ or $\delta = 0$) and compare the results with results obtained by numerical continuation of solutions of the fully nonlinear problem.

2.3. Fully nonlinear analysis of steady states

Some general remarks regarding boundary conditions:

In general, every solution $\vec{u}(x,t)$ can be expanded in a fourier basis

$$\vec{u}(x) = \int_{-\infty}^{\infty} \vec{u}_k(t) e^{ikx} dk\,. \tag{2.98}$$

For a solution in a finite domain of size l_x the integral reduces to a sum, whereby possible wavenumbers are $k_n = \frac{2n\pi}{l_x}$ for periodic boundary conditions or $k_n = \frac{n\pi}{l_x}$ for Neumann boundary conditions, respectively, with $n \in \mathbb{Z}$. Note that a domain with Neumann boundary conditions can always be embedded into a periodic domain by reflecting the solution profiles about one boundary and taking the resulting doubled domain as a

single period So the different boundary conditions may be comparable but they are not equivalent. This can easily be seen by rewriting the fourier expansion (2.98) into

$$\vec{u}(x) = \sum_{n\in\mathbb{N}} \vec{A}_n(t)\cos k_n x + \vec{B}_n(t)\sin k_n x = \sum_{n\in\mathbb{N}} \vec{C}_n(t)\cos\left(k_n x + \varphi_n\right). \tag{2.99}$$

Neumann boundary conditions, i.e.

$$\partial_x \vec{u}(x = \pm\frac{l_x}{2}) \stackrel{!}{=} 0\,, \tag{2.100}$$

require automatically

$$\vec{B}_n(t) = 0 \;\Leftrightarrow\; \varphi_n = \{0,\pi\}^{10} \quad \forall n\,, \tag{2.101}$$

whereas there is no restriction when periodic boundary conditions are used.
Therefore one can find all solutions that occur for Neumann boundary conditions in a setup with periodic boundary conditions (with double sozed domain) but not vice versa. As mentioned above, we use periodic boundary condition on a finite domain with length $l_x = 2$ from $x = -1$ to $x = +1$, so that the fitting wavenumbers are

$$k_n = \frac{2n\pi}{l_x} = n\pi\,. \tag{2.102}$$

For steady states ($\partial_t\phi = 0$) we can rewrite the Cahn-Hilliard part of (2.3):

$$\frac{d\mathcal{F}}{dt} = \int dx \frac{\delta\mathcal{F}}{\delta\phi}\partial_t\phi = \int dx \frac{\delta\mathcal{F}}{\delta\phi}\partial_{xx}\frac{\delta\mathcal{F}}{\delta\phi} = \frac{\delta\mathcal{F}}{\delta\phi}\partial_x\frac{\delta\mathcal{F}}{\delta\phi}\Big|_{-1}^{1} - \int dx \left(\partial_x\frac{\delta\mathcal{F}}{\delta\phi}\right)^2 \stackrel{!}{=} 0 \tag{2.103}$$

$$\Rightarrow \partial_x\frac{\delta\mathcal{F}}{\delta\phi} = 0 \tag{2.104}$$

$$\Rightarrow \frac{\delta\mathcal{F}}{\delta\phi} = \mu = const \tag{2.105}$$

In the first line we have used the Gauss' theorem, whereby the first term is evaluated at the boundaries and vanishes due to the periodic boundary conditions. We have introduced the integration constant μ, which corresponds to a chemical potential, as a third unknown. Therefore we also need a third equation. The third equation is the constraint of mass conservation of the Cahn-Hilliard field, i.e. we keep $\frac{1}{l_x}\int dx\phi = \phi_0$ constant.

[10] $\varphi_n = \pi \quad \forall n$ corresponds to $\vec{u} \to -\vec{u}$ symmetry.

Therefore the two-field system (2.3) for steady states becomes

$$-\frac{\kappa^2}{L^2}\partial_{xx}\phi + a\phi + \phi^3 + \gamma\psi - \mu = 0 \tag{2.106}$$

$$r\psi - (\frac{1}{L^2}\partial_{xx} + 1)^2\psi + \delta\psi^2 - \psi^3 - \gamma\phi = 0 \tag{2.107}$$

$$\phi_0 - \frac{1}{2}\int dx\phi = 0\,. \tag{2.108}$$

System (2.106)-(2.108) fulfills translation ($x \to x + x_0$) and reflection ($x \to -x$) symmetry. If $\mu = 0$ then it also has a $(\gamma, \phi, \psi) \to (-\gamma, -\phi, \psi)$ symmetry. If both, $\mu = 0$ and $\delta = 0$ then it is also invariant under inversion ($(x, \phi, \psi) \to (-x, -\phi, -\psi)$).
For this system (2.106) we discuss the bifurcation diagrams, its solutions in the cases of a short-scale instability with or without quadratic nonlinearity. For that matter the coupling strength γ will be our control parameter. The fixed parameters are

$$\kappa = 1,\ a = 1,\ r = -1,\ L = 2\pi,\ \phi_0 = 0\,. \tag{2.109}$$

2.3.1. Bifurcation behavior of the system without quadratic nonlinearity

We start with the case of a type I instability, see the associated dispersion relation in figure 2.1.
Figure 2.2 shows the bifurcation diagram of steady states, where the L^1-Norm of the deviation from the mean values, i.e.

$$||\delta\vec{u}||_{L^1} = \int dx\sqrt{(\phi - \phi_0)^2 + (\psi - \psi_0)^2} \tag{2.110}$$

$$\text{with} \quad \psi_0 = \frac{1}{2}\int dx\psi\,, \tag{2.111}$$

is plotted against the coupling strength γ.
Black solid lines correspond to stable states, other line styles and colors correspond to unstable states with respect to one, two, four or six eigenvalue(s), respectively. The horizontal line is the trivial state $\vec{u} = 0$. Starting from $\gamma = 0$ in positive or negative direction the trivial state looses stability and branches of structured solutions emerge. Every primary bifurcation of the trivial state is invariant under $\gamma \to -\gamma$ by exchanging ϕ to $-\phi$ in the eigenfunction of the critical eigenvalue. Here parameter L is set to 2π, hence the most critical wavenumber is

$$k_c \approx 6.2026 < 2\pi \tag{2.112}$$

according to (2.39). Though as mentioned above the possible wavenumbers due to the restriction of discretization are $k_n = n\pi$, i.e. the most critical and fitting wavenumber is $k_2 = 2\pi$, which gets unstable first. Then for higher values of γ modes of side band wavenumbers get unstable, too. In Figure 2.2 we see three primary bifurcations with

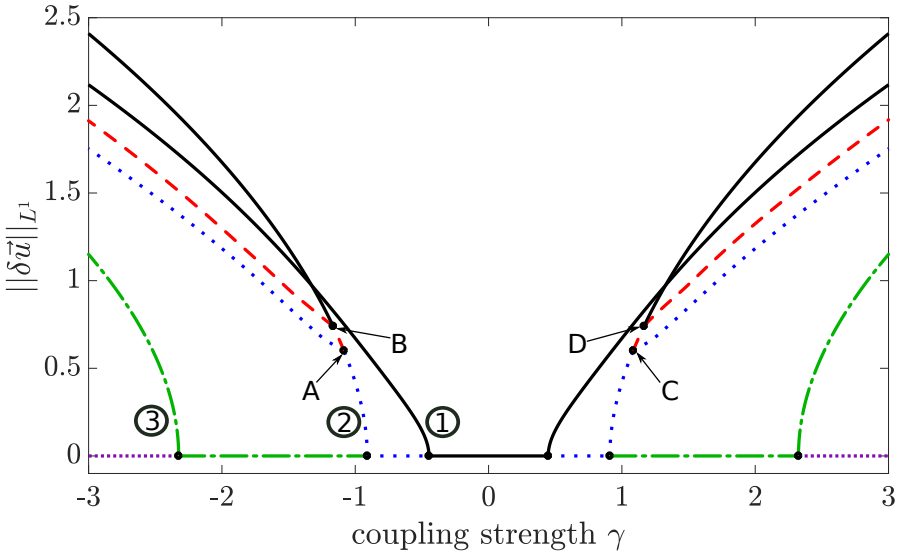

Figure 2.2: L^1-Norm of deviation $\delta\vec{u}$ against coupling strength γ for the occuring steady states of (2.106) with the fixed parameter (2.109). This is the special case without quadratic nonlinearity. Stable states are represented by black solid lines, unstable by red dashed, blue dotted, green dashed-dotted and violett densely dotted lines according to the amount of unstable eigenvalues (one, two, four and six, respectively). Secondary bifurcation points are labelled **A**, **B**, **C** and **D** and three primary bifurcation branches are labelled **1**, **2** and **3**.

$k = k_2, k_1, k_3$ for positive and three for negative coupling strengths, but of course there are further bifurcations for the next wavenumbers, but here we restrict ourselves to the pictured part of the bifurcation diagram to show the qualitative behavior. The associated critical coupling strengths for all primary bifurcations can be obtained in the linear problem as explained in chapter 2.1.

Figure 2.3 shows examples of solutions on the three primary nontrivial branches **1**, **2** and **3** for negative coupling strengths near the bifurcation points. As we have discussed the mode with wavennumber k_2 is the first emerging branch (stable, black solid line), then the sideband bifurcation solutions follow, here with wavenumber $k_1 = \pi$ first (blue dotted line) and then k_3 (green dashed dotted line), but both emerge as unstable solutions.

Due to the reflection symmetry the trivial state always gets unstable with respect to two modes with wavenumbers k and $-k$ simultaneously. Or in other words it looses stability to the cosine as well as to the sine mode with wavenumber k, therefore we find two new unstable eigenvalues [11] for the trivial state at each bifurcation.

All primary bifurcations are supercritical pitchforks of revolution and correspond to the breaking of translation symmetry with respect to the associated wavenumber of the eigenfunction found at the bifurcation point. Due to the periodic boundary conditions solutions with the same wavenumber but different phases are equivalent, which is why

[11] For Neumann boundary conditions we just have one unstable eigenvalue, because the sine mode does not fit to the boundary condition (see explanation at start of chapter 2.3)

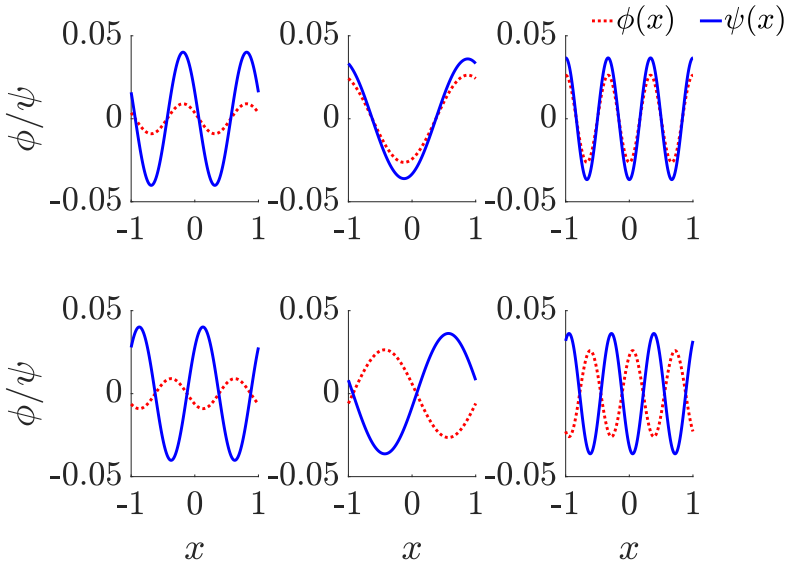

Figure 2.3: Solution profiles of primary nontrivial branches near the bifurcation point from trivial state. Red dotted lines correspond to Cahn-Hilliard field ϕ and solid blue lines to Swift-Hohenberg field ψ. Upper row shows solution profiles of the branches **1**, **2** and **3** from left to right. The lower row shows their counterparts for positive coupling strengths. Two panels of each column are related by $(\gamma, \phi, \psi) \to (-\gamma, -\phi, \psi)$ plus a shift.

this symmetry breaking relates infinite number of solutions continously with their phases. Therefore we have a pitchfork bifurcation of revolution [12]. Of course we can not take all possible phases into account, which would not yield any further information as one arbitrary phase solution. Hence, we project our system onto one phase φ_0 by using a so called phase condition. By this projection only one new branch emerges at each primary bifurcation though the trivial branch looses stability in terms of two eigenvalues (for sine and cosine which are related by a phase shift of $\pi/2$).

After discussing the bifurcation behavior of the trivial state, we turn towards the primary nontrivial branches and their, the secondary, bifurcations. Therefore we consider the symmetries of the solution profiles on these branches, namely reflection $(x, \phi, \psi) \to (-x, \phi, \psi)$, inversion $(x, \phi, \psi) \to (-x, -\phi, -\psi)$ and field inversion $(x, \phi, \psi) \to (x, -\phi, -\psi)$ symmetry (summarized in table 2.1). Note that these two discrete symmetries are the proper one to characterize the secondary bifurcations, because we will observe that these are the ones which are broken at the respective secondary bifurcations.

One observes that the modes with the critical wavenumber k_2 are stable, but all sideband modes emerge unstable. In the pictured part of the bifurcation diagram one sees that the first sideband modes gain stability after two secondary bifurcations, labelled **A** and **B** (for $\gamma > 0$ respectivly **C** and **D**). These are also pitchfork bifurcations but subcritical ones and with a discrete symmetry breaking, so that at each of these four bifurcations

[12] In the case of Neumann boundary conditions we would just have two solutions with phases $\varphi = 0$ or $\varphi = \pi$ (see (2.101)).

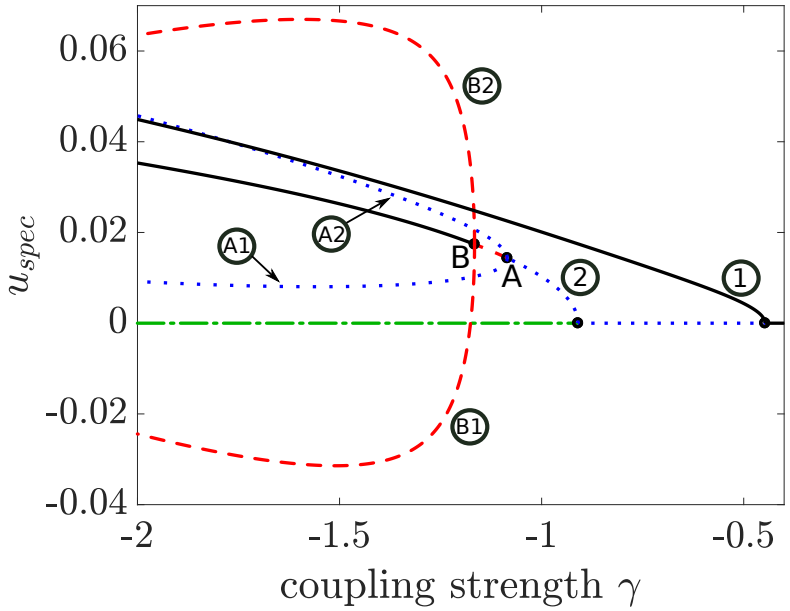

Figure 2.4: Unfolded representation (according to (2.114)) of the left hand side of bifurcation diagram 2.2, where the stability is indicated in the same way. Primary pitchfork bifurcations are not unfolded as this representation is still a projection onto one phase. Branches at secondary pitchfork bifurcations "**A**" and **B** are unfolded.

we find two emerging branches that are related by the respective broken symmetry .
In the chosen norm the two branches of each secondary pitchfork bifurcation lie on top of each other because of the associated symmetry break. Either the reflection or inversion are the transformations by which the different solution branches are related. Obviously the L^1 norm is invariant under these transformations, and so we can not distinguish between these solution profiles in figure 2.2.
But we can make them visible by choosing another representation, that separates them and "unfolds" the diagram.

The interplay of an unfolded bifurcation diagram and the solution profiles which will also be presented enable us to identify the bifurcation types and their associated symmetry breakings. To unfold the bifurcation diagram the solution profiles $\vec{u}(x)$ are integrated over the domain, i.e. from -1 to $+1$ and thereby weighted with the function

$$f(x) = 0.131x + 1.07 \tag{2.113}$$

that breaks the relevant symmetries. This means we calculate

$$u_{spec} = \int_{-1}^{1} \vec{u}(x) \cdot \begin{pmatrix} 1 \\ 1 \end{pmatrix} f(x)dx \tag{2.114}$$

for each profile. The solution of this procedure is not invariant under any relevant symmetry, so that two different branches have to separate. This separation is illustrated

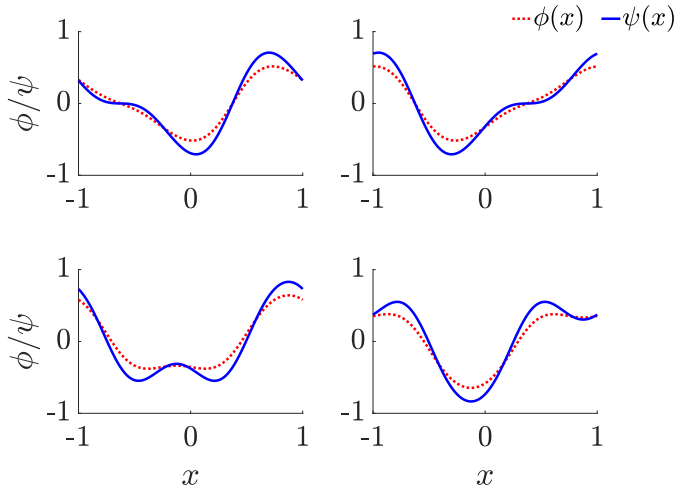

Figure 2.5: Solution profiles of secondary bifurcation branches which emerge from the main branch **2** (see figure 2.4). Upper row shows the two solution profiles of the branches **A1** and **A2**, respectively. In the lower row solution profiles of the branches **B1** and **B2**, emerging at bifurcation point **B** are depicted.

for the left hand side of the bifurcation diagram figure 2.4, i.e. for negative coupling strengths. One can identify the primary as well as the secondary bifurcation branches which are unfolded now, that means the two emerging branches at bifurcation points **A** and **B** do not lie onto each other [13]. Each bifurcation is linked to a broken symmetry, so we have a look at the solution profiles on the branches emerging at the secondary bifurcation points.

First, if we consider the upper row of figure 2.5 which shows the solutions on the blue dotted branches emerging from bifurcation point **A**, we see that the reflection symmetry [14] is broken but the solution profiles keep the inversion symmetry. Therefore the two solution profiles are related by the reflection symmetry. Through this subcritical pitchfork bifurcation the two emerging branches carry two unstable eigenvalues whereby the main branch gains stability by loosing one of the two unstable eigenvalues.
Then the remaining unstable eigenvalue on the main branch (red dashed line) is turned to a stable one in the second subcritical pitchfork bifurcation, labelled **B**, where the new emerging branches (red dashed) are related by the inversion symmetry but fulfill the reflection symmetry themselves (see lower row in figure 2.5). In this case the two emerging branches carry one unstable eigenvalue.
In table 2.1 we can also see that the chemical potential μ is zero for all listed branches except branch **B1**. The value zero of the chemical potential can be directly connected with the symmetries of the solution profiles. For branches **1**, **2**, **3** and **A1** the solution profiles are invariant under inversion which means that they are antisymmetric functions,

[13] At the primary pitchfork bifurcations still only one new branch emerge as we still project the whole pitchfork bifurcation of revolution onto one phase.
[14] In periodic boundary conditions reflection symmetry means that the solution is invariant under $x - x_0 \to -x - x_0$ for any arbitrary space point x_0 inside the domain.

Table 2.1: Symmetries and chemical potential of nontrivial branches for $\gamma < 0$. Branches are labelled in figure 2.2. Branches for positive coupling strengths are not listed. Their primary and secondary branches show the same symmetry breaking as the corresponding branches for negative coupling strengths.

Branch: / Symmetry:	**1**	**2**	**3**	**A1**	**B1**
Reflection	+	+	+	-	+
Inversion	+	+	+	+	-
chemical potential μ	0	0	0	0	$\neq 0$

i.e.

$$\vec{u}(x - x_0) = -\vec{u}(-x - x_0) \tag{2.115}$$

with respect to an axis going through space point x_0. If we evaluate any integral over the domain we are allowed to shift the solution by the value of x_0, because of the periodicity of the solution due to the periodic boundary conditions. After this shift the antisymmetry yields

$$\vec{u}(x) = -\vec{u}(-x)\,. \tag{2.116}$$

This property can be used to evaluate the mean values of the terms arising in the first component of the coupled system, see (2.106):

$$\psi_0 = \int_{-1}^{1} \psi(x)dx = \int_{-1}^{1} \psi(x)dx \Rightarrow \psi_0 = 0 \tag{2.117}$$

$$\int_{-1}^{1} \partial_{xx}\phi(x)dx = -\int_{-1}^{1} \partial_{xx}\phi(x)dx \Rightarrow \int_{-1}^{1} \partial_{xx}\phi(x)dx = 0 \tag{2.118}$$

$$\int_{-1}^{1} \phi^3(x)dx = -\int_{-1}^{1} \phi^3(x)dx \Rightarrow \int_{-1}^{1} \phi^3(x)dx = 0\,. \tag{2.119}$$

So by integrating (2.106) over the domain every of these three terms vanishes and therefore

$$\int_{-1}^{1} \mu dx = 2\mu \stackrel{!}{=} 0 \Rightarrow \mu = 0\,. \tag{2.120}$$

The secondary bifurcation behavior can be identified as an Eckhaus instability, because the sideband branch **2** is unstable with respect to the eigenfunctions plotted in figure 2.6. These eigenfunctions are simply the cosine respective the sine with the critical wavenumber $k_2 = 2\pi$ [15]. So before the sideband mode gains stability through the two secondary bifurcations, i.e. for smaller absolute value of γ, it lies into the unstable Eckhaus band. By increasing the absolute value of γ the stable band is broadened, so the first sideband mode leaves the unstable Eckhaus band, which corresponds to the bifurcation point **B** (or **D** for positive coupling strength). For further explanations and calculation of the Eckhaus instability see [14].

[15] In Neumann boundary conditions one just finds one unstable eigenfunction. The reason is similar to the explanation above, namely that only the cosine is compatible to the boundary conditions.

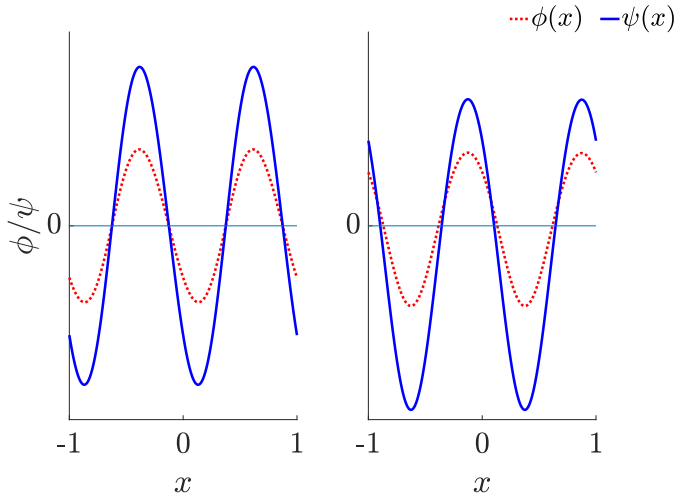

Figure 2.6: Critical eigenfunctions of linear stability consideration around the solutions of main branch **2**. Both eigenfunctions correspond to the most critical wavenumber. The eigenvalue of the left eigenfunction is positive until the bifurcation point **A** and the eigenvalue of the right one is stabilized in the pitchfork bifurcation **B**. Both bifurcations correspond to the Eckhaus instability.

In comparison with the solution profiles of branch **1** (see upper left panel in figure 2.3) we see that the eigenfunction in the right panel has the same phase and therefore the eigenfunction in the left panel is shifted by $\pi/2$. We observe that the sideband branch **2** gains stability in the pitchfork bifurcation point **A** related to the eigenfunction with shifted phase first and after that it gets totally stable through the pitchfork bifurcation **B** related to the eigenfunction with the same phase. So one can say that the eigenfunction with the same phase is the more critical or unstable one for the sideband mode.

We can already note that the bifurcation diagram 2.2 changes qualitatively if the quadratic nonlinearity is turned on as it breaks the inversion symmetry of the system and therefore no solution branches with inversion symmetry can occur. Especially the solutions of the primary branches fulfill inversion symmetry (see figure 2.3), which will not be the case for $\delta \neq 0$.
So far we have mainly considered the left hand side of the bifurcation diagram. On the first look it seems that the diagram is absolutly symmetric between left and right hand side by exchanging $\gamma \to -\gamma$ and $\phi \to -\phi$ in the corresponding solution profiles. But on a closer inspection, this symmetry is broken for the branches emerging at bifurcation points **B** and **D**, which is clear as we already mentioned that for these branches $\mu \neq 0$. And system (2.106) is only invariant under the symmetry $(\phi, \gamma) \to (-\phi, -\gamma)$ if $\mu = 0$.

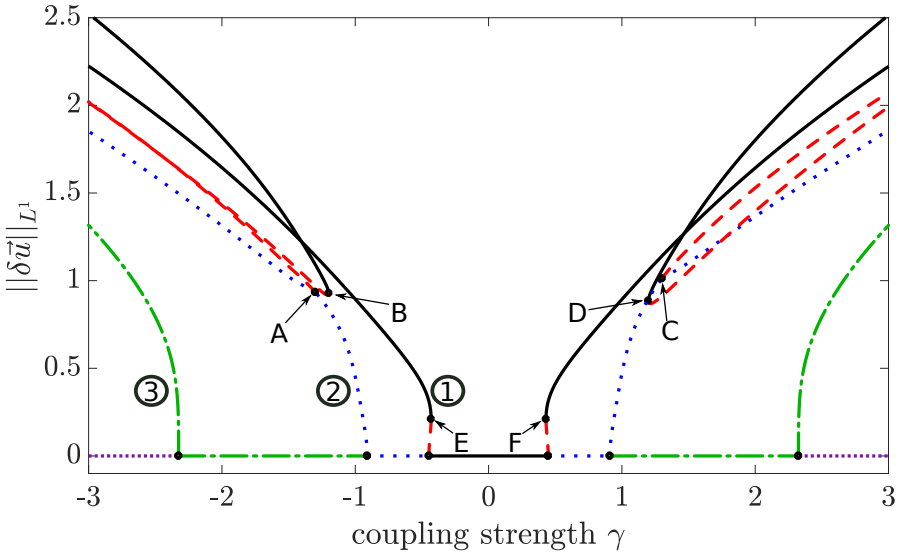

Figure 2.7: L^1-Norm of deviation $\delta\vec{u}$ against coupling strength γ for the occuring steady states of (2.106) with the fixed parameters of (2.109). The prefactor of the quadratic nonlinearity is adjusted to $\delta = 1$. Stable states are represented by black solid lines, unstable by red dashed, blue dotted, green dashed-dotted and violett densely dotted lines according to the amount of unstable eigenvalues (one, two, four and six, respectively). Secondary bifurcation points are labelled **A** and **C**. Folds (i.e. saddle-node bifurcations) are labelled **B**, **D**, **E** and **F**. Three of the main branches are labelled **1**, **2** and **3**.

2.3.2. Bifurcation behavior of the system with quadratic nonlinearity

Case 1: $\delta = 1$

Next we turn on the quadratic nonlinearity with $\delta = 1$ and obtain the bifurcation diagram shown in figure 2.7. As expected we can see qualitative changes. Of course, the positions of the primary bifurcation points do not change as they are determined by the linear problem. However, there is a change in the secondary bifurcations. Moreover, new saddle-node bifurcations **E** and **F** occur on the first primary branches. As the bifurcation branches have changed qualitatively, the corresponding solution profiles show also different behavior. We start the discussion of the qualitative changes with the solution profiles of the primary branches **1**, **2** and **3** and connect this to the modified secondary bifurcation behavior on branch **2**. Afterwards we briefly discuss the occuring saddle-nodes **E** and **F**.

The solution profiles near the primary bifurcations corresponding to branches **1**, **2** and **3** are illustrated in figure 2.8. In contrast to the solution profiles of these bifurcations in the case of $\delta = 0$ (see figure 2.3) here, the profiles do not fulfill inversion symmetry, because the quadratic nonlinearity breaks this symmetry. So they only have the remaining reflection symmetry, which can be broken in a secondary bifurcation which yields possible changes for the bifurcation points **A** and **B**.

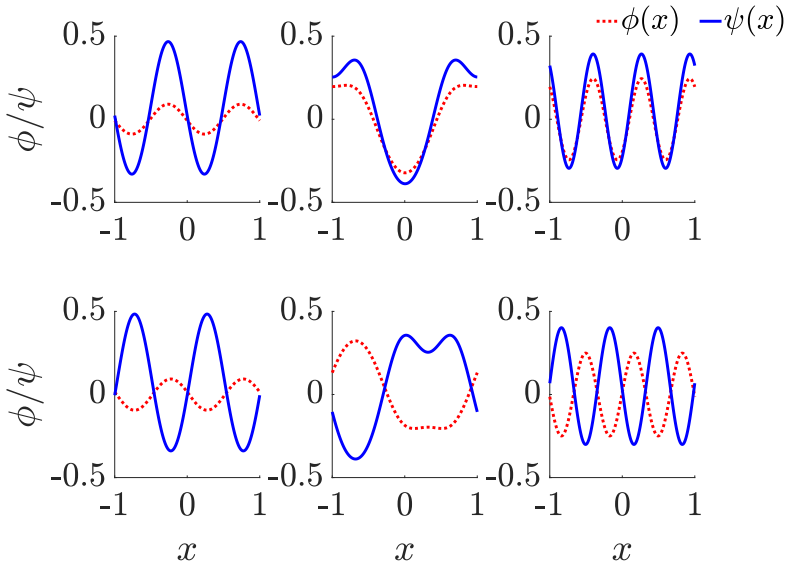

Figure 2.8: Solution profiles of primary nontrivial branches near their bifurcation points in the case $\delta = 1$. Red dotted lines correspond to Cahn-Hilliard field ϕ and solid blue lines to Swift-Hohenberg field ψ. Solution profiles in the upper row corrsponds to the branches **1**, **2** and **3** in figure 2.7 from left to right. The lower row shows their counterparts for positive coupling strengths. The two panels of each column are related by $(\gamma, \phi, \psi) \to (-\gamma, -\phi, \psi)$ plus a shift.

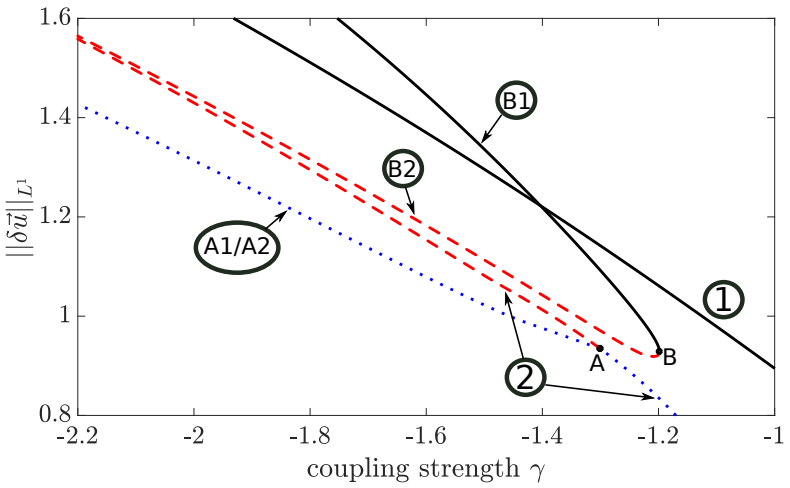

Figure 2.9: A detail view of the part of the bifurcation diagram 2.7 where the bifurcation point **A** and **B** are found. There we can examine the bifurcation behavior of branch **2**. Same labels and stability indicators as in figure 2.7 are used.

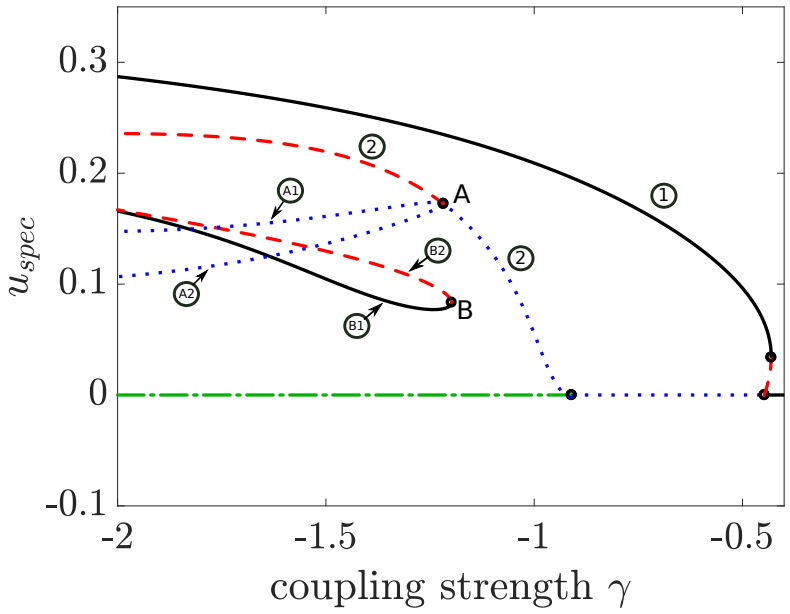

Figure 2.10: Unfolded representation (according to (2.114)) of the left hand side of bifurcation diagram 2.7, where the stability is indicated in the same way. Primary pitchfork bifurcation are not unfolded as it is still a projection onto one phase. Branches **A1** and **A2** emerging from the secondary pitchfork bifurcation **A** are unfolded.

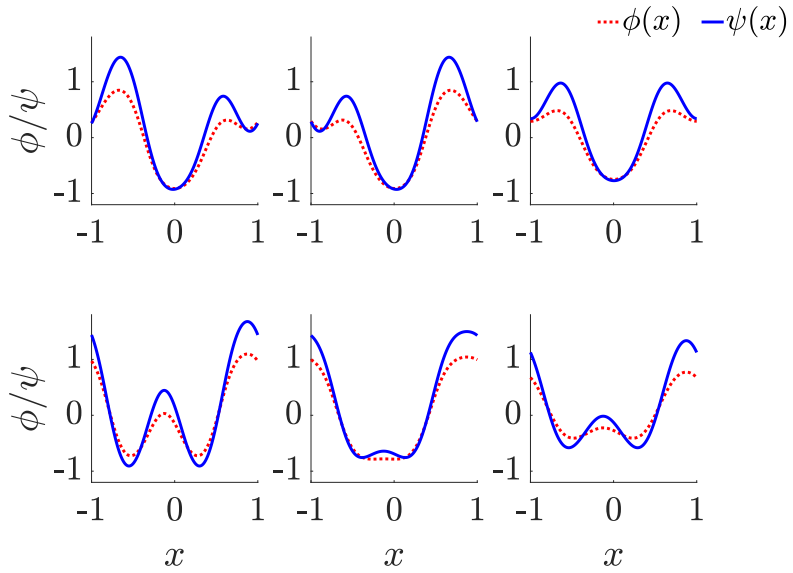

Figure 2.11: Lower row shows solutions of the saddle-node branches **B1** and **B2** in figure 2.9, whereby the node is on the left, the saddle in the middle and the solution at the saddle-node bifurcation **B** on the right. Analogous one can see the solutions of the emerging branches at the pitchfork bifurcation "**A**" in figure 2.9 in the upper row. The solution on the right is the one at the pitchfork bifurcation point **A** and the profiles in the left and in the middle panel correspond to branches **A1** and **A2**.

To study this in the framework of symmetry arguments we have to take a closer look at the relevant part in the bifurcation diagram as well as the solution profiles on each branch and at the bifurcation points. Again we consider negative coupling strength as we can observe the same qualitative bifurcation behavior for positive coupling strengths. A detail view of the interesting part of the secondary bifurcations on the left hand side of the bifurcation diagram is shown in figure 2.9 and the corresponding solution profiles are given in figure 2.11. A closer inspection of figure 2.9 reveals that there is only one secondary bifurcation left for the main branch **2**, where it gains stability with respect to one eigenvalue but then remains unstable with respect to another eigenvalue. This bifurcation point **A** is again a pitchfork bifurcation at which the emerging branches break reflection symmetry. Therefore, we use the weighted integral (2.114) again, to unfold the bifurcation diagram. Then we obtain figure 2.10 and we find two emerging branches **A1** and **A2** at pitchfork bifurcation **A**. These are unstable with respect to two eigenvalues. Regarding the corresponding solution profiles (upper row of figure 2.11) we see that the solution at the bifurcation point **A** (right panel) has reflection symmetry which is broken for the two solution profiles from branches **A1** and **A2**. Thus, similar to the case $\delta = 0$ the first secondary bifurcation breaks reflection symmetry as this symmetry is not attached to the quadratic nonlinearity.

Opposed to $\delta = 0$ there is no second secondary pitchfork bifurcation, but instead we observe a disconnected saddle-node bifurcation **B**. The reason for this difference is that in the case of $\delta = 0$ the second pitchfork bifurcation (bifurcation point **B** in figure 2.2) breaks inversion symmetry. Here, for $\delta = 1$, this is impossible as main branch **2** does not show the particular symmetry. Consequently, this symmetry can not be broken. In other words, the original pitchfork bifurcation is a non-generic codimension-2 bifurcation, so two parameters (here γ and δ) at specific values need to occur. As the specific value for δ is zero the original pitchfork bifurcation is split into the main branch and a saddle-node bifurcation in the case for $\delta \neq 0$. Thereby, the stable part of the original main branch (black solid line in figure 2.2) becomes the node of the saddle-node branches (B1) and one of the emerging branches in the original pitchfork bifurcations merges together with the unstable part of the main branch. If we consider the solution profiles of branches **B1** and **B2** (see lower row of figure 2.11) we see that they are still invariant under reflection as the quadratic nonlinearity has no effects on this symmetry. Starting from the solution at the saddle-node bifurcation **B** (right panel), the difference between the stable (node) and unstable (saddle) branch is, that the saddle becomes more structured whereas the node becomes less structured. As the node has been the stable part of the main branch **2** in the case of $\delta = 0$ the solution on the node gets closer to the original solution of the main branch.

The last qualitative difference between the cases $\delta = 0$ and $\delta = 1$ is the stability property of the first primary branch **1**. We observe that this branch emerges unstable in a subcritical pitchfork bifurcation and gains stability at the saddle-node bifurcation **E**. To understand this behavior one can consider stability analysis of steady state solutions in

the framework of the obtained amplitude equations (2.42) and (2.43). From the well known stability analysis of a classical real Ginzburg-Landau equation one obtains the Eckhaus instability for all sideband modes which we have briefly discussed for the case $\delta = 0$. In addition to the instability of the sideband modes this analysis shows that the first emerging branch is always stable which is not true for the case $\delta \neq 0$. So this characteristic can not be explained by an Eckhaus instability, but by the so-called Matthew-Cox instability [16]. This instability is quite generic for pattern formations with a conservation law. Here, we do not calculate this instability explicitly, because this has already been done in [18] and [5]. The origin of this instability is the interplay between the conservation law of field ϕ and the coupling between the pattern mode $A(X,T)$ and the neutral mode $B_\phi(X,T)$ through the quadratic nonlinearity. Together, both properties result in the coupled amplitude equation system (2.42) and (2.43). First, without conservation law the neutral mode $B_\phi(X,T)$ would be determined by (2.30), similar to equation (2.31) and no amplitude equation as (2.43) would arise. Then only a Ginzburg-Landau equation for the pattern mode $A(X,T)$ would remain. And second, without quadratic nonlinearity no coupling between neutral and pattern mode is possible as the coefficients α_2 and β_2 in equations (2.42) and (2.43) are proportional to δ.

Case 2: $\delta = 1.8$

Next, we intensify the quadratic nonlinearity by setting $\delta = 1.8$. If we look at the equation system (2.4) there is only a qualitative change between $\delta = 0$ and $\delta \neq 0$. However, we can also observe different bifurcation behavior in figure 2.13 as we increase δ from 1 to 1.8. This bifurcation diagram looks quite complicated, because each of the three main branches **1**, **2** and **3** undergoes different changes which we explain in the following. First, branch **3** and its corresponding branch for positive coupling strength emerge subcritically. Thus, they start unstable with respect to five eigenvalues and gain stability to one of these eigenvalues through the saddle-node bifurcations **M** and **N**, respectively. Surprisingly, branch **2** does not show this subcritical behavior, although it is a sideband mode as well as branch **3**. But instead of becoming subcritical we observe a hysteris bifurcation by the appearance of two new saddle-node bifucations **H** and **G** (as well as **K** and **J** for positive coupling strengths). At a critical value of δ they merge together on branch **2** and drift apart when δ is further increased. Together they form a hysteris bifurcation of branch **2**. So branch **2** still emerges supercritically with two unstable eigenvalues, but looses stability to a third one at **H** and regains this stability at **G**. Afterwards it undergoes the pitchfork bifurcation **A** in the qualitative same manner as before. Of course it is still disconnected from the saddle-node bifurcation **B** because of the broken inversion symmetry.

The third different bifurcation behavior is found for the first main branch **1** which is split into two parts, **1** and **1'**. Thereby, the saddle-nodes **E** and **F** found in bifurcation diagram 2.7 vanish. In comparison to the bifurcation behavior for $\delta = 1$ (see figure 2.7)

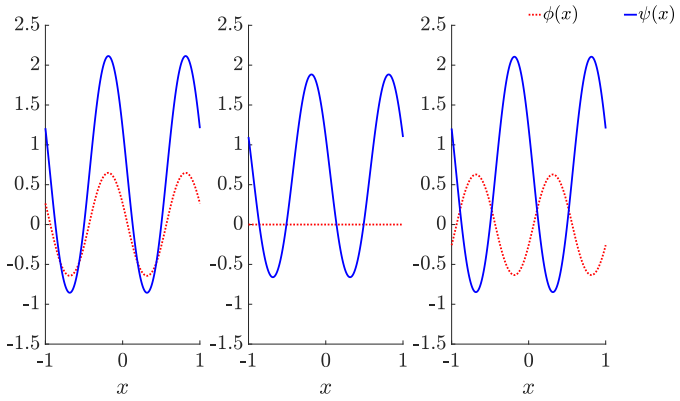

Figure 2.12: Three solution profiles of branch **1'** for $\delta = 2$. The left panel shows the solution profile at $\gamma \approx -1$. In the middle the solution profile at $\gamma = 0$ is depicted and in the right panel the solution profiles corresponds to $\gamma \approx 1$. This illustrates the transition from $\phi(x)$ to $-\phi(x)$ while γ changes its sign.

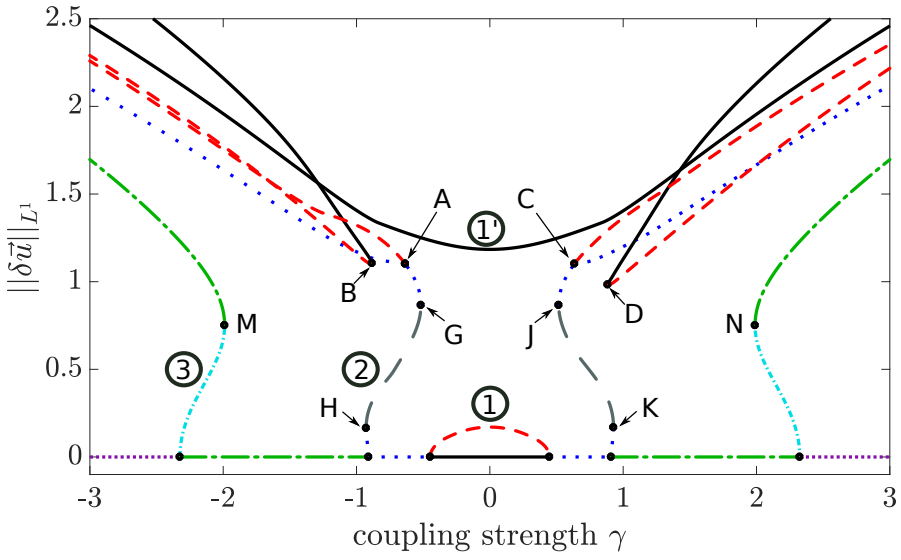

Figure 2.13: L^1-Norm of deviation $\delta\vec{u}$ against coupling strength γ for the occuring steady states of (2.106) with the fixed parameters of (2.109). The prefactor of the quadratic nonlinearity is adjusted to $\delta = 1.8$. Stable states are represented by black solid lines, unstable by red densely dashed, blue dotted, grey dashed, green dashed-dotted, turquoise densely dashed-dotted and violett densely dotted lines according to the amount of unstable eigenvalues (one, two, three, four, five and six, respectively). Secondary bifurcation points are labelled **A** and **C**. Folds (i.e. saddle-node bifurcations) are labelled **B**, **D**, **G**, **H**, **J**, **K**, **M** and **N**. Three of the main branches are labelled **1**, **2** and **3**.

we can explain which mechanism between $\delta = 1$ and $\delta = 1.8$ has lead to that splitting. By increasing the value of δ the subcritical behavior of the first primary branches was enhanced, so that the saddle-nodes **E** and **F** drifted to $\gamma = 0$ where they merged together. Hence, the unstable parts as well as the stable parts of the two branches merged together to the new branches **1** and **1'**, respectively. The connection between the primary branches for negative to positive coupling strengths is done by the transformation $(\gamma, \phi, \psi) \to (-\gamma, -\phi, \psi)$. So obviously, this merging at $\gamma = 0$ is only possible if $\phi(x) = 0$ for the corresponding solution. This is shown in figure 2.12 where the solution profiles from branch **1'** are shown for different values of γ.

Case 3: $\delta > 1.8$

Obviously the coefficient δ has great influence on the bifurcation behavior of our system. Now, we examine the bifurcation behavior in two more cases, $\delta = 1.95$ and $\delta = 2$ (see top and bottom panel of figure 2.14). Besides, we show results of fold continuations (see figure 2.15) which are helpful to understand the transitions between the bifurcation diagrams. Here, fold continuation means that we follow the folds while varying δ and let γ free to be adjusted numerically. First, comparing the bifurcation diagrams for $\delta = 1.8$ (figure 2.13) and $\delta = 1.95$ we recognize a change at branch **2**. Due to an increasing value of δ the hysterisis behavior becomes stronger and its width increases. Hence, the saddle-nodes **G** and **J** drift more and more towards $\gamma = 0$ until they eliminate each other for $\delta \approx 1.93$. While the saddle-nodes eliminates each other the corresponding branches merge together. Thus, branch **2** and its counterpart for positive coupling strength merge and thereby, they split into branches **2** and **2'**. This mechanism is similar to the one in the previous case where branch **1** and its counterpart have formed the branches **1** and **1'**.

At first, the pitchfork bifurcations **A** and **C** are not influenced by this merging and stay onto branch **2'**. However, they also drift towards each other for increasing δ until they eliminates themselves for $\delta \approx 1.97$. Thus, the bifurcation branches of branch **2'** (blue dotted) merge together to one new branch. Thereby, branch **2'** and this new branch split into two separated branches. The result of this procedure can be seen in the bifurcation diagram for $\delta = 2$ (bottom panel of figure 2.14).

Finally, we turn to figure 2.15. There the results of fold continuation are displayed in red (for folds in the negative γ range) and in green (for folds in the positive γ range). The bifurcation diagram for $\delta = 2$ is also plotted by blue dotted lines. With that in the background, it is easier to compare the fold branches with the folds discovered in all the previous bifurcation diagrams. Each fold branch has a different line style and consists of at least two fold labels [16]. The reason for this is that each fold in the negative γ range has a fold as counterpart for positive coupling strengths. For each of these fold pairs there exists one critical value of δ. At this value the folds eliminates each other at the

[16] Except of the fold branches **M** and **N**. However, they would also merge together if the fold continuation has been run to even higher values of δ

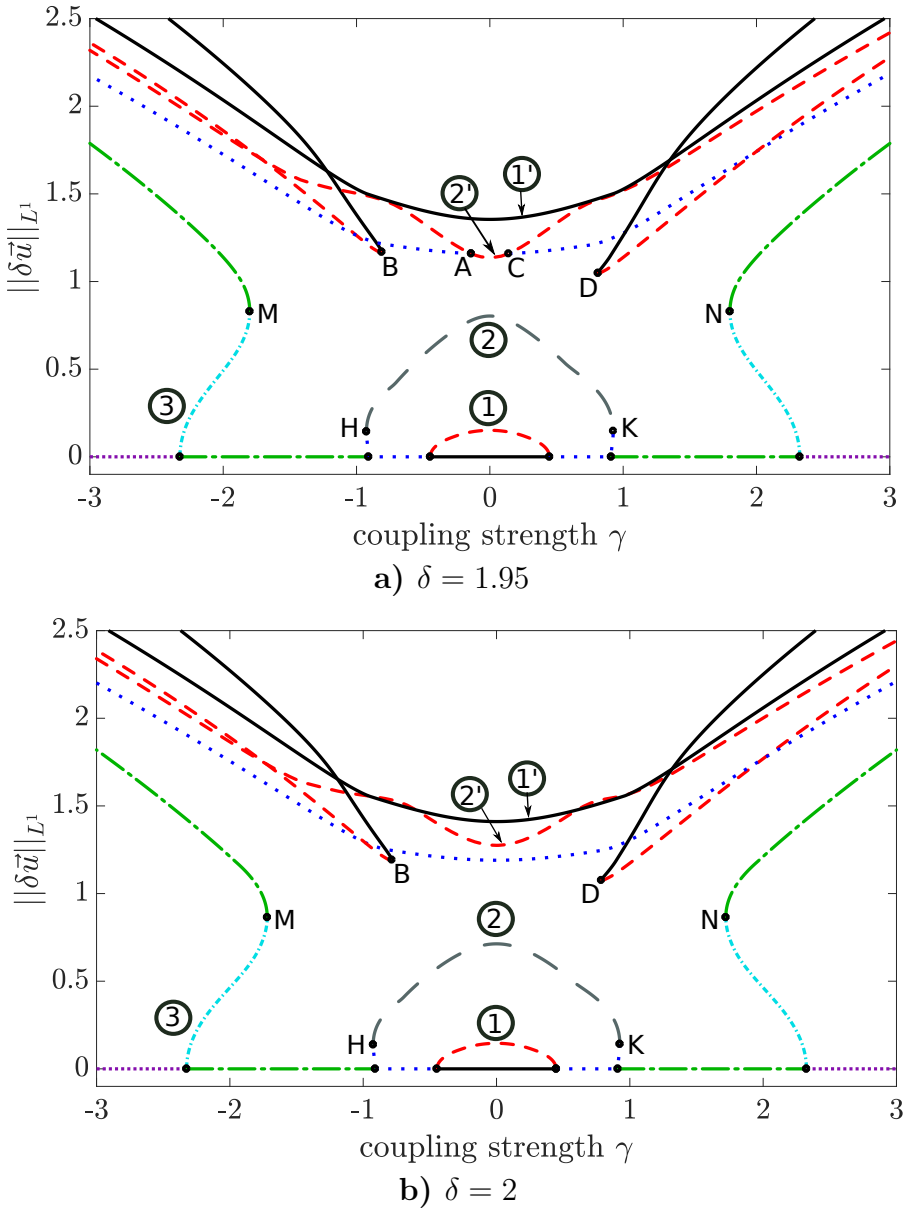

Figure 2.14: L^1-Norm of deviation $\delta\vec{u}$ against coupling strength γ for the occuring steady states of (2.106) with the fixed parameters of (2.109).The prefactor of the quadratic nonlinearity is adjusted to $\delta = 1.95$ in panel a) and to $\delta = 2$ in panel b). Stable states are represented by black solid lines, unstable by red densely dashed, blue dotted, grey dashed, green dashed-dotted, turquoise densely dashed-dotted and violett densely dotted lines according to the amount of unstable eigenvalues (one, two, three, four, five and six, respectively). Labels are explained in the text.

coupling strength $\gamma = 0$ (indicated by all the black dots at the vertical line $\gamma = 0$ in figure 2.15). Therefore each fold branch consists of two folds which also is indicated by the color transition from red to green as γ crosses zero and becomes positive.
On the basis of these fold branches it is easy to verify the bifurcation behavior discussed previously and to make further observations for even higher values of δ which have not been considered yet. Starting with the fold branches **M** and **N** we see that they emerge right at the bifurcation point of the blue dotted lines. This emergence corresponds to the transition from a super- to a subcritical behavior of branch **3** and its counterpart. For increasing δ the drift towards each other and without a lot of imagination we can assume that they will hit and eliminate each other at a higher critical value of δ. These fold continuations has been run up to $\delta = 2$. Therefore these fold branches end up at the fold of the connected blue dotted solution branches. Next, we consider fold branches **E** and **F**. At first, it seems that they do not emerge at the bifurcation point of the blue dotted line. However, the reason for this is that this fold continuation fails near the trivial branch and the branch could not be followed till the end. Regarding the Matthew-Cox instability we know that the primary branch **1** change from super- to subcritical (also observed for $\delta = 1$) behavior. Therefore, we are allowed to interpolate the fold branches **E** and **F** down to the trivial branch where they emerge at the onset of the Matthew-Cox instability.
A more complex behavior is found for the folds **H** and **G** which are connected to the blue dotted primary branch **2**. Together they form the hysterisis bifurcation examined for the bifurcation diagram 2.13 with $\delta = 1.8$. We can observe that their fold branches emerge from a kind of saddle-node bifurcation of folds (left black dot between **H** and **G**). For increasing δ the folds move apart until **G** hits it counterpart **J**. So this is just the procedure already explained by comparing the different bifurcation diagrams 2.13 and 2.14a).
The last think we examine are the fold branches **B** and **G**. We have not already seen that they also merge together in previous diagrams, because δ was too small. This merging is not too surprising after discussing the other fold branches. However, we also observe two additional special points for each fold branch. These points were numerically found as folds. Hence, these points could behave similarly to the saddle-node bifurcations of the fold branches **H** and **G**. In order to provide clarification one should try to exit the fold continuation between the special points and continuate again in the coupling strength. Then one could get further solution branches whose symmetry and stability properties provides additional information. The study of this bifurcation behavior is of main importance since the stable solution branches are involved directly.

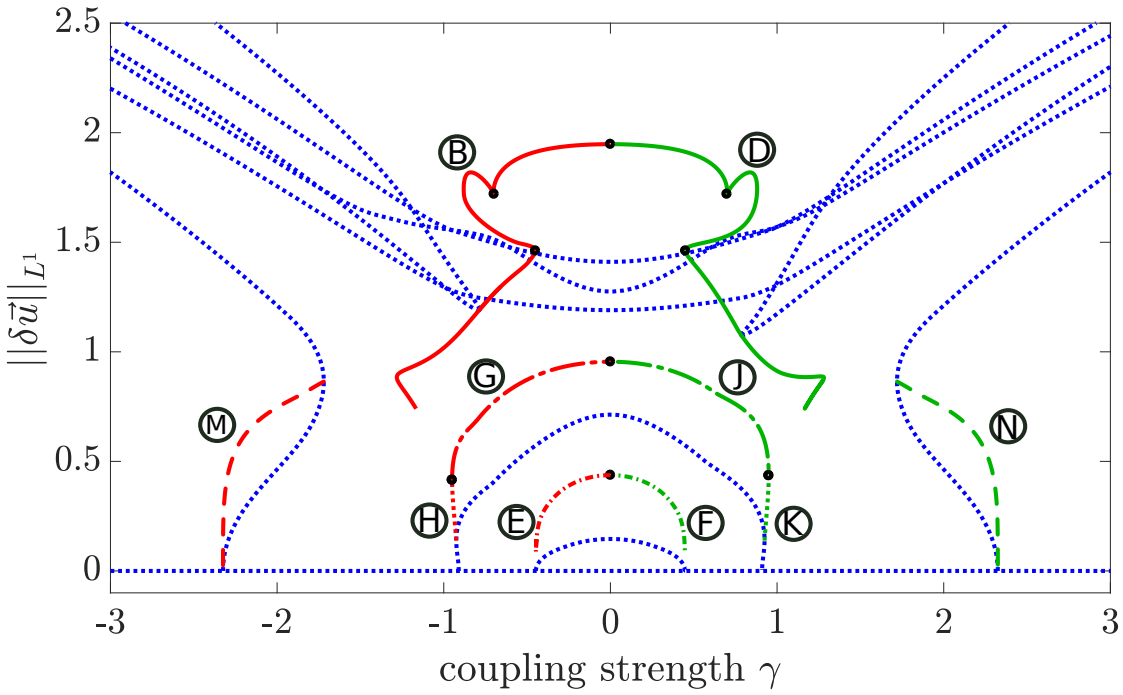

Figure 2.15: L^1-Norm of deviation $\delta\vec{u}$ against coupling strength γ. The results of fold continuation by varying δ are depicted in red and green lines (red lines for the negative γ range, and green lines for positive γ range, respectively). Different fold continuations are distinguished by different line styles and their labels. The whole bifurcation diagram 2.14b) for $\delta = 2$ is indicated by blue dotted lines as a background orientation.

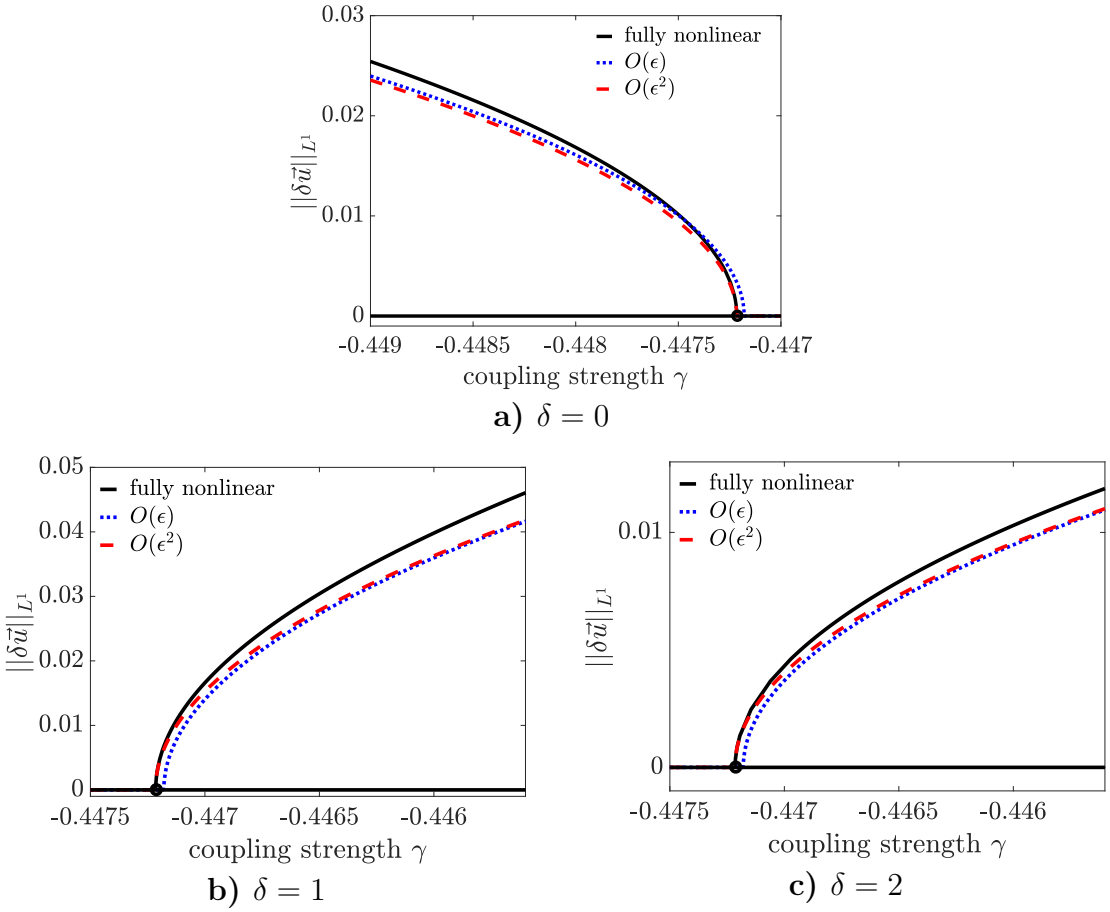

Figure 2.16: Comparison of the fully nonlinear branch **1** (black solid) and the corresponding solution branches derived from amplitude equations in first (blue dotted) and second (red dashed) order (see chapter 2.2.2). This is done for three different values of δ.

2.4. Comparison between weakly nonlinear and fully nonlinear solutions

At the end of the examination of the short-scale instability we compare the fully nonlinear results with solutions of the amplitude equation (2.89) or (2.82), derived in chapter 2.2. Q has to fulfill constraint (2.97) in which n correspond to the different critical wavenumbers. For the most critical mode k_2 it has to be

$$2\pi = k_2 \stackrel{!}{=} Q + k_c = \frac{2n\pi}{l_x} - k_c + k_c \stackrel{l_x=2}{=} n\pi \qquad (2.121)$$
$$\Rightarrow n = 2\,.$$

Each panel in figure 2.16 depicts a detail view of a bifurcation diagram close to the primary bifurcation where branch **1** emerges for a particular value of δ. Here, we do not consider stability and use solid, dashed and dotted lines to distinguish between fully nonlinear and weakly nonlinear calculations to first and second order in ϵ. The solid blue

line refers to the numerical obtained fully nonlinear steady states, whereas the dotted and dashed lines correspond to branches of the solutions derived from the amplitude equations in chapter 2.2.2. Thereby, the dotted line is the solution branch at $O(\epsilon)$ and the dashed one is the solution branch at $O(\epsilon^2)$. For each case we can observe the same. Obviously the first order does not get the bifurcation point precisely. This is, however, corrected in the second order. At this point one could be confused why the first order solution branch do not ly onto the fully nonlinear branch at least at the bifurcation point. The reason of this deviation is that the first suitable critical mode in our system is restricted by the discretization and is therefore not the most critical mode which would appear in an infinite domain. However, the derivation of the amplitude equations starts from the point where the most critical mode unregarded of discretization (in an infinite domain, respectively) has zero growth rate. Thus, we expand around the bifurcation point of an infinite domain and in that case the first order solution branch would lie exactly on the fully nonlinear branch at the bifurcation point. However, in our case branch **1** deviates a little from that most critical mode due to discretization. Therefore it is possible that the second order is closer to the fully nonlinear branch right from the beginning.
Furthermore, we observe that the weakly nonlinear approximations are only good one close to the bifurcation point. The approximations for the sideband mode which correspond to $n = 1$ and $n = 3$ in (2.121) are not shown here, because they do not fit very well to the fully nonlinear branches. This is no surprise, since the weakly nonlinear analysis assumes that the band width of unstable wavenumbers is small ($\sim O(\epsilon)$). However, the first two sideband modes (branches **2** and **3** in the bifurcation diagrams) deviate from the critical mode by $\delta k = \pi$. All in all the approximated solution branches are not very useful for quantitative considerations, but nevertheless this comparison could verify that our construction of amplitude equations of first and second oder is correct. For this work this is of greater importance since we pursue a more general meaning of these investigations.

2.5. Weakly nonlinear analysis – Large-scale instability

Now, we consider the large-scale instability for our coupled system

$$\partial_t \vec{u} = \begin{pmatrix} \partial_{xx}\left(-\frac{\kappa^2}{L^2}\partial_{xx}\phi + a\phi + \phi^3 + \gamma\psi\right) \\ r\psi - (\frac{1}{L^2}\partial_{xx} + 1)^2\psi + \delta\psi^2 - \psi^3 - \gamma\phi \end{pmatrix}, \tag{2.122}$$

i.e. the critical wavenumber is $k_c = 0$ as shown in figure 2.1.
The linearized problem has already been considered in chapter 2.1, where one can finds the critical coupling strength $\gamma_{c,l}$ of the long-scaled instability (see (2.17)) as well as the eigenvector $\vec{w}$ (see (2.18)).
The adjoint eigenvector [17] is

$$\vec{w}^\dagger = \begin{pmatrix} 1 \\ 0 \end{pmatrix}. \tag{2.124}$$

Again the coupling strength should be slightly above [18] the critical coupling strength $\gamma_{c,l}$ i.e.

$$\gamma = \gamma_{c,l} + \epsilon^2 . \tag{2.125}$$

Similar to the analysis of the long scale instability in the uncoupled Cahn-Hilliard equation (see chapter 1.2) we introduce slow time and long space-scales as

$$X = \epsilon x \qquad T = \epsilon^4 t . \tag{2.126}$$

These scales result from the qualitative behavior near the onset of instability. If equation (2.125) holds then the width of the linear unstable wavenumber band is of order ϵ and the height of the maximal growth rate inside this band is of order ϵ^4.
Next, we discuss which terms and scalings we need in a proper ansatz for the weakly nonlinear analysis. Due to the absence of a nonzero wavenumber we do not have higher harmonics as in ansatz (2.22) and just the neutral mode $B(X,T)$ at different orders in ϵ arises.
The occuring nonlinearities are B^2 and B^3.
Due to the vanishing second component in the adjoint eigenvector, one knows that the amplitude equation will be obtained in the Cahn-Hilliard equation. Therefore the terms $\partial_T B$, $\partial_{XX}(\gamma - \gamma_{c,l})B$ and the first occuring nonlinearity in second space derivative should be in balance.
The suitable ansatz depends on the parameter δ which scales the quadratic nonlinearity, because if δ is of order 1 the quadratic nonlinearity is the one of lowest order, i.e. the

[17] In this case the adjoint Jacobian is

$$\underline{\mathbf{J}}^\dagger = \underline{\mathbf{J}}^\intercal = \begin{pmatrix} 0 & -\gamma \\ 0 & r-1 \end{pmatrix} \tag{2.123}$$

[18] We choose the plus sign in (2.17). For the minus sign we have to be slightly under the critical coupling strength

strongest nonlinearity, whereas if δ is of order ϵ or even zero the cubic nonlinearity arises in the amplitude equation.
Therefore we consider two different cases of strong and weak quadratic nonlinearity. We start with the strong quadratic nonlinearity, i.e. we start with $\delta = 1$.
The suitable ansatz reads

$$\begin{aligned}\begin{pmatrix} \phi_1 \\ \psi_1 \end{pmatrix} =& \epsilon^2 \vec{w} B^0(X,T) + \epsilon^4 \begin{pmatrix} B^1_\phi(X,T) \\ B^1_\psi(X,T) \end{pmatrix} \\ &+ \epsilon^6 \begin{pmatrix} B^2_\phi(X,T) \\ B^2_\psi(X,T) \end{pmatrix} + O(\epsilon^8)\,. \end{aligned} \tag{2.127}$$

Then the equations at different orders in ϵ become:

$$O(\epsilon^2): \quad 0 = 0 \tag{2.128}$$

$$0 = 0 \tag{2.129}$$

$$O(\epsilon^4): \quad 0 = 0 \tag{2.130}$$

$$\begin{aligned} 0 =& (r-1)B^1_\psi - \frac{2}{L^2}\frac{\gamma_{c,l}}{r-1}\partial_{XX}B^0 + \left(\frac{\gamma_{c,l}}{r-1}\right)^2 \delta (B^0)^2 \\ &- \gamma_{c,l} B^1_\phi - (\gamma - \gamma_{c,l}) B^0 \end{aligned} \tag{2.131}$$

$$\begin{aligned} O(\epsilon^6): \quad \partial_T B^0 =& \partial_{XX}\left(-\frac{\kappa^2}{L^2}\partial_{XX}B^0 + aB^1_\phi + \right. \\ &\left. \gamma_{c,l} B^1_\psi + (\gamma - \gamma_{c,l})\frac{\gamma_{c,l}}{r-1} B^0 \right) \end{aligned} \tag{2.132}$$

$$\begin{aligned} \frac{\gamma_{c,l}}{r-1}\partial_T B^0 =& (r-1)B^2_\psi - \frac{\gamma_{c,l}}{r-1}\frac{1}{L^4}\partial_{XX}B^0 \\ &- \frac{2}{L^2}\partial_{XX}B^1_\psi + 2\frac{\gamma_{c,l}}{r-1}\delta B^0 B^2_\psi - \left(\frac{\gamma_{c,l}}{r-1}B^0\right)^3 - \\ &- \gamma_{c,l} B^2_\phi - \gamma_1 B^1_\phi \end{aligned} \tag{2.133}$$

Now, we rewrite (2.131) as

$$\begin{aligned} &- \frac{2}{L^2}\frac{\gamma_{c,l}}{r-1}\partial_{XX}B^0 + \left(\frac{\gamma_{c,l}}{r-1}\right)^2 \delta (B^0)^2 - (\gamma - \gamma_{c,l}) B^0 \\ =& (1-r)B^1_\psi + \gamma_{c,l} B^1_\phi \\ =& \frac{1-r}{\gamma_{c,l}}\left(\gamma_{c,l} B^1_\psi + aB^1_\phi\right) \end{aligned}$$

$$\Leftrightarrow \quad \gamma_{c,l}B^1_\psi + aB^1_\phi = \frac{\gamma_{c,l}}{1-r}\Big(-\frac{2}{L^2}\frac{\gamma_{c,l}}{r-1}\partial_{XX}B^0 + \left(\frac{\gamma_{c,l}}{r-1}\right)^2 \delta(B^0)^2 - (\gamma-\gamma_{c,l})B^0\Big) \tag{2.134}$$

and insert (2.134) into (2.132), whereby we use

$$a = \frac{\gamma^2_{c,l}}{1-r}\,. \tag{2.135}$$

This yields

$$\partial_T B^0 = \partial_{XX}\Bigg[-\frac{\kappa^2}{L^2}\partial_{XX}B^0 + (\gamma-\gamma_{c,l})\frac{\gamma_{c,l}}{r-1}B^0 + \frac{\gamma_{c,l}}{1-r}\left(-\frac{2}{L^2}\frac{\gamma_{c,l}}{r-1}\partial_{XX}B^0 + \left(\frac{\gamma_{c,l}}{r-1}\right)^2\delta(B^0)^2 - (\gamma-\gamma_{c,l})B^0\right)\Bigg] \tag{2.136}$$

Arranging the terms in (2.136) one obtains the amplitude equation for $B^0(X,T)$:

$$\partial_T B^0 = \partial_{XX}\Bigg[-\frac{1}{L^2}\left(\kappa^2 - 2\left(\frac{\gamma_{c,l}}{1-r}\right)^2\right)\partial_{XX}B^0 - 2(\gamma-\gamma_{c,l})\frac{\gamma_{c,l}}{1-r}B^0 + \left(\frac{\gamma_{c,l}}{1-r}\right)^3\delta(B^0)^2\Bigg] \tag{2.137}$$

Now we can reintroduce the original scales and drop all ϵ as it just indicates the size scales, but has no physical meaning. This yields the physical field in $O(\epsilon^2)$:

$$\begin{pmatrix}\phi_1\\ \psi_1\end{pmatrix} = \vec{w}B^0(x,t) \tag{2.138}$$

$$\text{with} \quad \partial_t B^0 = \partial_{xx}\Bigg[-\frac{1}{L^2}\left(\kappa^2 - 2\left(\frac{\gamma_{c,l}}{1-r}\right)^2\right)\partial_{xx}B^0 - 2(\gamma-\gamma_{c,l})\frac{\gamma_{c,l}}{1-r}B^0 + \left(\frac{\gamma_{c,l}}{1-r}\right)^3\delta(B^0)^2\Bigg] \tag{2.139}$$

We see that (2.139) is the Sivashinsky equation. So the type III-instability of the coupled system behaves similar to the uncoupled Cahn-Hilliard equation and the amplitude equation itself provides a type III-instability, but there are some differences.
On the one hand the quadratic nonlinearity occurs in the amplitude equation (2.139) although we consider $\phi_0 = 0$ [19]. The reason is that the quadratic nonlinearity of the Swift-Hohenberg part couples into the amplitude equation. On the other hand the prefactors in the amplitude equation have changed in comparison to the ones in the original

[19] In this case the amplitude equation of the Cahn-Hilliard equation is the Cahn-Hilliard equation itself

Cahn-Hilliard equation, which we can briefly discuss. Therefore we keep in mind that

$$a > 0 \,\text{and}\, r < 0\,. \tag{2.140}$$

As

$$\frac{1}{L^2}\left(\kappa^2 - 2\left(\frac{\gamma_{c,l}}{1-r}\right)^2\right) < \frac{\kappa^2}{L^2} \tag{2.141}$$

we see that the prefactor of the stabilizing term $\sim -\partial_{xxxx}B$ is decreased which broadens the band of instability with respect to the steady state solution $B^0(x,t) = b_0 = const$ of (2.139).
The prefactor of the other linear term proportional to $\partial_{xx}B^0$ is

$$-2(\gamma - \gamma_{c,l})\frac{\gamma_{c,l}}{1-r} = -2\frac{\gamma - \gamma_{c,l}}{\gamma_{c,l}}a\,. \tag{2.142}$$

This term provides linear instability. Linear instability sets in if

$$|\gamma| > |\gamma_{c,l}|\,. \tag{2.143}$$

Independent of the sign, the quadratic nonlinear term $\sim \partial_{xx}\left[\left(B^0\right)^2\right]$ always acts destabilizing. The corresponding prefactor

$$\left(\frac{\gamma_{c,l}}{1-r}\right)^3 \delta \tag{2.144}$$

is enhanced by the absolut value of δ. So long as $\delta = O(1)$ we have to incorporate the next order of the physical field to obtain a saturating term proportional to $\partial_{xx}\left[\left(B^0\right)^3\right]$. Another way to obtain a physical useful amplitude equation is to start with a weak quadratic nonlinearity, i.e. with $\delta = O(\epsilon)$. Then the suitable ansatz reads

$$\begin{aligned}\begin{pmatrix}\phi_1\\ \psi_1\end{pmatrix} =& \epsilon\vec{w}B^0 + \epsilon^2\begin{pmatrix}B^1_\phi\\ B^1_\psi\end{pmatrix}\\ &+\epsilon^3\begin{pmatrix}B^2_\phi\\ B^2_\psi\end{pmatrix} + O(\epsilon^4)\,.\end{aligned} \tag{2.145}$$

With the same procedure as above one gets similar equations, but with the remarkable difference that the cubic and quadratic nonlinearity contribute at same order, so the amplitude equation, obtained at order ϵ^5, is

$$\begin{aligned}\partial_T B^0 = \partial_{XX}\Bigg[&-\frac{1}{L^2}\left(\kappa^2 - 2\left(\frac{\gamma_{c,l}}{1-r}\right)^2\right)\partial_{XX}B^0 - 2(\gamma-\gamma_{c,l})\frac{\gamma_{c,l}}{r-1}B^0\\ &+\left(\frac{\gamma_{c,l}}{1-r}\right)^3\delta(B^0)^2 + \left(1-\left(\frac{\gamma_{c,l}}{1-r}\right)^3\right)(B^0)^3\Bigg]\,.\end{aligned} \tag{2.146}$$

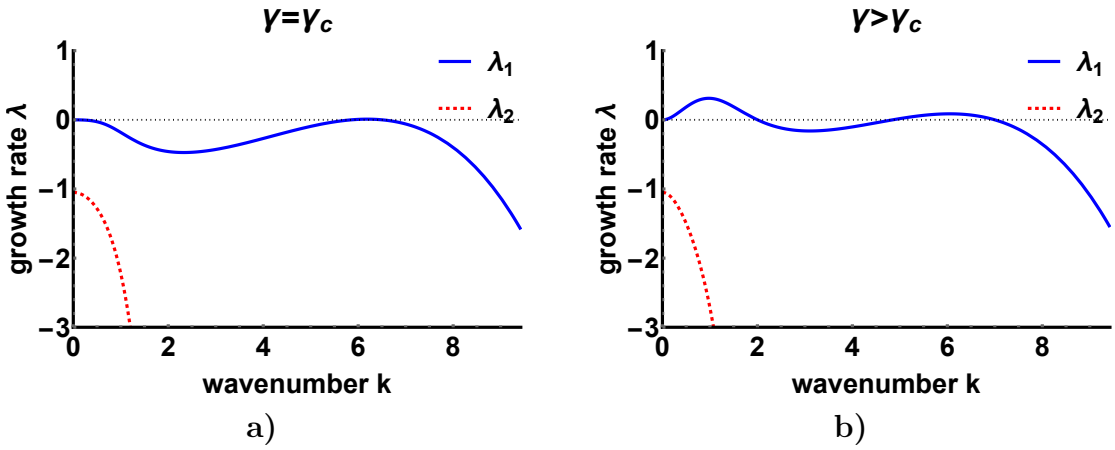

Figure 2.17: Dispersion relations near the codimension-2 instability. The fixed parameters for panels a) and b) are $r = -0.05$, $\kappa = 4$, $L = 2\pi$ and $a = a_c \approx 0.79$ (according to (2.151)). In the left panel the system is at onset of instability for $\gamma = \gamma_c \approx 0.82$. In the right panel the system is slightly above the onset for $\gamma > \gamma_c$.

Here, the prefactor of the cubic nonlinearity acts stabilizing as long as

$$\gamma_{c,l} < 1 - r\,. \tag{2.147}$$

2.6. Weakly nonlinear analysis – Codimension-2 instability

So far we have studied the cases where either the short- (chapter 2.2) or the long- (chapter 2.5) scale instability occur. It is very interesting and challenging to study the system at the codimension-2 point, where both, the short and long-scale instability become unstable simultaneously.
The solution of the linearized problem for zero eigenvalues is

$$\begin{pmatrix} \phi_1 \\ \psi_1 \end{pmatrix} = c_0\vec{w} + \vec{v}\left(c_1 e^{ik_c x} + c_1^* e^{-ik_c x}\right)\,. \tag{2.148}$$

with the eigenvectors $\vec{w}$ and $\vec{v}$ already defined in (2.13) and (2.10), respectively. For the linearized solution there is no difference to the case where only the short-scale instability occurs, because the neutral mode has always zero growth rate.
However, for the codimension-2 point the dispersion relation crosses zero for small k and at $k = k_c$ as depicted in figure 2.17. Instead of one there are two parameters which have to be adjusted to critical values in order that this codimension-2 point is reached. We use the coupling strength γ and the parameter a. From previous linear investigations (see chapter..) we know that the critical values for the coupling strength are

$$\gamma_{c,s}^2 = \left(\frac{\kappa^2}{L^2}k_c^2 + a\right)\left[\left(1 - \frac{1}{L^2}k_c^2\right)^2 - r\right] \quad \text{and} \quad \gamma_{c,l}^2 = (1-r)a \tag{2.149}$$

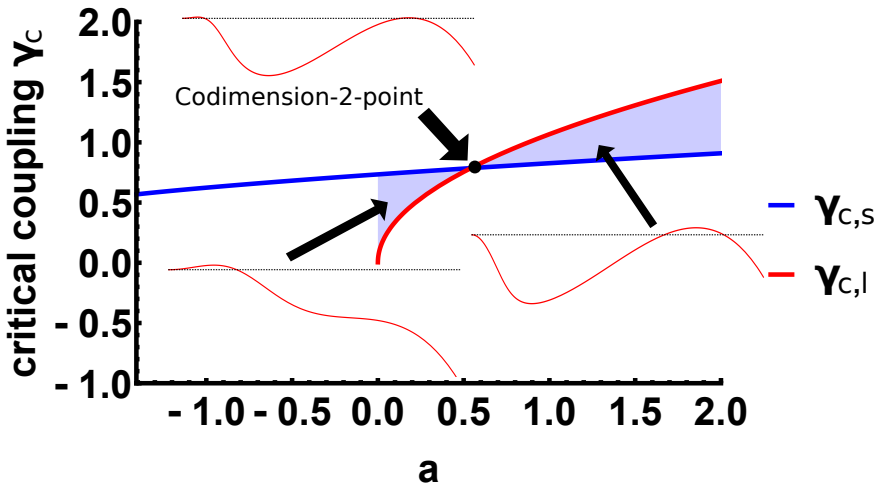

Figure 2.18: Critical coupling strength $\gamma_c(a)$ as function of a. Blue: $\gamma_{c,s}$ for short-scale instability. Red: $\gamma_{c,l}$ for long-scale instability. The crossing point depicts the codimension-2 point. Blue shaded areas are connected to the respective codimension-1 instabilities. A representative dispersion relation is plotted for each instability.

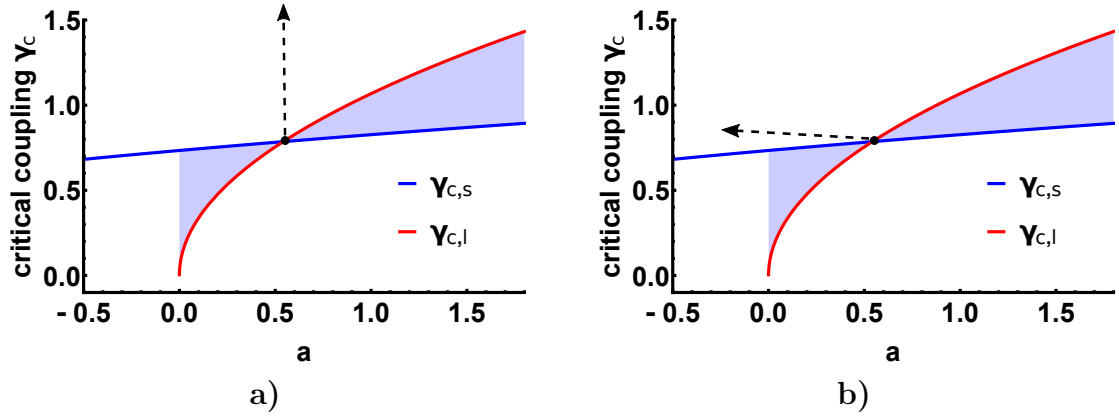

Figure 2.19: Two possible pathways in parameter space at the onset of the codimension-2 instability. Path a) is connected to equations (2.152) and (2.153). Path b) is connected to equations (2.164) and (2.165)

to obtain the short-scale and the long-scale instability, respectively.
These two critical coupling strengths are plotted as functions of the parameter a in figure 2.18. At the codimension-2 point both are equal, which yields the critical value a_c if we use :

$$\gamma_{c,s} \overset{!}{=} \gamma_{c,l} \tag{2.150}$$

$$\Leftrightarrow a_c = 2\kappa^2 \left(-1 + \sqrt{1-r}\right) . \tag{2.151}$$

According to (2.150) the codimension-2 point is the intersection point in figure 2.18. The codimension-1 instabilities are depicted by the blue shaded areas. We see that for $a < a_c$ the long-scale instability and for $a > a_c$ the short-scale instability occur, respectively. Next, we employ a weakly nonlinear analysis at this codimension-2 instability. For that various questions arise:

- Which spatial and temporal scales do we need to introduce?
- How do the two instabilities couple and which amplitude equations are obtained?
- We have two critical parameters, so we are free to choose different pathway inside the (a, γ)-plane. Do different pathways require different analysis and maybe lead to different amplitude equations?

On the basis of the last question we employ the analysis on two different pathways in the (a, γ)-plane, which are illustrated in figure 2.19. Note, that this is done more qualitatively, such that the occuring coefficients are not listed anywhere. We start with the pathway depicted in the left panel. This vertical line corresponds to

$$a = a_c \tag{2.152}$$

$$\gamma = \gamma_c + \epsilon^2 , \tag{2.153}$$

i.e. we vary γ slightly above its critical value and keep $a = a_c$ constant.
Due to previous discussions we introduce long space- and timescales as

$$X = \epsilon x \qquad T_s = \epsilon^2 t \qquad T_l = \epsilon^4 t . \tag{2.154}$$

The spacescale X results from the band of unstable wavenumbers whose width is of order ϵ for both instabilities. However, the heights of the maximal growth rates are different for the two instabilities. Therefore, we introduce two timescales. Thereby, T_s results from the short-scale instability and T_l results from the long-scale instability, respectively.
Next, we explain how the proper scalings for the amplitudes are found. For this we examine which terms we have to balance. Due to the short-scale instability the amplitude equation of A^0 contains a linear term proportional to $(\gamma - \gamma_c)A^0$. This term should be in balance with the first occuring nonlinearities. These could be $A^0 B^0$ and $|A^0|^2 A^0$. Hence, either $A^0 \sim \epsilon$ or $B^0 \sim \epsilon^2$ or both. One of these relations have to be fulfilled

otherwise we would obtain a linear equation. But the amplitudes must not be greater than these relations otherwise the linear instability term $(\gamma - \gamma_c)A^0$ has no significance anymore. Then it is no longer a weakly nonlinear analysis. Now, we consider the long-scale instability. Hence, the neutral mode B^0 also becomes linear unstable. Thus, the amplitude equation of B^0 contains a linear term proportional to $\partial_{XX}\Big((\gamma-\gamma_c)B^0\Big)$. This term should also be in balance with the first occuring nonlinearities. Here, the possible nonlinearities are $\partial_{XX}\Big(\left(B^0\right)^2\Big)$ and $\partial_{XX}\Big(|A^0|^2\Big)$. Hence, either $A^0 \sim \epsilon^2$ or $B^0 \sim \epsilon^2$ or both.
In sum, we conclude that the possible scaling with maximal greatest amplitudes is given by

$$A^0 \sim \epsilon^2 \quad \text{and} \quad B^0 \sim \epsilon^2 \,. \tag{2.155}$$

Then the suitable ansatz is given by

$$\begin{aligned}\begin{pmatrix} \phi_1 \\ \psi_1 \end{pmatrix} =& \epsilon^2 \left[\vec{v}\left(A^0(X,T_s,T_l)e^{ik_c x} + c.c\right) + \vec{w}B^0(X,T_s,T_l)\right] \\ &+ \epsilon^3 \left[\begin{pmatrix} A^1_\phi(X,T_s,T_l) \\ A^1_\psi(X,T_s,T_l) \end{pmatrix} e^{ik_c x} + c.c.\right] \\ &+ \epsilon^4 \left[\begin{pmatrix} A^2_\phi(X,T_s,T_l) \\ A^2_\psi(X,T_s,T_l) \end{pmatrix} e^{ik_c x} + \begin{pmatrix} C^0_\phi(X,T_s,T_l) \\ C^0_\psi(X,T_s,T_l) \end{pmatrix} e^{2ik_c x} + c.c. \right. \\ &\left. + \begin{pmatrix} B^1_\phi(X,T_s,T_l) \\ B^1_\psi(X,T_s,T_l) \end{pmatrix}\right] + O(\epsilon^5)\,. \end{aligned} \tag{2.156}$$

Without going into details we finally obtain coupled amplitude equations at order ϵ^4 and ϵ^6, respectively, which read

$$\partial_{T_s} A^0 = \alpha_1 A^0 + \alpha_2 A^0 B^0 + \alpha_3 \partial_{XX} A^0 \tag{2.157}$$

$$\partial_{T_s} B^0 = 0 \tag{2.158}$$

$$\partial_{T_l} B^0 = \partial_{XX}\left[\beta_1 \partial_{XX} B^0 + \beta_2 B^0 + \beta_3 (B^0)^2 + \beta_4 |A^0|^2\right]. \tag{2.159}$$

It might be confusing that these amplitude equations evolve on different timescales, but these timescales can be recombined by reintroducing the original timescale t:

$$\partial_t A^0 = \epsilon^2 \partial_{T_s} A^0 + \epsilon^4 \partial_{T_l} A^0 \tag{2.160}$$

Here, the smallness parameter ϵ indicates the size scales of the two contributions. We note that the time evolution $\partial_{T_s} A^0$ is much greater and similar to (2.55), where we have considered higher order terms in the amplitude, the time evolution $\partial_{T_l} A^0$ is a higher order correction. Hence, we are allowed to neglect that term. However, the time evolution of B^0 has no contribution on the timescale T_s. Thus, we have to consider the second

contribution, i.e.

$$\partial_t B^0 = \epsilon^2 \partial_{T_s} B^0 + \epsilon^4 \partial_{T_l} B^0 = \epsilon^4 \partial_{T_l} B^0 \,. \tag{2.161}$$

After ordering the terms with the help of ϵ we can finally reincorporate into the particular terms what gives us the final amplitude equations:

$$\partial_t A^0 = \alpha_1 A^0 + \alpha_2 A^0 B^0 + \alpha_3 \partial_{xx} A^0 \tag{2.162}$$

$$\partial_t B^0 = \partial_{xx} \left[\beta_1 \partial_{xx} B^0 + \beta_2 B^0 + \beta_3 (B^0)^2 + \beta_4 |A^0|^2 \right] . \tag{2.163}$$

Next, we consider another pathway in the (a, γ)-plane. The second pathway is illustrated in the right panel of figure 2.19. This path in parameter space corresponds to

$$a = a_c - \epsilon \tag{2.164}$$

$$\gamma = \gamma_{c,s}(a) + \epsilon^2 \,, \tag{2.165}$$

i.e. we follow a path slightly above the blue curve in figure 2.19 in the left direction. The multiscales are introduced by the following implications:

$$a - a_c \sim \epsilon \Rightarrow \gamma - \gamma_{c,l} \sim \epsilon \Rightarrow X_l = \sqrt{\epsilon} x \qquad T_l = \epsilon^2 t \tag{2.166}$$

$$\gamma - \gamma_{c,s} \sim \epsilon^2 \Rightarrow X_s = \epsilon x \qquad T_s = \epsilon^2 t \,. \tag{2.167}$$

We see that both instabilities evolves on the same timescale $T_s = T_l = T = \epsilon^2 t$, but in return we get two different space-scales X_l and X_s.
Analogous examination of reaching a balance between linear and nonlinear terms gives us the suitable ansatz:

$$\begin{aligned} \begin{pmatrix} \phi_1 \\ \psi_1 \end{pmatrix} =& \epsilon^{3/2} \vec{v} \left(A^0(X_l, X_s, T) e^{ik_c x} + c.c \right) + \epsilon^2 \left[\vec{w} B^0(X_l, X_s, T) + \left(\vec{A^1}(X_l, X_s, T) e^{ik_c x} + c.c \right) \right] \\ &+ \epsilon^{5/2} \left(\vec{A^2}(X_l, X_s, T) e^{ik_c x} + c.c \right) \\ &+ \epsilon^3 \left[\left(\vec{A^3}(X_l, X_s, T) e^{ik_c x} + c.c \right) + \vec{C^0}(X_l, X_s, T) e^{2ik_c x} + c.c \right] + O(\epsilon^{7/2}) \,. \end{aligned} \tag{2.168}$$

Then the coupled amplitude equations obtained at order $\epsilon^{7/2}$ and ϵ^4, respectively are given by:

$$\partial_T A^0 = \alpha_1 A^0 + \alpha_2 A^0 B^0 + \alpha_3 \partial_{X_s X_s} A^0 \tag{2.169}$$

$$\partial_T B^0 = \partial_{X_l X_l} \left[\beta_1 \partial_{X_l X_l} B^0 + \beta_2 B^0 + \beta_4 |A^0|^2 \right] \tag{2.170}$$

Reintroducing the original scales yields the final amplitude equations

$$\partial_t A^0 = \alpha_1 A^0 + \alpha_2 A^0 B^0 + \alpha_3 \partial_{xx} A^0 \tag{2.171}$$

$$\partial_t B^0 = \partial_{xx} \left[\beta_1 \partial_{xx} B^0 + \beta_2 B^0 + \beta_4 |A^0|^2 \right] \tag{2.172}$$

We note that different amplitude equations can be deduced in the proximity of a codimension-2 instability. The derived amplitude equations as well as the multiscales depend on the path in parameter space.

3. Conclusion and outlook

In this work we have considered a coupled system consisting of a Cahn-Hilliard and a Swift-Hohenberg equation. In the introduction we have argued why this kind of model system is worth to investigate from a theoretical point of view. Furthermore, we have noted on which kind of experiments it might be applied.
The studied system has two main properties: First, it is a system which couples a conserved and a non-conserved quantity. Second, both uncoupled equations form gradient dynamics. Then, the coupling terms determine if this variational structure is broken or not.
The purpose of this work was to give first theoretical analyses for the simplest possible coupling which keeps the gradient dynamics. We have used an analytical access by employing linear and weakly nonlinear analysis as well as a numerical access by continuation of the fully nonlinear problem. Analytically we have found two qualitatively different codimension-1-instabilities: The long-scale instability arising from the Cahn-Hilliard behavior and the short-scale one which is well known from the Swift-Hohenberg equation. The coupling between the two equations yields to a third possible instability of codimension two, where both instabilities appear simultaneously. The weakly nonlinear analysis of these instabilities was a key issue in this work. It was possible to derive amplitude equations in each case. On the basis of these equations and their derivation we could deduce the consequences of the interplay between conserved and non-conserved properties.
Especially, in the case of the short-scale instability discussed in chapter 2.2 the zero growth rate at $k = 0$ which reflects the conserved property yields coupled amplitude equations of pattern and neutral modes. At linear order in the smallness parameter ϵ these coupled amplitude equations also form gradient dynamics with a corresponding free energy. However, this variational structure is broken at second order. In previous investigation [16] this kind of amplitude system was studied qualitatively and a new instability, the Matthew-Cox instability, was found. Here, we have used the amplitude equations for quantitative comparison with the bifurcation diagram obtained by numerical continuation of the fully nonlinear problem. For comparison we have solved the amplitude equations in first and second order. We have seen that the solution in second order is improved compared to the one obtained in first order. However, both solutions only approximate the fully nonlinear result in the proximity of the bifurcation point (see figure 2.16), but the validity range of the approximations was not too important. Instead our main focus was to explain how the equations obtained through the weakly nonlinear analysis have to be connected in order to yield the amplitude equations in second order. Of course, in many investigations one needs to consider higher order terms but mostly it is done by symmetry arguments or the final merging of the equations is skipped or even left out. From this point of view the comparison between the weakly nonlinear approximations and the fully nonlinear solution branches can be understood

as confirmation that this nontrivial merging is the correct procedure. Moreover, one can use this general method for other systems in order to compare weakly nonlinear results with numerical or experimental data.
Furthermore, the bifurcation diagram obtained by the fully nonlinear treatment was discussed near the short-scale instability. There, we have found that the coefficient δ of the quadratic nonlinearity affects the bifurcation behavior in three ways: First, if it is nonzero the quadratic nonlinearity breaks the inversion symmetry of the system. Therefore, pitchfork bifurcations which break this symmetry are split into saddle-node bifurcations. Second, if the quadratic nonlinearity is strong enough, i.e. if δ crosses a critical value, the primary bifurcations can change from supercritical to subcritical. Surprisingly, we have also found hysterisis bifurcations instead of the transition from super- to subcritical (see figure 2.13). Further work can tackle this hysterisis by considering higher orders in the amplitude equations. And third, an increasing value of δ leads to further merging and splitting of branches. This complex behavior has been studied by fold continuation and numerical linear stability analyses.
Besides, symmetry considerations have been connected to the transition from $\delta = 0$ to $\delta \neq 0$. Thereby a question related to the choice of the definition of inversion symmetry could arise. In this work we have defined inversion by

$$(x, \phi, \psi) \to (-x, -\phi, -\psi)\,. \tag{3.1}$$

Another possible definition of inversion as field inversion is given by

$$(x, \phi, \psi) \to (x, -\phi, -\psi)\,. \tag{3.2}$$

The system of equations shows the same properties for both definitions of inversion, so both seem to be equal. However, only the first definition (3.1) is the proper one to characterize the bifurcation behavior. In table 2.1 we have listed the symmetries of the relevant branches and found that each bifurcation is related to one broken symmetry. But this is only the case if we define inversion symmetry by (3.1) and the other definition (3.2) would not fit. In that case the solution profiles on branch A1 would not be invariant under reflection as well as under inversion. Therefore, the question arises, how it is possible to predict the proper symmetries already on the basis of the equations. This general question is related to group theory and maybe a kind of irreducible representations of the problem and could be part of further work.
Besides, the short-scale instability we have also studied the long-scale and the codimension-2 instability analytically by linear and weakly nonlinear considerations (chapter and , respectively). Throughout these analyses we have explained how and why the different ansatzes and multiscales in the weakly nonlinear analysis are chosen, which is of general significance. Especially the treatment of the codimension-2 point was quite interesting since the freedom of varying two instead of one critical parameter has lead to different

amplitude equations according to different pathways in parameter space. Further work could consider how these different amplitude equations differ from each other by their solutions and the stability behavior of their solutions.

However, the main task of further work on this class of systems is the study of the nonvariational case, i.e. the case where complex eigenvalues can occur. Therefore, one uses coupling terms which break the gradient dynamics. Then, the solution variety is not limited by this property anymore and travelling waves instabilities are possible. Here, we give an outlook by deriving the amplitude equations for a short-scale instability in the nonvariational case, where two complex conjugated eigenvalues become unstable, i.e. we start a study of a travelling wave instability.

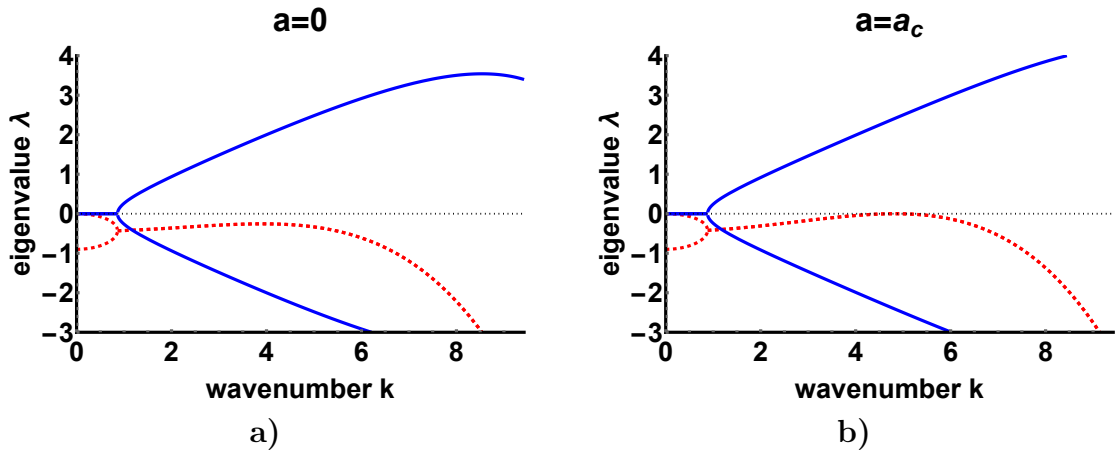

Figure 3.1: Dispersion relation of (3.7). The real parts of the eigenvalues are depicted in red dashed lines. The imaginary parts are depicted in blue solid lines. The fixed parameters for panels a) and b) are $\gamma = 0.5$, $r = 0.1$, $\kappa = 0.2$, $L = 2\pi$ and $\sigma = 1$. In a) the trivial fixpoint is stable while $a = 0$. In b) the short scale instability sets in when $a = a_c$ with a_c from (3.14).

3.1. Outlook – Nonvariational coupling with a travelling wave instability

Here, we consider a nonvariational coupling such that the two-field system is given by

$$\partial_t \begin{pmatrix} \phi \\ \psi \end{pmatrix} = \begin{pmatrix} \partial_{xx}\left(-\frac{\kappa^2}{L^2}\partial_{xx}\phi + a\phi + \phi^3 - \gamma\psi\right) \\ r\psi - (\frac{1}{L^2}\partial_{xx} + 1)^2\psi + \delta\psi^2 - \psi^3 - (\gamma - \sigma)\phi \end{pmatrix}. \tag{3.3}$$

In the limit $\sigma \to 0$ we obtain the variational case discussed before. In figure 3.1 we see that in some parameter space system (3.3) becomes unstable in a short-scale instability with complex eigenvalues. We start with the linearized problem and derive amplitude equations in the case of being close to the onset of instability.

3.1.1. Linearized problem

Again the trivial fixpoint is given by

$$\begin{pmatrix} 0 \\ 0 \end{pmatrix}. \tag{3.4}$$

The linearized problem around the trivial fixpoint is given by

$$\begin{pmatrix} -k^2\left(\frac{\kappa^2}{L^2}k^2+a\right) & -\gamma k^2 \\ -(\gamma-\sigma) & r-\left(-\frac{1}{L^2}k^2+1\right)^2 \end{pmatrix}\vec{v}=\lambda\vec{v} \tag{3.5}$$

$$\underbrace{\begin{pmatrix} -k^2\left(\frac{\kappa^2}{L^2}k^2+a\right)-\lambda & -\gamma k^2 \\ -(\gamma-\sigma) & r-\left(-\frac{1}{L^2}k^2+1\right)^2-\lambda \end{pmatrix}}_{:=\underline{\mathbf{J}}}\vec{v}=0\,. \tag{3.6}$$

and the eigenvalues are

$$\lambda_{1,2}(k)=\frac{1}{2}\left[c(k)+s(k)\pm\sqrt{\left(c(k)-s(k)\right)^2+4k^2\gamma(\gamma-\sigma)}\right]\,, \tag{3.7}$$

with the abbreviations

$$c(k)=-k^2\left(\frac{\kappa^2}{L^2}k^2+a\right)\quad\text{and}\quad s(h)=r-\left(-\frac{1}{L^2}k^2+1\right)^2\,. \tag{3.8}$$

Here, we demand that at onset of instability the eigenvalues are purely imaginary, i.e.

$$\lambda_{1,2}(k_c)=\pm i\omega\,,\omega\in\mathbb{R}\,. \tag{3.9}$$

Together with (3.7) this yields

$$c(k_c)+s(k_c)\stackrel{!}{=}0\quad\text{and}\quad\omega=\frac{1}{2}\sqrt{-\left(c(k)-s(k)\right)^2+4k^2\gamma(\sigma-\gamma)}\,. \tag{3.10}$$

In this case the coupling strength γ only influences the imaginary part of the eigenvalue at onset of instability. Therefore, we have to use another parameter to adjust the instability and let the system become unstable. The chosen parameter is a. Then, we obtain the critical value a_c from the first condition of (3.10) where the instability sets in:

$$a_c=-\frac{\kappa^2}{L^2}k_c^2+\frac{1}{k_c^2}\left[r-\left(-\frac{1}{L^2}k^2+1\right)^2\right]\,. \tag{3.11}$$

The nonvanishing critical wavenumber k_c can be obtained by the maximum condition for the real part of the eigenvalues at onset, i.e. by

$$\partial_k\left[\mathrm{Re}\big(\lambda_{1,2}(k)\big)\right]\Big|_{k=k_c}\stackrel{!}{=}0\,, \tag{3.12}$$

which yields

$$k_c^2 = \frac{L^2}{1+\kappa^2 L^2}\left(1 - \frac{L^2 a_c}{2}\right)$$
$$k_c^2 = L^2\sqrt{\frac{1-r}{1+L^2\kappa^2}}\,, \tag{3.13}$$

where we have inserted the expression for a_c (3.11).
In this case it is easy to find the expression for k_c (3.13), because only the real part of the eigenvalues is relevant for this calculation. But again we will find the same expression in the weakly nonlinear analysis which can be used as a check of the following weakly nonlinear analysis. Now, we insert (3.13) into (3.11) which yields

$$a_c = \frac{2\left(L^2 - \sqrt{\kappa^2 L^2 + 1}\sqrt{-L^4(r-1)}\right)}{L^4}\,. \tag{3.14}$$

Before we make this investigation we write down the solution of the linearized problem. The eigenvectors corresponding to the eigenvalues are

$$\lambda_1(k_c) = +i\omega: \qquad \vec{v}_1 = \begin{pmatrix} 1 + i\frac{\omega}{c(k_c)} \\ \frac{\sigma-\gamma}{c(k_c)} \end{pmatrix} \tag{3.15}$$

$$\lambda_2(k_c) = -i\omega: \qquad \vec{v}_2 = \begin{pmatrix} 1 - i\frac{\omega}{c(k_c)} \\ \frac{\sigma-\gamma}{c(k_c)} \end{pmatrix} \tag{3.16}$$

We note that the eigenvectors are complex conjugated to each other due to the complex conjugated eigenvalues and the purely real matrix $\underline{\mathbf{J}}$, so we can use

$$\vec{v}_2 = \vec{v}_1^{\,*}\,. \tag{3.17}$$

Then the solution of the linearized problem becomes

$$\vec{u} = A\vec{v}_1 e^{i(k_c x + \omega t)} + a\vec{v}_1^{\,*} e^{i(k_c x - \omega t)}\,. \tag{3.18}$$

Thereby A is the coefficient of the left travelling wave and a is the coefficient of the right travelling one.
Furthermore we need the adjoint eigenvectors [20]

$$\vec{v}_1^{\,\dagger} = \left(-i\frac{c(k_c)}{2\omega}, \frac{1}{2}\left(\frac{c(k_c)}{\sigma-\gamma} + i\frac{c(k_c)^2}{(\sigma-\gamma)\omega}\right)\right) \quad \text{and} \quad \vec{v}_2^{\,\dagger} = \left(\vec{v}_1^{\,\dagger}\right)^* \tag{3.20}$$

to apply the fredholm alternative in the following investigation.

[20] In this case the adjoint Jacobian is

$$\underline{\mathbf{J}}^\dagger = \begin{pmatrix} c(k) - \lambda^* & -(\gamma - \sigma) \\ -\gamma k^2 & s(k) - \lambda^* \end{pmatrix} \tag{3.19}$$

3.1.2. Derivation of amplitude equations

We start the weakly nonlinear analysis by introducing the smallness parameter ϵ as

$$a - a_c = \epsilon^2 \tag{3.21}$$

and the multiscales

$$X = \epsilon x\,, \quad T_1 = \epsilon t\,, \quad T_2 = \epsilon^2 t\,. \tag{3.22}$$

In contrast to the short-scale instability in the variational regime two slow timescales occur. The amplitude of the most critical mode grows on the timescale T_2 similar to the case of the variational system. The relation $T_2 = \epsilon^2 t$ results from the height of the real part of the eigenvalue, because $\mathrm{Re}(\lambda)(a, k_c) \sim \epsilon^2$ if a fulfills (3.21). The other timescale $T_1 = \epsilon t$ also occurs because $\mathrm{Im}(\lambda)(a, k_c) - \omega \sim \epsilon$. That means that deviations from the frequency of the physical field at the onset of instability develop on this timescale.
Besides the new space- and timescales we make an ansatz similar to (2.22). Here it is given by:

$$\begin{aligned}
\vec{u} = \begin{pmatrix} \phi_1 \\ \psi_1 \end{pmatrix} =& \epsilon \left(\vec{v}_1 A^0(X, T_1, T_2) e^{ik_c x + i\omega t} + \vec{v}_1^{*} a^0(X, T_1, T_2) e^{ik_c x - i\omega t} + c.c \right) \\
&+ \epsilon^2 \Big[\vec{A}^1(X, T_1, T_2) e^{ik_c x + i\omega t} + \vec{a}^1(X, T_1, T_2) e^{ik_c x - i\omega t} \\
&\quad + \vec{C}^0(X, T_1, T_2) e^{2ik_c x + 2i\omega t} + \vec{c}^{\,0}(X, T_1, T_2) e^{2ik_c x - 2i\omega t} \\
&\quad + \vec{D}^0(X, T_1, T_2) e^{2ik_c x} + \vec{E}^0(X, T_1, T_2) e^{2i\omega t} + c.c. \\
&\quad + \vec{B}^0(X, T_1, T_2) \Big] + O(\epsilon^3)
\end{aligned} \tag{3.23}$$

The difference is that at linear order in ϵ we have twice as many contributions as in ansatz (2.22), because of the two complex conjugated eigenvalues. Therefore we also have more contributions at second order, but in principle it is the same procedure. We note that we do not have to consider amplitude equation of A and a, because they would have the same form. To obtain the other equation one has to exchange all capital letters to small letters and vice versa and change the sign of ω. Therefore, we do not mention all equation, instead one can just apply this transformation to obtain the missing ones. At linear order in ϵ we obtain the linearized problem which has already been solved in the previous chapter. At second order we obtain by projecting onto the respective fourier modes the following equations:

$O(\epsilon^2)$:

~ 1 :

$$\underline{\mathbf{J}}\Big|_{k=0,\,\omega=0} \begin{pmatrix} B_\phi^0 \\ B_\psi^0 \end{pmatrix} = \begin{pmatrix} 0 \\ 2\delta v_\psi^2 \left[|a^0|^2 + |A^0|^2\right] \end{pmatrix} \tag{3.24}$$

$\sim e^{ik_c x + i\omega_c t}$:

$$\begin{aligned} \underline{\mathbf{J}}\Big|_{k=k_c,\,\omega=\omega_c} \vec{A}^1 &= -\vec{v}_1 \partial_{T_1} A^0 \\ &+ \begin{pmatrix} 2i\left[\frac{2\kappa^2}{L^2} k_c^3 v_\phi + k_c(a_c v_\phi + \gamma v_\psi)\right] \\ -4i\frac{k_c}{L^2}\left(1 - \frac{k_c^2}{L^2}\right) v_\psi \end{pmatrix} \partial_X A^0 \end{aligned} \tag{3.25}$$

$\sim e^{2ik_c x + 2i\omega t}$:

$$\underline{\mathbf{J}}\Big|_{k=2k_c,\,\omega=2\omega_c} \vec{C}^0 = \begin{pmatrix} 0 \\ \delta v_\psi^2 \left(A^0\right)^2 \end{pmatrix} \tag{3.26}$$

$\sim e^{2ik_c x}$:

$$\underline{\mathbf{J}}\Big|_{k=2k_c,\,\omega=0} \vec{D}^0 = \begin{pmatrix} 0 \\ 2\delta v_\psi^2 A^0 a^0 \end{pmatrix} \tag{3.27}$$

$\sim e^{2i\omega_c t}$:

$$\underline{\mathbf{J}}\Big|_{k=0,\,\omega=2\omega_c} \vec{E}^0 = \begin{pmatrix} 0 \\ 2\delta v_\psi^2 A^0 \left(a^0\right)^* \end{pmatrix} \tag{3.28}$$

Equation systems (3.26) - (3.28) determine the amplitudes $\vec{C}^0$, $\vec{D}^0$ and $\vec{E}^0$ as functions of the amplitudes A^0, a^0 and their complex conjugates. The first component of (3.24) yields $0 = 0$ due to the conserved property, but the second component relates B_ψ to B_ϕ, A^0, a^0 and their complex conjugates. Equation system (3.25) can be used to employ the Fredholm alternative. This yields:

$$\left(\vec{v}_1^\dagger\right)^* \cdot \left[-\vec{v}_1 \partial_{T_1} A^0 + \begin{pmatrix} 2i\left[\frac{2\kappa^2}{L^2} k_c^3 v_\phi + k_c(a_c v_\phi + \gamma v_\psi)\right] \\ -4i\frac{k_c}{L^2}\left(1 - \frac{k_c^2}{L^2}\right) v_\psi \end{pmatrix} \partial_X A^0 \right] = 0 \tag{3.29}$$

We sort the solvability condition (3.29) into real and imaginary part:

$$\text{real:} \quad k_c^2 = L^2 \sqrt{\frac{1-r}{1+L^2\kappa^2}} \tag{3.30}$$

$$\text{imaginary:} \quad \partial_{T_1} A^0 = \omega_1 \partial_X A^0 \tag{3.31}$$

$$\begin{aligned} \text{with} \quad \omega_1 = -\frac{k_c}{\omega_c} \Bigg[&\gamma(\gamma - \sigma) + k_c^2 a_c \left(\frac{2}{L} + a_c\right) + \frac{k_c^4}{L^4}\left(2\kappa^2 + a_c(3L^2\kappa^2 - 2)\right) \\ &+ \frac{k_c^6}{L^6} 2\kappa^2 \left(L^2\kappa^2 - 1\right) \Bigg] \end{aligned} \tag{3.32}$$

Analogous to the variational case, the solvability condition in second order provides the expression for the critical wavenumber k_c, which has been already calculated in the previous chapter. In contrast to the variational case we also obtain a first amplitude equation (3.32) from the imaginary part of the solvability condition. This equation reflects the first correction of the frequency ω_c. This correction is of order ϵ and therefore appears on the timescale $T_1 = \epsilon t$.
At next order we find the evolution of amplitude A^0 and the slower timescale T_2. We project the third order in ϵ onto the fourier mode $e^{ik_c x + i\omega t}$ and employ the Fredholm alternative analogously. Then, we obtain the amplitude equation

$$\begin{aligned}\partial_{T_2} A^0 =& \alpha_1 A^0 + \alpha_2 A^0 B_\phi^0 \\ &+ \alpha_3 |A^0|^2 A^0 + \tilde{\alpha}_3 |a^0|^2 A^0 + \alpha_4 \partial_{XX} A^0 \,,\end{aligned} \tag{3.33}$$

with the complex parameters α_i and $\tilde{\alpha}_3$ given in table B.2. Again, we need the amplitude equation for B_ϕ^0 to obtain a self-contained system. Therefore we the evolution of B_ϕ^0 on both timescales. At $O(\epsilon^3)$ we find

$$\partial_{T_1} B_\phi^0 = 0 \tag{3.34}$$

and at fourth order in ϵ we obtain:

$$\partial_{T_2} B_\phi^0 = \partial_{XX} \left[a_c B_\phi^0 - \frac{\gamma}{1-r} \big((\gamma - \sigma) B_\phi^0 - 2\delta v_\psi^2 \left(|A^0|^2 + |a^0|^2 \right) \big) \right]. \tag{3.35}$$

Finally, we want to combine both time evolutions. Again, we reintroduce the original timescale:

$$\begin{aligned}\partial_t A^0 =& \epsilon \partial_{T_1} A^0 + \epsilon^2 \partial_{T_2} A^0 \\ &= \epsilon \omega_1 \partial_X A^0 + \epsilon^2 \Big[\alpha_1 A^0 + \alpha_2 A^0 B_\phi^0 \\ &+ \alpha_3 |A^0|^2 A^0 + \tilde{\alpha}_3 |a^0|^2 A^0 + \alpha_4 \partial_{XX} A^0 \Big]\end{aligned} \tag{3.36}$$

$$\begin{aligned}\partial_t B_\phi^0 =& \epsilon \partial_{T_1} B_\phi^0 + \epsilon^2 \partial_{T_2} B_\phi^0 \\ =& \epsilon^2 \partial_{XX} \Big[a_c B_\phi^0 - \frac{\gamma}{1-r} \big((\gamma - \sigma) B_\phi^0 - 2\delta v_\psi^2 \left(|A^0|^2 + |a^0|^2 \right) \big) \Big]\end{aligned} \tag{3.37}$$

We remind us that ϵ indicates the size scale of the corresponding term it is multiplied with. Now, ϵ can be reincorporated in the terms of (3.36) and (3.32) which yields the final amplitude equations in the original scales:

$$\partial_t A^0 = \omega_1 \partial_x A^0 + \alpha_1 A^0 + \alpha_2 A^0 B_\phi^0 + \alpha_3 |A^0|^2 A^0 + \tilde{\alpha}_3 |a^0|^2 A^0 + \alpha_4 \partial_{xx} A^0 \tag{3.38}$$

$$\partial_t B_\phi^0 = \partial_{xx} \Big[a_c B_\phi^0 - \frac{\gamma}{1-r} \big((\gamma - \sigma) B_\phi^0 - 2\delta v_\psi^2 \left(|A^0|^2 + |a^0|^2 \right) \big) \Big] \tag{3.39}$$

At this point we finish our considerations in the framework of this work. We have seen that the weakly nonlinear analysis in the case of complex eigenvalues is quite more involved, but techniqually similar to the analysis of the codimension-2 instability in the variational case.
Further investigations should start with the amplitude equation system (3.38) and (3.39). Finding (travelling wave) solutions and investigate their stability are possible and interesting tasks. Furthermore, it is worth to study the bifurcation behavior in a fully nonlinear consideration and compare it to the solutions given by the amplitude equations. Maybe the Matthew-Cox instability can be found similarly or even another instability determines the system behavior.

A. Literatur

[1] Vaeth M Appell J. In: *Elemente der Funktionalanalysis*. Vieweg Teubner Verlag, 2005. Chap. Die Fredholm-Alternative.

[2] TB Benjamin and F Ursell. "The stability of the plane free surface of a liquid in vertical periodic motion". In: *Proc. Roy. Soc. A: Math. Phys. Eng. Sci.* Vol. 225. 1163. The Royal Society. 1954, pp. 505–515.

[3] S Ciliberto and JP Gollub. "Chaotic mode competition in parametrically forced surface waves". In: *J. Fluid Mech.* 158 (1985), pp. 381–398.

[4] P Coullet and G Iooss. "Instabilities of one-dimensional cellular patterns". In: *Phys. Rev. Lett.* 64.8 (1990), p. 866.

[5] SM Cox. "The envelope of a one-dimensional pattern in the presence of a conserved quantity". In: *Phys. Lett. A* 333.1 (2004), pp. 91–101.

[6] S Douady. "Experimental study of the Faraday instability". In: *J. Fluid Mech.* 221 (1990), pp. 383–409.

[7] M Faraday. "On the forms and states assumed by fluids in contact with vibrating elastic surface". In: *Phil. Trans. R. Soc. Land.* 121 (1831), pp. 319–346.

[8] LS Fisher and AA Golovin. "Instability of a two-layer thin liquid film with surfactants: Dewetting waves". In: *J. of Colloid and Interface Science* 307.1 (2007), pp. 203–214.

[9] C Godrèche. In: *Solids far from Equilibrium*. Vol. 1. Cambridge University Press, 1991. Chap. 3.

[10] C Godrèche. In: *Solids far from Equilibrium*. Vol. 1. Cambridge University Press, 1991. Chap. 2.

[11] AA Golovin, AA Nepomnyashchy, and LM Pismen. "Interaction between short-scale Marangoni convection and long-scale deformational instability". In: *Physics of Fluids* 6.1 (1994), pp. 34–48.

[12] A van Harten. "On the validity of the Ginzburg-Landau equation". In: *J. Nonlin. Sci.* 1.4 (1991), pp. 397–422.

[13] E Knobloch. "Pattern selection in long-wavelength convection". In: *Phys. D: Nonlin. Phen.* 41.3 (1990), pp. 450–479.

[14] L Kramer and W Zimmermann. "On the Eckhaus instability for spatially periodic patterns". In: *Phys. D: Nonlinear Phenomena* 16.2 (1985), pp. 221–232.

[15] K. Kumar. "Linear theory of Faraday instability in viscous liquids". In: *Proc. Roy. Soc. A: Math. Phys. Eng. Sci.* Vol. 452. 1948. The Royal Society. 1996, pp. 1113–1126.

[16] PC Matthews and SM Cox. "Pattern formation with a conservation law". In: *Nonlinearity* 13.4 (2000), p. 1293.

[17] HW Müller et al. “Analytic stability theory for Faraday waves and the observation of the harmonic surface response”. In: *Phys. Rev. Lett.* 78.12 (1997), p. 2357.

[18] MRE Proctor. “Finite amplitude behaviour of the Matthews–Cox instability”. In: *Phys. Lett. A* 292.3 (2001), pp. 181–187.

[19] G Pucci, MB Amar, and Y Couder. “Faraday instability in floating liquid lenses: the spontaneous mutual adaptation due to radiation pressure”. In: *J. Fluid Mech.* 725 (2013), pp. 402–427.

[20] G Pucci et al. “Mutual adaptation of a Faraday instability pattern with its flexible boundaries in floating fluid drops”. In: *Phys. Lett. A* 106.2 (2011), p. 024503.

[21] R Seydel. *Practical bifurcation and stability analysis*. Vol. 5. Springer Science & Business Media, 2009.

[22] GI Sivashinsky. “Instabilities, pattern formation, and turbulence in flames”. In: *Ann. Rev. Fluid Mech.* 15.1 (1983), pp. 179–199.

[23] U Thiele et al. “Localized states in the conserved Swift-Hohenberg equation with cubic nonlinearity”. In: *Phys. Rev. E* 87.4 (2013), p. 042915.

[24] H Uecker, D Wetzel, and JDM Rademacher. “pde2path-A Matlab package for continuation and bifurcation in 2D elliptic systems”. In: *NUMER MATH THEORY ME* 7.1 (2014), pp. 58–106.

[25] EP Zemskov, VK Vanag, and IR Epstein. “Amplitude equations for reaction-diffusion systems with cross diffusion”. In: *Phys. Rev. E* 84.3 (2011), p. 036216.

B. Appendix

Table B.1: List of parameters which occur in amplitude and algebraic equations of chapter 2.2. The corresponding equations are (2.58), (2.59), (2.60), (2.60), (2.68) and (2.69)

parameter	expression
α_1	$-\frac{2\left(2L^2k_c^2-k_c^4+L^4(r-1)\right)}{L^4\gamma_c\left(\frac{\left(r-\left(\frac{k_c^2}{L^2}-1\right)^2\right)^2}{\gamma_c^2k_c^2}+1\right)}(\gamma-\gamma_c)$
α_2	$\frac{2\delta\gamma_c}{(r-1)\left(\frac{\left(r-\left(\frac{k_c^2}{L^2}-1\right)^2\right)^2}{\gamma_c^2k_c^2}+1\right)}$
α_3	$\frac{2\delta^2\left(\frac{1}{\frac{\gamma_c^2}{\frac{4\kappa^2k_c^2}{L^2}+a}-\left(1-\frac{4k_c^2}{L^2}\right)^2+r}+\frac{2}{r-1}\right)+\frac{3\left(-2L^2k_c^2+k_c^4+L^4(-r)+L^4\right)^4}{L^{16}\gamma_c^4}+3}{\frac{\left(r-\left(\frac{k_c^2}{L^2}-1\right)^2\right)^2}{\gamma_c^2k_c^2}+1}$
α_4	$-\frac{\frac{\left(2L^2k_c^2-k_c^4+L^4(r-1)\right)\left(\left(2L^2k_c^2-k_c^4+L^4(r-1)\right)\left(9a\kappa^2L^2k_c^2+10\kappa^4k_c^4+3a^2L^4\right)+L^6\gamma_c^2\left(7\kappa^2k_c^2+3aL^2\right)\right)}{L^{10}\gamma_c^2k_c^2\left(\kappa^2k_c^2+aL^2\right)}+\frac{2\left(L^2-3k_c^2\right)}{L^4}}{\frac{\left(r-\left(\frac{k_c^2}{L^2}-1\right)^2\right)^2}{\gamma_c^2k_c^2}+1}$
α_5	$-\frac{\left(r-\left(1-\frac{k_c^2}{L^2}\right)^2\right)\left(-2aL^{12}\gamma_c^2k_c-\frac{2L^8\gamma_c^2\left(\left(2L^2k_c^2-k_c^4+L^4(r-1)\right)\left(2\kappa^2k_c^2+aL^2\right)+L^6\gamma_c^2\right)}{k_c\left(\kappa^2k_c^2+aL^2\right)}-4\kappa^2L^{10}\gamma_c^2k_c^3\right)}{L^{12}\gamma_c^4k_c^2\left(\frac{L^2\left(r-\left(1-\frac{k_c^2}{L^2}\right)^2\right)}{k_c^2\left(\kappa^2k_c^2+aL^2\right)}-1\right)}$
α_6	$\frac{2k_c\left(\left(2L^2k_c^2-k_c^4+L^4(r-1)\right)^2\left(\kappa^2k_c^2+aL^2\right)\left(2\kappa^2k_c^2+aL^2\right)+L^{12}\gamma_c^4+\kappa^2L^6\gamma_c^2k_c^2\left(2L^2k_c^2-k_c^4+L^4(r-1)\right)\right)}{L^8\gamma_c^3(L^2k_c^2(2-aL^2)-k_c^4(\kappa^2L^2+1)+L^4(r-1))}(\gamma-\gamma_c)$
α_7	$-\frac{4\delta\left(2L^2k_c^2-k_c^4+L^4(r-1)\right)\left(2\kappa^2k_c^2+aL^2\right)}{L^6(r-1)\gamma_ck_c\left(\frac{L^2\left(r-\left(\frac{k_c^2}{L^2}-1\right)^2\right)}{k_c^2\left(\kappa^2k_c^2+aL^2\right)}-1\right)}$

α_8	$$-\frac{1}{L^{12}k_c^2\left(\frac{L^2\left(r-\left(1-\frac{k_c^2}{L^2}\right)^2\right)}{k_c^2\left(aL^2+\kappa^2k_c^2\right)}-1\right)\gamma_c^4}\Bigg[\left(r-\left(1-\frac{k_c^2}{L^2}\right)^2\right)\left(-6k_c^{13}+36L^2k_c^{11}+18L^4(r-5)k_c^9\right.$$ $$+\frac{6\left(\gamma_c^2L^6+\left(aL^2+2\kappa^2k_c^2\right)\left((r-1)L^4+2k_c^2L^2-k_c^4\right)\right)k_c^9}{aL^2+\kappa^2k_c^2}+120L^6k_c^7-72L^6rk_c^7$$ $$-\frac{24L^2\left(\gamma_c^2L^6+\left(aL^2+2\kappa^2k_c^2\right)\left((r-1)L^4+2k_c^2L^2-k_c^4\right)\right)k_c^7}{aL^2+\kappa^2k_c^2}-18L^8\left(r^2-6r+5\right)k_c^5$$ $$-\frac{12L^4(r-3)\left(\gamma_c^2L^6+\left(aL^2+2\kappa^2k_c^2\right)\left((r-1)L^4+2k_c^2L^2-k_c^4\right)\right)k_c^5}{aL^2+\kappa^2k_c^2}+36L^{10}k_c^3+36L^{10}r^2k_c^3-12L^{10}\kappa^2\gamma_c^2k_c^3$$ $$-\frac{16L^{10}\delta^2\kappa^2\gamma_c^2k_c^3}{r-1}-72L^{10}rk_c^3+\frac{24L^6(r-1)\left(\gamma_c^2L^6+\left(aL^2+2\kappa^2k_c^2\right)\left((r-1)L^4+2k_c^2L^2-k_c^4\right)\right)k_c^3}{aL^2+\kappa^2k_c^2}$$ $$-\frac{8L^{10}\delta^2\kappa^2\gamma_c^2k_c^3}{-\left(1-\frac{4k_c^2}{L^2}\right)^2+\frac{\gamma_c^2}{\frac{4\kappa^2k_c^2}{L^2}+a}+r}-6L^{12}k_c+6L^{12}r^3k_c-18L^{12}r^2k_c-6aL^{12}\gamma_c^2k_c-\frac{8aL^{12}\delta^2\gamma_c^2k_c}{r-1}$$ $$\left.+18L^{12}rk_c+\frac{6L^8(r-1)^2\left(\gamma_c^2L^6+\left(aL^2+2\kappa^2k_c^2\right)\left((r-1)L^4+2k_c^2L^2-k_c^4\right)\right)k_c}{aL^2+\kappa^2k_c^2}-\frac{4aL^{12}\delta^2\gamma_c^2k_c}{-\left(1-\frac{4k_c^2}{L^2}\right)^2+\frac{\gamma_c^2}{\frac{4\kappa^2k_c^2}{L^2}+a}+r}\right)\Bigg]$$
α_9	$$\frac{1}{L^8\gamma_c^2k_c\left(L^2k_c^2\left(aL^2-2\right)+k_c^4\left(\kappa^2L^2+1\right)+L^4(-(r-1))\right)}\Bigg[2\Big(L^8k_c^4\big(2(r-1)\big(2a^2+9a\kappa^2+5\kappa^4(r-1)\big)$$ $$-3\gamma_c^2\big(a-4\kappa^2\big)\big)+2L^6k_c^6\big(-4\kappa^2\gamma_c^2+5a^2+3a\kappa^2(r+1)+18\kappa^4(r-1)\big)+L^4k_c^8\big(-5a^2$$ $$+18a\kappa^2-8\kappa^4(r-5)\big)+aL^{12}(r-1)\big(\gamma_c^2+a(r-1)\big)+2L^{10}k_c^2\big(a$$ $$\left.+3\kappa^2(r-1)\big)\big(\gamma_c^2+a(r-1)\big)-12\kappa^2L^2k_c^{10}\big(a+\kappa^2\big)-2\kappa^4k_c^{12}\big)\right]$$
α_{10}	$\frac{2\left(\left(2L^2k_c^2-k_c^4+L^4(r-1)\right)\left(2\kappa^2k_c^2+aL^2\right)+L^6\gamma_c^2\right)}{L^4\gamma_ck_c(\kappa^2k_c^2+aL^2)}$
β_1	$\frac{\gamma_c^2+a(r-1)}{r-1}$
β_2	$-\frac{2\delta\gamma_c}{r-1}$
β_3	$\frac{\gamma_c}{r-1}$
β_4	$-\frac{2\delta}{r-1}$
γ_1	$-\frac{\gamma_c}{\frac{4\kappa^2k_c^2}{L^2}+a}$
γ_2	$-\frac{\delta}{\frac{\gamma_c^2}{\frac{4\kappa^2k_c^2}{L^2}+a}-\left(1-\frac{4k_c^2}{L^2}\right)^2+r}$

Table B.2: List of parameters which occur in amplitude equations (3.38) in the case of the travelling wave instability

parameter	expression
α_1	$\frac{i(a-a_c)v_\phi\left(L^2a_ck_c^4+\kappa^2k_c^6\right)}{2L^2w}$
α_2	$\frac{i\delta v_\psi\left(L^2a_c+\kappa^2k_c^2\right)\left(L^2a_ck_c^4+iL^2wk_c^2+\kappa^2k_c^6\right)}{L^4(r-1)w}$
α_3	$\frac{3ik_c^4v_\phi^2v_\phi^*\left(a_c+\frac{\kappa^2k_c^2}{L^2}\right)}{2w}+\frac{1}{2}\left(-\frac{k_c^2\left(a_c+\frac{\kappa^2k_c^2}{L^2}\right)}{\sigma-\gamma}+\frac{ik_c^4\left(a_c+\frac{\kappa^2k_c^2}{L^2}\right)^2}{w(\sigma-\gamma)}\right)$ $\left(-\frac{2\delta^2L^4v_\psi^3}{-\frac{2\gamma L^6k_c^2(\gamma-\sigma)}{2L^2a_ck_c^2+8\kappa^2k_c^4+iL^2w}-8L^2k_c^2+16k_c^4+L^4(-r+2iw+1)}+\frac{4\delta^2v_\psi^3}{r-1}+3v_\psi^3\right)$
$\tilde{\alpha}_3$	$\frac{3iv_\phi^2v_\phi^*\left(L^2a_ck_c^4+\kappa^2k_c^6\right)}{L^2w}+\frac{1}{2}\left(-\frac{k_c^2\left(a_c+\frac{\kappa^2k_c^2}{L^2}\right)}{\sigma-\gamma}+\frac{ik_c^4\left(a_c+\frac{\kappa^2k_c^2}{L^2}\right)^2}{w(\sigma-\gamma)}\right)$ $\left(-\frac{4\delta^2L^4v_\psi^3}{-\frac{2\gamma L^6k_c^2(\gamma-\sigma)}{2L^2a_ck_c^2+8\kappa^2k_c^4}-8L^2k_c^2+16k_c^4+L^4(1-r)}+\frac{4\delta^2v_\psi^3}{r-1}+\frac{4\delta^2v_\psi^3}{r-2iw-1}+6v_\psi^3\right)$
α_4	$\frac{i}{2L^2w}\left(\frac{\kappa^2k_c^2}{L^2}+a_c\right)\Big(\frac{1}{\kappa^2k_c^4+L^2a_ck_c^2+iL^2w}4i\kappa^2\Big(-4i\kappa^2v_\phi k_c^3$ $-\frac{\left(a_cL^2+\kappa^2k_c^2\right)v_\phi\left(a_cv_\phi L^6+\gamma v_\psi L^6+2\kappa^2k_c^2v_\phi L^4+\frac{2\left(L^2-k_c^2\right)\left(\kappa^2k_c^4+L^2a_ck_c^2+iL^2w\right)v_\psi}{\gamma-\sigma}\right)k_c^3}{L^6w}$ $-2i\left(a_ck_cv_\phi L^2+\gamma k_cv_\psi L^2\right)k_c^3\Big)-6\kappa^2v_\phi k_c^2+\frac{1}{\kappa^2k_c^4+L^2a_ck_c^2+iL^2w}\Big)2iL^2a_c$ $\Big(-4i\kappa^2v_\phi k_c^3-\frac{1}{L^6w}\left(a_cL^2+\kappa^2k_c^2\right)v_\phi\Big(a_cv_\phi L^6$ $+\gamma v_\psi L^6+2\kappa^2k_c^2v_\phi L^4+\frac{2\left(L^2-k_c^2\right)\left(\kappa^2k_c^4+L^2a_ck_c^2+iL^2w\right)v_\psi}{\gamma-\sigma}k_c^3\Big)$ $-2i\left(a_ck_cv_\phi L^2+\gamma k_cv_\psi L^2\right)\Big)k_c-L^2a_cv_\phi-L^2\gamma v_\psi$ $+\frac{1}{\kappa^2k_c^4+L^2a_ck_c^2+iL^2w}\Big(L^2\Big(-\frac{1}{L^{14}w^2}\left(a_cL^2+\kappa^2k_c^2\right)^2v_\phi\Big(a_cv_\phi L^6+\gamma v_\psi L^6+2\kappa^2k_c^2v_\phi L^4$ $+\frac{2\left(L^2-k_c^2\right)\left(\kappa^2k_c^4+L^2a_ck_c^2+iL^2w\right)v_\psi}{\gamma-\sigma}\Big)^2k_c^6\Big)-\frac{1}{L^8w}\Big(4i\kappa^2\left(a_cL^2+\kappa^2k_c^2\right)v_\phi\Big(a_cv_\phi L^6+$ $\gamma v_\psi L^6+2\kappa^2k_c^2v_\phi L^4+\frac{2\left(L^2-k_c^2\right)\left(\kappa^2k_c^4+L^2a_ck_c^2+iL^2w\right)v_\psi}{\gamma-\sigma}\Big)k_c^6$ $-\frac{2i\left(a_cL^2+\kappa^2k_c^2\right)\left(a_cv_\phi+\gamma v_\psi\right)\left(a_cv_\phi L^6+\gamma v_\psi L^6+2\kappa^2k_c^2v_\phi L^4+\frac{2\left(L^2-k_c^2\right)\left(\kappa^2k_c^4+L^2a_ck_c^2+iL^2w\right)v_\psi}{\gamma-\sigma}k_c^4\right)}{L^6w}\Big)\Big)k_c^2$ $+\frac{\left(L^2-3k_c^2\right)\left(a_cL^2+\kappa^2k_c^2\right)\left(-i\kappa^2k_c^6-iL^2a_ck_c^4+L^2wk_c^2\right)v_\psi}{L^8w(\gamma-\sigma)}$

Acknowledgements

Finally I want to say “thank you” to all persons who contributed during the last year with their support, explanations and advices:

- First of all I want to thank my supervisor, Uwe Thiele, for providing me a topic on which I could learn a lot during the last year, for giving me the opportunity to employ my own ideas and for all the great discussions.
- Sebastian Engelnkemper, for explaining me the usage of *pde2path* for all the valuable advices and for proofreading a part of my thesis
- Fenna Stegemerten, for always being willing to help, for helpful discussions about my analytical results and for proofreading of my thesis
- All members of the group, for the great year and for the fantastic atmosphere

Declaration of Academic Integrity

Hereby, I confirm that this thesis on "Nonlinear analysis of coupled dissipative systems with a conservation law" is solely my own work and that I have used no sources or aids other than the ones stated. All passages in my thesis for which other sources, including electronic media, have been used, be it direct quotes or content references, have been acknowledged as such and the sources cited.

(date and signature of student)

I agree to have my thesis checked in order to rule out potential similarities with other works and to have my thesis stored in a database for this purpose.

(date and signature of student)